Stability Studies of Poly(3-hexylthiophene) and Synthesis and Characterization of Some Metallo-Supramolecular Polymers

A thesis submitted by

Prasanta Jyoti Goutam

to

Indian Institute of Technology Guwahati

for the award of the degree of

Doctor of Philosophy

Department of Chemistry
Indian Institute of Technology Guwahati
Guwahati - 781039
India

November, 2011

Statement

The work contained in this thesis titled '**Stability Studies of Poly(3-hexylthiophene) and Synthesis and Characterization of Some Metallo-Supramolecular Polymers**' has been carried out by me under the supervision of Dr. Parameswar Krishnan Iyer, Associate Professor, Department of Chemistry, Indian Institute of Technology Guwahati. This work has not been submitted elsewhere for the award of any degree.

Prasanta Jyoti Goutam

Department of Chemistry,
Indian Institute of Technology Guwahati,
Guwahati – 781039, India.

November, 2011

Certificate

It is certified that the work contained in the thesis entitled '**Stability Studies of Poly(3-hexylthiophene) and Synthesis and Characterization of Some Metallo-Supramolecular Polymers**' by Prasanta Jyoti Goutam, a student of Department of Chemistry, Indian Institute of Technology Guwahati, for the award of the degree of Doctor of Philosophy has been carried out under my supervision. This work has not been submitted elsewhere for any degree.

Dr. Parameswar Krishnan Iyer

Associate Professor,
Department of Chemistry,
Indian Institute of Technology Guwahati
Guwahati – 781039, India.

November, 2011

Dedicated To My Parents

Acknowledgements

At this stage of ending my PhD period, I must appreciate the people around me all throughout my academic journey, without whom this thesis would not have been a reality.

Firstly, I would like to express my sincere gratitude to my thesis supervisor Dr. Parameswar Krishnan Iyer for introducing me to an interdisciplinary area of research. I earnestly thank him for his astute guidance, encouragement, inspiration and creative and scientific ideas, which helped me to enhance my knowledge.

I sincerely thank and appreciate the members of my doctoral committee, Professor Bhisma Kumar Patel, Professor Seenipandian Ravi and Dr. Ashish Kumar Gupta for periodic assessments, crucial comments and suggestions which certainly helped me a lot in betterment of my thesis.

I am thankful to Dr. Pravat Kumar Giri, Department of Physics and Dr. Aloke Kumar Ghoshal, Department of Chemical Engineering of Indian Institute of Technology for their cooperation and suggestion in our collaborative works.

I am thankful to all faculties and scientific staff associated with me at the Department of Chemistry, Indian Institute of Technology Guwahati who were always helpful.

I remain thankful to the Central Instruments Facility (CIF), IIT Guwahati for different characterization facilities. I am grateful to Chandan da, Kula da and Singh da from CIF for their help at every stages of my research.

With my friends, seniors and juniors my PhD period became cherishably wonderful and will be echoing forever in corridors my mind. I am blessed with friendship of my friends-Sonit, Akashi, Krishna, Bibek, Susanda, Upasana, Mahfuz, Shamim, Aboni, Arindom, Raja, Ramesh, Mrigendra, Prasenjit, Dhruba and Rupam. I am going to treasure the fantastic moments shared. I am very lucky to have extremely cooperative and friendly seniors – Pranjol da, Bolin da, Gunin da, Manash da, Sahid da, Ballav da, Sankar da. My lab juniors – Atul, Ratna, Muthu, Sukanti, Meenakshi, Radhakrishna, Sameer, Bhim and Suresh made my experiences with them unforgettable with their help and care. I must specially thank Dilip, Francis, Karthik and Subhojit for their scientific helps at different stages of my work. Thanks go to all other departmental seniors, batch mates and juniors for making my days memorable with them. I am thankful to Swarup Sir, Swapnali baideu, Bhaskar da, Jayashree ba and Madhurjya for offering me homely atmosphere at different times within IITG campus.

I gratefully acknowledge the funding source, Council of Scientific and Industrial Research (CSIR), India.

I gratefully acknowledge all my teachers at Jorhat Engineering Collegiate L. P. School, Jorhat Govt. Boys H. S. and M. P. School, J. B. College Jorhat, Govt. Science College Jorhat and Indian Institute of Technology Guwahati for whom what I am today. I sincerely acknowledge Dr. Aboni Chandra Goswami, Govt. Science College Jorhat, for his best teachings, constant motivations and precious advices which are of great impact on me. I acknowledge Prasanta Kumar Bordoloi sir for his helps, support and motivations right from my graduation days.

Finally, my PhD endeavour could not be completed without the endless love, unending support, tolerance and blessings from my family. I would like to express my sincere gratitude to my family members and relatives for their encouragement and patience.

Prasanta

Abstract

The thesis entitled '**Stability Studies of Poly(3-hexylthiophene) and Synthesis and Characterization of Some Metallo-Supramolecular Polymers'** is divided into two parts. First part discusses stability of poly(3-hexylthiophene), an important conjugated polymer. Second part discusses synthesis and characterization of some metallo-supramolecular polymers.

Poly(3-hexylthiophene) (P3HT)) is a very important conjugated polymer which finds wide applications in optoelectronics. Despite the vast and many more applications of P3HT, very modest effort has been devoted to understand their detailed thermal decomposition behavior. Mostly available literature only discusses basic thermal studies without any established thermal decomposition route. We could realize that insight into the details changes of P3HT, that take place when they are subjected to high temperatures, especially during device fabrication is important area to be focused. We took up the project and a plausible degradation route is proposed based on the experimental details acquired from gas chromatography, Raman spectroscopy, FTIR spectroscopy, powder X-ray diffractometry, scanning electron microscopy and transmission electron microscopy. Moreover, photo stability of P3HT is not good enough and it degrades in organic solvents containing dissolved molecular oxygen when irradiated with ultraviolet light. We could show that preparation of composites of P3HT with appropriate amounts of multiwalled carbon nanotubes (MWCNT) result in superior photostability of P3HT. UV visible and fluorescence spectroscopy have been used as primary tools to study the photostability of P3HT and its composites. This enhanced photostability of P3HT on preparing composites with MWCNT in addition to its easy processability directly from solution makes these composites immensely important for optoelectronic applications. Photoluminescence quenching of P3HT upon addition of carbon nanotubes was an important phenomenon that we observed. We could establish the nature as 'static quenching' from the results of photoluminescence spectroscopy and time resolved photoluminescence spectroscopy.

Metallo-supramolecular polymers potentially offer the functionality of the metal ion along with the processability of the polymer and this makes them advantageous over the conventional polymers. Designing of efficient ditopic monomers with effective metal binding sites has been a wide area of research. Recently, interest has developed in synthesizing terpyridine ligand based metallo-supramolecular polymers as because they form chelate with metal ions which increase the stability of the polymeric systems. Coordination behavior of benzimidazole, 2-substituted benzimidazoles and benzothiazoles, towards transition metal ions are well established. Looking into the important biological activities of the benzothiazole nucleus, and its similarities in binding modes with benzimidazole as well as availability of easy synthetic methods, we pursued the synthesis of benzothiazole based ditopic monomers and used it for metallo-supramolecular polymer formation. One of our monomer, apart from forming polymers, showed well ability in selectively recognizing resorcinol from among the other toxic benzene metabolites. Another monomer, with a pentaethylene based ethereal spacer showed remarkable propensity to fold in solution by supramolecular interaction selectively upon addition of K^+. Monomer – K^+ folded unit self assemble upon addition of Zn^{2+} ion and results a unique supramolecular polymeric system. We could establish this interesting behavior with experimental results as well as supportive theoretical calculations by DFT method.

Contents

Part A

Chapter A1

INTRODUCTION

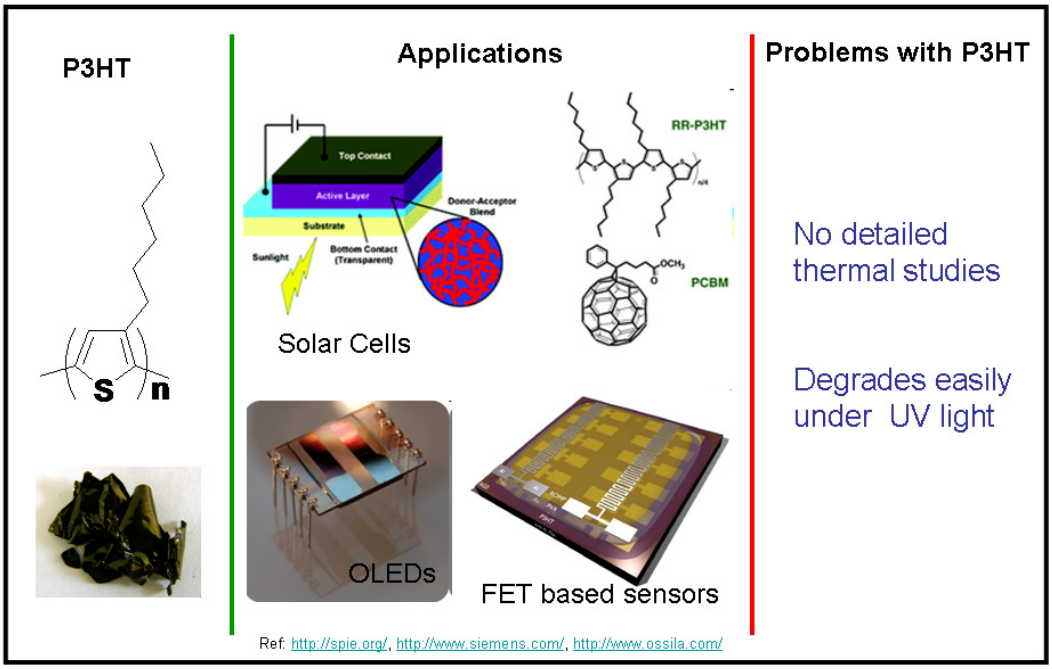

Poly(3-hexylthiophene) (P3HT) is one of the most extensively studied conducting polymer for optoelectronic device applications. Although its physicochemical properties are very much promising, they still pose a number of fundamental problems. P3HT degrades rapidly under UV light which causes problem in devices. Moreover, till date no detail thermal studies are made to establish its thermal stability. In this thesis, the cause and solution to problems associated with stability of P3HT are elaborated. Need of investigations to ascertain details of thermal stability of P3HT and search for enhancement of photostability of the polymer in its composites are established.

A1.1Conjugated Polymers

Materials capable of simultaneously presenting the properties of organic polymers and of semiconductors have become a subject of considerable interest for both academic and industrial researchers in different domains of chemistry, solid-state physics and electrochemistry [1]. In this perspective, conjugated polymers (CPs) were proclaimed as futuristic new materials that would lead to the next generation of electronic and optical devices. In late 1970's Alan J. Heeger, Alan G. MacDiarmid and Hideki Shirakawa have changed the view on plastics that they insulate, they are opposite of metals, they do not conduct electricity, with their discovery that polyacetylene polymer can be made conductive almost like a metal [2]. Design and development of inexpensive renewable energy sources and fabrication of devices with best power efficiency stimulates scientific research as energy is the most important global concern of the scientific community to save the future of the planet [3]. New technologies are coming up with the discoveries of polymer light-emitting diodes (LEDs) [4], organic transistors [5] and organic solar cells etc [6-7].

The class of polymer is called 'conjugated polymer' because of the alternating single and double / triple bonds in the polymer chain. Due to the conjugation in their chains, it enables the electrons to delocalize throughout the whole system and thus many atoms may share them. The delocalized electrons move around the whole system and become charge carriers to make them conductive. Several examples of conjugated conducting polymers are polyacetylene, polypyrrole, polyaniline and polythiopene (Figure 1) [8].

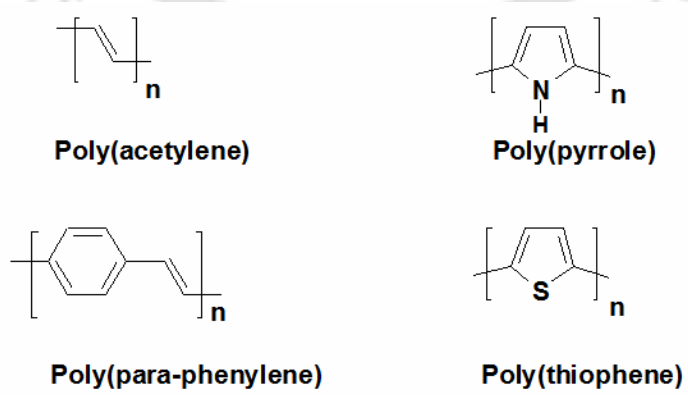

Figure 1 Different important conjugated polymers.

A1.2 Polythiophenes

Among the various possible strategies for modification of CPs the synthesis of a functional CP from a substituted monomer in respect to the prerequisites of preserving its relevant electronic, optical, and electrochemical properties [9] implies a detailed comprehension of the structural effects of substitution (inductive, mesomeric and steric) at the various stages of organization of the material. Ease of synthesis due to better reactivity of monomer, modification of macromolecular properties (planarity of the conjugated system, mean effective conjugation length intrachain conductivity, electronic and electrochemical properties) and modification of macroscopic properties (crystallinity, morphology, porosity, mechanical properties and macroscopic conductivity electrochemical properties) are achieved with betterment in substituted polythiophenes [1] Alkyl chains in β position enhance their solubility in organic solvents and thereby enhances the ease of processing for device applications. Alkyl chains in β position also facilitate characterizations in alkylthiophenes [10]. These features make polythiophenes an important representative class of conjugated polymer, which can form some of the most environmentally [11] and thermally stable materials that can be used as electrical conductors, nonlinear optical devices, polymer LEDs, electrochromic or smart windows, photoresists, antistatic coatings, sensors, batteries, electromagnetic shielding materials, artificial noses and muscles, solar cells, electrodes, microwave absorbing materials, new types of memory devices, nanoswitches, optical modulators and valves, imaging materials, polymer electronic interconnects, nanoelectronic and optical devices, and transistors [12]. Polythiophene and its derivatives work very well in some of the above applications and less impressively in other devices. Creative new design and development strategies of new polythiophenes has led to interesting new materials and enhanced performance in certain devices. The ability of molecular designers to understand how to gain control over the structure, properties, and function in polythiophenes continues to make the synthesis of polythiophenes a critical subject in the development of new advanced materials [7]. A number of 3-substituted poly(alkylthiophenes), namely poly(3-alkylthiophene) (P3AT) (Figure 2) have been prepared by electrochemical or chemical oxidation of appropriately 3-substituted thiophenes [13].

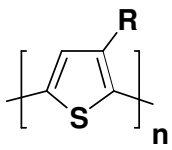

R=Hexyl, octyl, bromohexyl etc.

Figure 2 Chemical structure of poly(3-alkylthiophene).

A1.3 Synthesis of poly(3-alkylthiophene)

A1.3.1 Electrochemical polymerization

In electro chemical method of preparation of polythiophenes, a potential is applied across a solution containing thiophene or substituted thiophene and an electrolyte. Conductive polythiophene is recovered as product on the anode (Scheme 1). Initially, oxidation of monomer generates a radical cation which then couples with a second radical cation to produce a dihydro dimer dication. This leads to a neutral dimer after loss of two protons. The dimer which is more easily oxidized than the monomer, gets oxidized to its radical cation and then couple with another monomer radical. This process repeats until the polymer becomes insoluble in the electrolytic medium and precipitates onto anode [1].

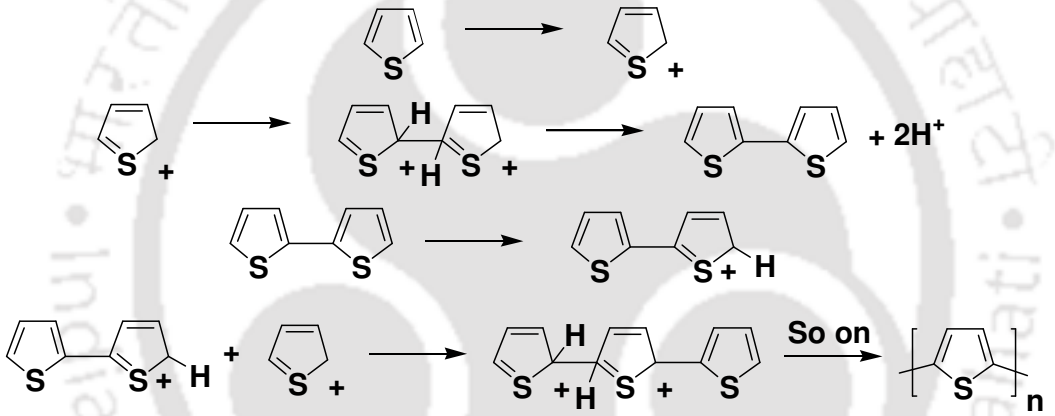

Scheme 1 Electrochemical polymerization of thiophene.

A1.3.2 Transition metal catalyzed reactions

Elsenbaumer was first to report synthesis of poly(3-alkylthiophene)(P3AT). Later, Sugimoto synthesized P3AT by treating 3-alkylthiophene with FeCl3 in chloroform [14-18] (Scheme 2).

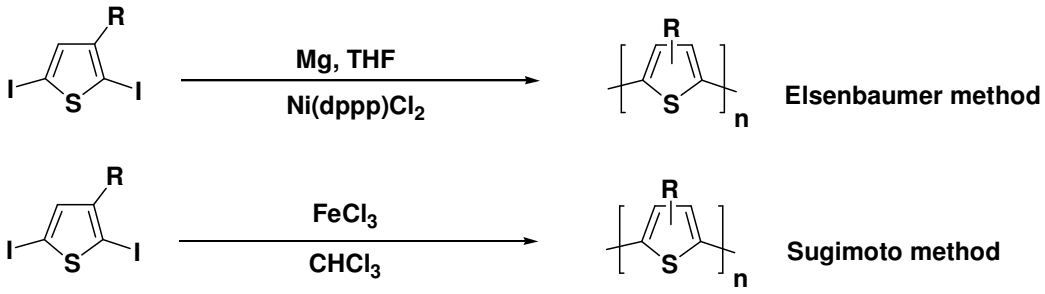

Scheme 2 Different methods for synthesis of polythiophenes using transition metal catalyst.

A1.3.3 Synthesis of regioregular poly(3-alkylthiophene)

Electrochemical and chemical methods lead to random couplings in P3ATs. This gives only 50-80% of head-to-tail (HT) coupling, the remaining part is regioirregular. Coupling of 3–substituted thiophene at the 2- and 5- positions leads to three different regiochemical dimeric units, head-to-head(HH), head-to-tail(HT) and tail-to-tail(TT) diads as shown in (Figure 3). This leads to four chemically distinct triads region isomers, i.e., HT-HT, HT-HH, TT-HT and TT- HH as shown in (Figure 4). Irregularly substituted polythiophenes have structures where unfavorable H-H coupling cause a sterically driven

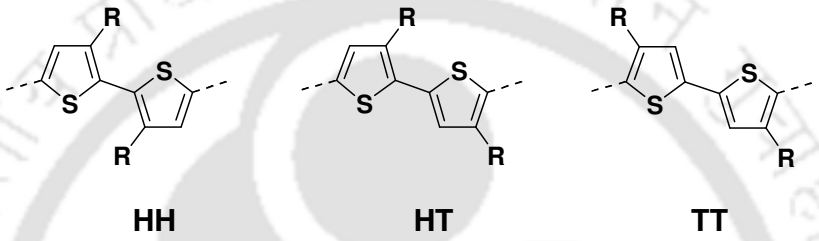

Figure 3 Regiochemical diads of P3AT.

twist of thiophene rings, resulting in loss of conjugation. Regioregular H-T poly(3-alkylthiophene)(rr-P3AT) can easily access a low energy planar conformation, leading to highly conjugated polymer [19].

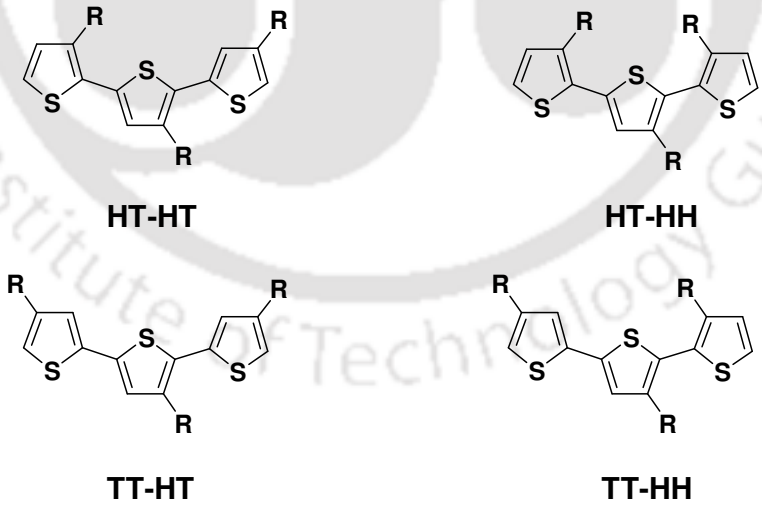

Figure 4 Regiochemical triads of P3AT.

McCullough et al. reported the first synthesis of rrP3HTs, yielding nearly 100% regioregular polymer [20]. The key to this method is the regio specific generation of 2-

bromo-5-bromomageniso-3-alkylthiophene, which is generated by reaction of 2-bromo-3-alkylthiophene with LDA at -78 °C followed by the addition of $MgBr_2.OEt_2$. The bifunctional intermediate is then polymerized with catalytic amount of $Ni(dppp)Cl_2$ using Kumada cross coupling method, affording rrP3AT in 44- 66% yield (Scheme 3).

The resulting rrP3AT afford HT-HT region regularity of 98-100% as seen by NMR study and the Mn values are typically 20k-40k with a PDI of 1.4. Another approach reported by Rieke et al. involves the regio specific formation of an organo zinc compound by

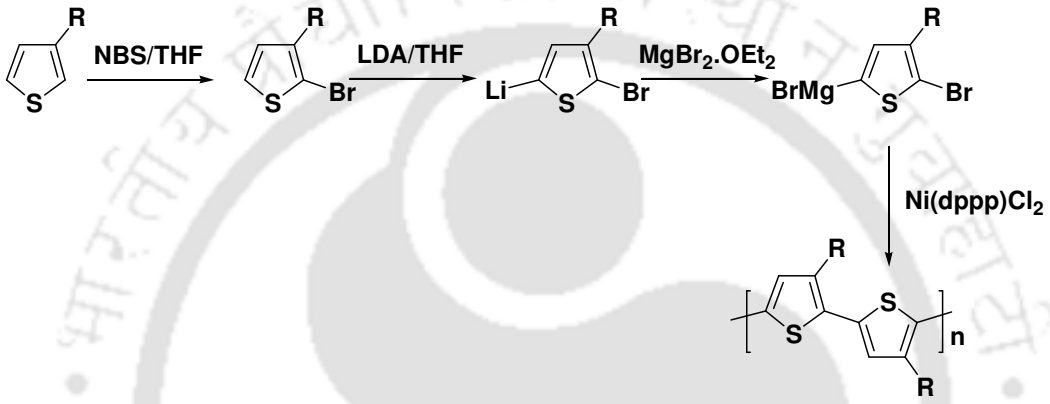

Scheme 3 McCullough method of rrP3AT synthesis.

reaction of 2,5-dibromo-3-alkylthiophene with highly reactive zinc , and subsequent nickel catalysed polymerization [21-24] (Scheme 4). The choice of catalyst used in the aryl –aryl coupling has a strong influence on regioregularity of the resulting polymer.

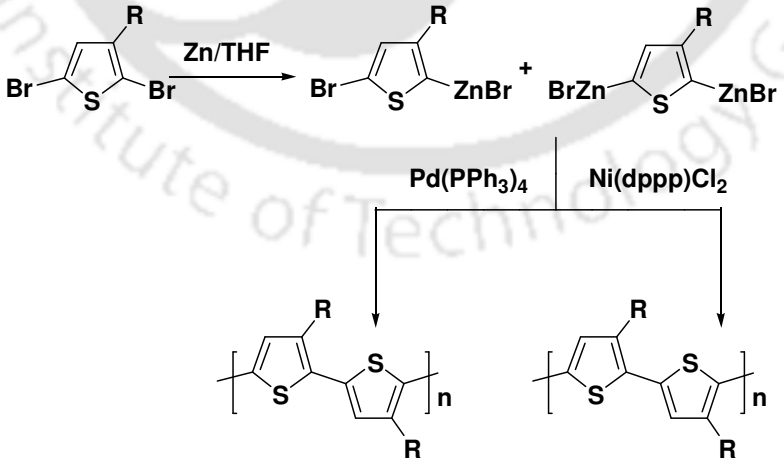

Scheme 4 Rieke method of rrP3AT synthesis.

Use of $Pd(PPh_3)_4$ leads to a regiorandom polymer whereas $Ni(dppp)Cl_2$ leads to a regioregular polymer. Molecular weights of polymers prepared by these methods falls in

the range of 24k-34k with PDI of 1.4. To overcome the drawbacks of the above methods (use of cryogenic temp, multistep procedure and use of highly reactive zinc) McCullough et al. in 1999 described an economical new synthesis for the rrP3ATs known as Grignard

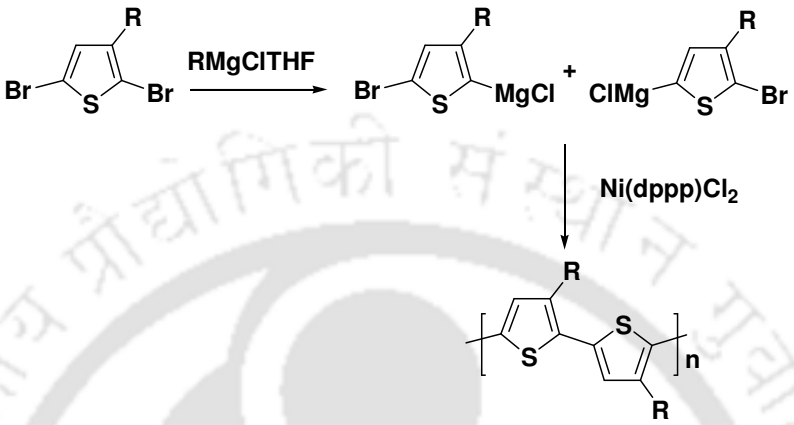

Scheme 5 GRIM method of rrP3AT synthesis.

metathesis (GRIM) method [25,26]. In this method, 2,5-dibromo-3-alkylthiophene is treated with 1 equivalent of RMgCl (R=alkyl) to form mixtures of intermediates as shown in Scheme 5 in the ratio of 85:15 to 75:25. The Mn values of rrP3ATs synthesized by these methods are 20k-40k with PDI in the range of 1.2-1.4.

A1.4 Problems with poly(3-alkylthiophenes)

Although their structure and physicochemical properties are very much promising, poly(3-alkylthiophenes) still pose a number of fundamental problems [1]. Chemical stability of conducting polymers has attracted enormous debate, because lithography processes used during submicrometer device fabrication involves exposure to intense UV light or electron beam irradiation [27]. This usually causes the photodegradation/bleaching of the organic materials. Such degradation occurs via the classical route of photooxidation where scission is initiated by photolysis of trace amounts of transition-metal salts [28]. From above discussion on synthesis of poly(alkylthiophene)s, it is evident that such metal impurities are obviously added in trace amounts in the process of synthesis. Various methods have been used to improve the thermal, mechanical, electrical, and optical properties of conducting polymers, such as introducing alkyl groups into the main chain, synthesis of soluble precursors, copolymerization and preparation of conducting polymer composites [7, 12].

A1.5 Conducting polymer composites

Preparation of conducting polymer composites with advanced material is a recent development where advantages of both the polymer and the composite forming material are achieved together. Recently, conducting polymer-carbon nanotube composites were widely studied to make a large scale enhancement in the physical, mechanical, optical, and conducting properties [29-34]. The multiwalled carbon nanotube (MWCNT)-poly(3-octylthiophene) (P3OT) composites show a 5 order increase in conductivity of the composites than that of the pure polymer [35]. However, the optical absorption spectra of the P3OT-single-walled carbon nanotubes (SWNT) did not change significantly up to 5 wt % SWCNT no significant ground-state interaction between the two materials, causing no charge transfer [36]. In the SWCNT-poly-(ethylene dioxythiophene) (PEDOT) composites, the electroluminescence, current (I)-voltage (V) data, and photoluminescence suggest an electronic interaction between SWCNT and PEDOT; the electronic interaction originates from the hole trapping nature of SWCNT in a hole-conducting polymer [37]. Hence, from literature survey it is apparent that poly(3-alkylthiophene) (P3AT)-CNT nanocomposites exhibit interesting physical, optical, and conductivity properties, but the reason for such improvement is not clearly understood and there lie scope of research [38].

A1.6 Poly(3-hexylthiophene)

The discovery of ultrafast charge transfer in p-conducting polymer/fullerene composites by Sariciftci in 1992 [39] brought a crucial milestone in the field of polymer solar cells. The high asymmetry between the forward and back electron transfer rate (9 order of magnitude)[40] allows the use of cell architectures with one photo active composite layer instead of donor acceptor bilayer devices. The advantage of the blend is an increased

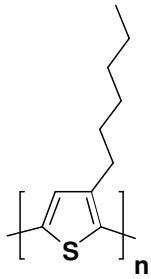

Figure 5 Chemical structure of poly(3-hexylthiophene)

donor acceptor interface and a shortened distance for exciton diffusion (created on the polymer) to reach it. Regioregular poly(3-hexylthiophene) (P3HT) appears to be one of the best materials till date for such devices. It combines the commercial availability with sufficient solubility, a low band gap relative to the most conjugated polymers and a high degree of intermolecular order leading to high charge carrier motilities [41]. Hence, it is less surprising that the recent best results were obtained using this material [42].

A1.7 Scope of the work

Despite vast applications of P3HT, it has serious problem of photostability. P3HT in optoelectronic devices has been a challenge due to its degradation in the presence of light during fabrication and operation. The prime reason for this degradation is the effect of organic/nonaqueous solvents while processing and the presence of dissolved molecular oxygen in addition to the exposure or irradiation of UV or visible light. According to Holdcroft, degradation takes the form of both reduced π-conjugation and chain scission. The former manifests itself as photobleaching and is largely the product of photosensitization and reaction of singlet oxygen. Chain scission occurs via the classical route of photooxidation where scission is initiated by photolysis of trace amounts of transition-metal salts. In the case of poly(3-hexylthiophene), prepared by chemical oxidation using $FeCl_3$, the photoactive impurities are iron(III) salts. Free-radical attack on thienyl rings provides an additional, but minor route to photobleaching. Similar polymers prepared electrochemically and by Grignard polycondensation reactions also undergo photochain scission but to a lesser degree than polymers prepared by $FeCl_3$. The variation in rates of scission is attributed to differences in the nature and concentration of the impurities. Cause and path of photodegradation of P3HT in well established in literature [27-28, 43]. This helps in taking care the fabrication process and to enhance the performances of devices made out of it.

P3HT are subjected to high temperatures especially during device fabrication. Surprisingly, very modest effort has been devoted to understand their thermal decomposition behavior which would provide an insight into the changes that take place under thermal conditions. Literature available [44-49] only discusses basic thermal studies without proposing any degradation pathway. We observed, an established thermal degradation pathway would certainly help to ascertain thermal parameters for fabrication of devices using P3HT. We took up the project and could successfully formulate and study the systematic stepwise degradation mechanism of P3HT under thermal conditions in inert atmosphere as described in Chapter A2 of this thesis. As discussed above, severe

problem of photo stability is associated with P3HT. Yet meager or practically no efforts have been made to prevent the photodegradation of conjugated polymers. In the scope of this thesis, we have taken up a systematic study on enhancing the photostability of P3HT by preparing nanocomposites with carbon nanotubes in Chapter A3.

P3HT composites with carbon nanotubes show high photoluminescence quenching even if very minor quantities of carbon nanomaterial is blended. However, despite this observation of significant quenching behavior, the nature of this photoluminescence quenching (static or dynamic) has not yet been determined. In Chapter A4, we have taken up the to study the nature of photoluminescence quenching of P3HT in the presence of CNTs.

References

[1] Roncali, J. *Chem. Rev.* **1992**, *92*. 711.

[2] *The official website of the Nobel prize*, http://www.nobelprize.org/nobel_prizes/chemistry/laureates/2000/chemadv.pdf

[3] Tang, C. W. *Appl. Phys. Lett.* **1986**, *48*, 183.

[4] Burroughes, J. H.; Bradley, D. D. C.; Brown, A. R.; Marks, R. N.; Mackay, K.; Friend, R. H.; Burns, P. L.; Holmes, A. B. *Nature*, **1990**, *347*,539.

[5] Katz, H. E. *J. Mater. Chem.* **1997**, *7*, 369.

[6] Gunes, S.; Neugebauer, H.; Sariciftci N. S. *Chem. Rev.* **2007**, *107*, 1324.

[7] McCullough R. D. *Adv. Mater.* **1998**, *10(2)*, 93.

[8] Patil A. O.; Heeger A. J.; Wudl, F. *Chem. Rev*, **1988**, *88*, 183.

[9] Springborg, M. *J. Phys: Condens. Matter* **1992**, *4*, 101.

[10] Mucci, A.; Schenetti, L. *Macromol. Chem. Phys.* **1995**, *196*, 2687.

[11] Baker, G. L. *Electronic and Photonic Applications of Polymers; Bowden, M. J., Turner, Eds.* ACS Advances in Chemistry Series 210; American Chemical Society: Washington, DC, **1988**.

[12] Skotheim, T.; Reynolds, J.; Elsenbamer, R.; Dekker, M. *Handbook of Conducting Polymers, 2nd ed.* Marcel Dekker: New York, **1998**.

[13] Reynolds, J. R.; Pomerantz, M. *In Electroresponsive Molecular and Polymeric Systems; Skotheim, T. A., Ed.* Dekker: New York, **1991**.

[14] Yoshino, K.; Hayashi, S.; Sugimoto, R. *Jap. J. Appl. Phys. Part 2-Lett.* **1984,** *23 (12)*, L899.

[15] Yamamoto,T.; Maruyama, T.; Zhou, Z. H.; Miyazaki, Y.; Kanbara, T.; Sanechika, K.*Synth. Met.* **1991,** *41*, 345.

[16] Jen, K. Y.; Miller, G. G.; Elsenbaumer, R. L. *J. Chem. Soc.-Chem. Comm.* **1986,** *17*, 1346.

[17] Jow, T. R.; Jen, K. Y.; Elsenbaumer, R. L.; Shacklette, L. W.;Angelopoulos,M.; Cava, M. P. *Synth. Met.* **1986,** *14*, 53.

[18] Elsenbaumer, R. L.; Jen, K. Y.; Oboodi, R. *Synth. Met.* **1986,** *15*, 169.

[19] Sato, M. A.; Morii, H. *Macromolecules* **1991,** *24*, 1196.

[20] McCullough, R. D.; Lowe, R. D.; Jayaraman, M.; Anderson, D. L. *J. Org. Chem.* **1993,** *58*, 904.

[21] Wu, X. M.; Chen, T. A.; Rieke, R. D. *Macromolecules* **1995,** *28*, 2101.

[22] Chen, T. A.; Obrien, R. A.; Rieke, R.D. *Macromolecules* **1993,** *26*, 3462.

[23] Chen, T. A.; Rieke, R. D. *Synth. Met.* **1993,** *60*, 175.

[24] Chen, T. A.; Wu, X. M.; Rieke, R. D. *J. Am. Chem. Soc.* **1995,** *117*, 233.

[25] Loewe, R. S.; Ewbank, P. C.; Liu, J. S.; Zhai, L.; McCullough, R. D. *Macromolecules* **2001,** *34*, 4324.

[26] Iovu, M. C.; Sheina, E. E.; Gil, R. R.; McCullough, R. D. *Macromolecules* **2005,** *38*, 8649.

[27] Holdcroft, S. *Macromolecules* **1991**, *24*, 4834.

[28] Holdcroft S. *Macromolecules* **1991**, *24*, 2119.

[29] O'Connell, M. J.; Boul, P.; Ericson, L. M.; Huffman, C.; Wang, Y.; Haroz, E.; Kuper, C.; Tour, J.; Ausman, K. D.; Smalley, R. E. *Chem. Phys. Lett.* **2001**, *342*, 265.

[30] Tang, B. Z.; Xu, H. *Macromolecules* **1999**, *32*, 2569.

[31] Hughes, M.; Chen, G. Z.; Shaffer, M. S. P.; Fray, D. J.; Windle, A. H. *Chem. Mater.* **2002**, *14*, 1610.

[32] Bandyopadhyaya, R.; Nativ-Roth, E.; Regev, O.; Yerushalmi-Rozen, R. *Nano Lett.* **2002**, *2*, 25.

[33] Riggs, J. E.; Guo, Z.; Carroll, D. L.; Sun, Y.-P. *J. Am. Chem. Soc.* **2000**, *122*, 5879.

[34] Hill, D. E.; Lin, Y.; Rao, A. M.; Allard, L. F.; Sun, Y. P. *Macromolecules* **2002**, *35*, 9466.

[35] Musa, I.; Baxendale, M.; Amaratunga, G. A. J.; Eccleston, W. *Synth. Met.* **1999**, *102*, 1250.

[36] Kymakis, E.; Amaratunga, G. A. J. *Synth. Met.* **2004**, *142*, 161.

[37] Woo, H. S.; Czerw, R.; Webster, S.; Carroll, D. L.; Park, J. W.; Lee, J. H. *Synth. Met.* **2001**, *116*, 369.

[38] Kuila, B. K.; Malik, S.; Batabyal, S. K.; Nandi, A. K. *Macromolecules* **2007**, *40*, 278.

[39] Sariciftci, N. S.; Smilowitz, L.; Heeger, A. J.; Wuld, F. *Science* **1992**, *258*, 1474.

[40] Brabec, C. J.; Zerza, G.; Cerullo, G.; De Silvestri, S.; Luzzati, S.; Hummelen, J. C.; Sariciftci, N. S. *Chem. Phys. Lett.* **2001**, *340*, 232.

[41] Sirringhaus, H. S.; Brown, P. J.; Friend, R. H.; Nielsen, M. M.; Bechgaard, K.; Langefeld-Voss, B. M. W.; Spiering, A. J. H.; Janssen, R. A. J.; Meijer, E. W.; Herwig, P.; de Leeuw, D. M. *Nature* **1999**, *401*, 685.

[42] Al- Ibrahim, M.; Roth, H. K.; Zhokhavets, Gobsch, U. G.; Sensfuss, S. *Solar Energy Mat. And Solar Cell* **2005**, *85*, 13.

[43] Abdou, M. S. A.; Holdcroft, S. *Macromolecules* **1993**,*26*, 2954.

[44] Chiang, C. K.; Fincher Jr, C. R., Park, Y. W.; Heeger, A. J. Shirakawa, H.; Louis, E. J. *Phys Rev Lett* **1977**, *39(17)*, 1098.

[45] Reynolds, J. R.; Chien, J. C. W.; Lillya, C. P. *Macromolecules* **1987**, *20*, 1184.

[46] Pyo, M.; Reynolds, J. R. *J Chem Soc Chem Commun* **1993**, 258.

[47] Cirpan, A.; Alkan, S.; Toppare, L.; Hepuzer, Y.; Yagci, Y. *J Polym Sci Part A Polym Chem* **2002**, *40(23)*, 4131.

[48] Yildiz, U. H.; Sahin, E.; Akhmedov, I. M.; Tanyeli, C.; Toppare, L. *J Polym Sci Part A Polym Chem* **2006**, *44(7)*, 2215.

[49] Folch, I.; Borros, S.; Amabilino, D. B.; Veciana, J. *J Mass Spectrom* **2000**, *35*, 550.

Chapter A2

DEGRADATION PATHWAY OF POLY(3-HEXYLTHIOPHENE) UNDER THERMAL CONDITIONS

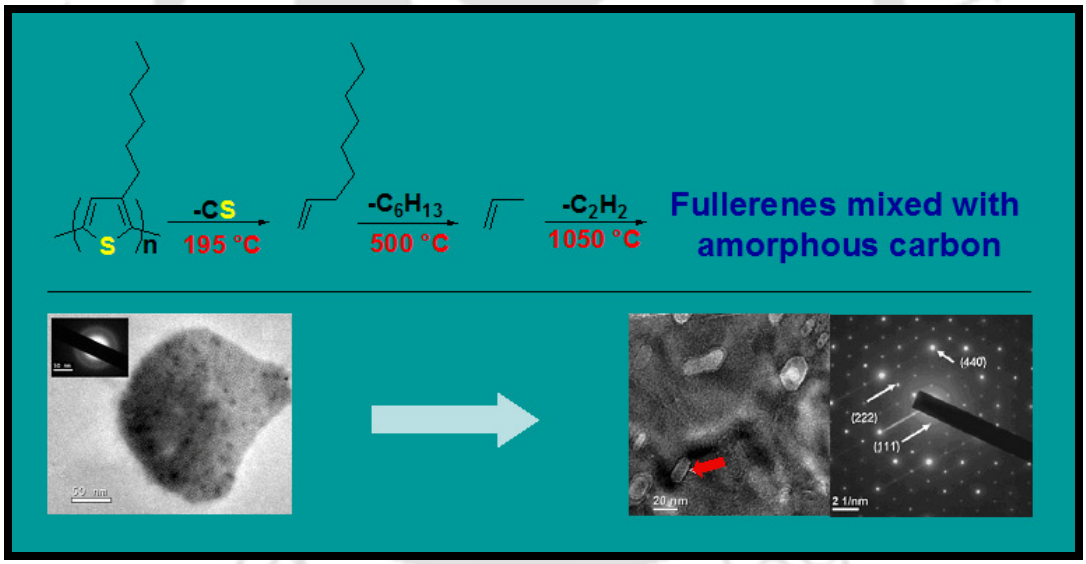

Thermal degradation of Poly(3-hexylthiopene) (P3HT) was studied under nitrogen environment. A plausible degradation route is proposed based on the experimental details acquired from thermogravimetric analysis (TGA), gas chromatography (GC), Raman spectroscopy, FTIR spectroscopy, powder X-ray diffractometry (XRD), scanning electron microscopy (SEM) and transmission electron microscopy (TEM). Degradation of P3HT starts at around 195°C with release of lighter units like CS. Further increase in the temperature results in detachment of the hexyl chain from P3HT and the residue obtained at 1050 °C contains fullerenes mixed with amorphous carbon.

A2.1 Prologue

Polythiophenes and their derivatives are a very important class of conjugated polymers which find applications as electrical conductors, nonlinear optical devices, polymer LEDs, electrochromic or smart windows, photo resists, antistatic coatings, sensors, batteries, electromagnetic shielding materials, artificial noses and muscles, solar cells, electrodes, microwave absorbing materials, new types of memory devices, nanoswitches, optical modulators and valves, imaging materials, polymer electronic interconnects, nanoelectronic and optical devices and transistors [1]. Despite the above vast and many more applications of P3HT, very less effort has been devoted to understand their thermal decomposition behavior [2–7]. Studying the thermal degradation of P3HT would also provide an insight into the changes that take place when they are subjected to high temperatures especially during device fabrication. We have also analyzed degraded samples at various temperatures using Raman, FTIR spectroscopy, powder XRD, SEM, TEM and proposed a plausible degradation route. The residue collected finally at 1050 ^{o}C was well characterized and confirmed to be fullerenes mixed with amorphous carbon. Gas chromatography (GC) technique was used to understand the evolved gaseous products at various stages of degradation.

A2.2 Experimental Section

A2.2.1 Chemicals and Solvents

Chemicals were used as received without any further purification. All solvents, procured from Merck, were used after purification by standard purification techniques [8].

A2.2.2 Synthesis of Poly(3-hexylthiophene)

The synthesis of P3HT was accomplished by oxidative polymerization process using anhydrous $FeCl_3$ as catalyst following the literature procedure [9]. 3-hexylthiophene 0.5 g (2.97 mmol) in 5 mL of freshly distilled $CHCl_3$ was added to a stirred solution of 3.06 g of anhydrous $FeCl_3$ (11.88 mmol) in 30 mL of freshly distilled $CHCl_3$. The reaction vessel was purged with nitrogen and stirred for 2 h at room temperature. The black precipitate which formed was filtered, washed with methanol and then added to 200 mL of $CHCl_3$ and 10 mL of concentrated aqueous ammonia and stirred for 15 minutes at room temperature. Some insoluble red-orange material was filtered. The $CHCl_3$ solution was washed several times with water and dried using anhydrous $CaSO_4$. The solvent was removed in vacuo to give a dark brown film sticking on the wall of the round bottom flask used. Low molecular

weight products were removed by adding a concentrated $CHCl_3$ solution of this compound into 50 mL of methanol. The product then was filtered and dried under vacuum resulting again a film on the round bottom flask. The sample is dried in room temperature for 12 h to give 0.215 g (61%) of pure P3HT.

^{1}H NMR δ: 6.97 (s), 2.79 (br), 2.60 (br), 1.850-1.250 (m), 0.908 (br).
^{13}C NMR δ: 140.13, 133.93, 130.73, 128.84, 31.91, 30.73, 29.68, 29.48, 22.86, 14.32.
UV visible ($CHCl_3$) : λ_{max} 443 nm, Fluorescence ($CHCl_3$) $\lambda_{Emission}$ 573 nm (ex. 453 nm)
GPC analysis: Weight average molecular weight, Mw = 50,400, PDI-1.05.

A2.2.3 Instrumentation

Thermogravimetry experiments were carried out in a TGA instrument of Mettler TOLEDO, model no. TGA/SDTA 851e under nitrogen environment for a range of temperature 25 °C –1050 °C. Nitrogen flow rate was maintained at 40–50 mL min^{-1} according to the specification of the equipment. Experiments were done at 10 K min^{-1} heating rate. Three samples collected at three different temperatures (neat P3HT sample at room temperature, 500 °C and 1050 °C) are used for different methods of characterizations.

SEM images of neat P3HT sample and degraded samples collected at 500 °C and 1050 °C from the TGA analysis were recorded in a LEO 1430 VP Scanning Electron Microscope. TEM imaging and SAED patterns were recorded in a JEOL JEM 2100 Transmission Electron Microscope. Raman spectra of the samples were taken in the solid form using 488 nm Ar^+ ion laser source in backscattering geometry. FTIR spectra were recorded in a Perkin Elmer Spectrum One FTIR spectrometer. Powder XRD patterns were recorded in a Bruker AXS D8 Advance fully automatic Powder X-ray Diffractometer. Digital photographs of P3HT samples were taken using a Nikon Coolpix 8400 digital camera fitted to a Nikon SMZ-645 binocular stereo zoom microscope.

Evolved gases from the thermal degradation of P3HT were analyzed in a Varian 3800 Gas Chromatograph (GC). The separation was performed on a mild-polarity column, VF-200 ms (30 m length, 0.25 mm film thickness, 0.25 mm ID) composed of 100% trifluropropyl methyl siloxane phase.

A2.3 Result and discussion

A2.3.1 TGA analysis

The pretreated P3HT film, dark brown in color (Figure 1a), breaks into smaller pieces on

thermal treatment in TGA instrument (Figure 1b and Figure 1c). The original brown film changes into black in color in 500 °C and 1050 °C collected samples. The 1050 °C collected sample is darker in contrast than the 500 °C collected sample. The TGA and DTA curves are plotted together to identify the weight loss at different temperatures (Figure 2). Three significant weight losses can be distinctly identified. The first observable weight loss is at approximately 195 °C. Till this temperature 21% of the total weight is lost. The second, which is the major weight loss, is observed at around 473 °C accounting 64% loss from the original weight. Total 90% weight is lost from the original weight is observed till the end of the experiment. To ascertain this fragmentation pattern, calculated weight

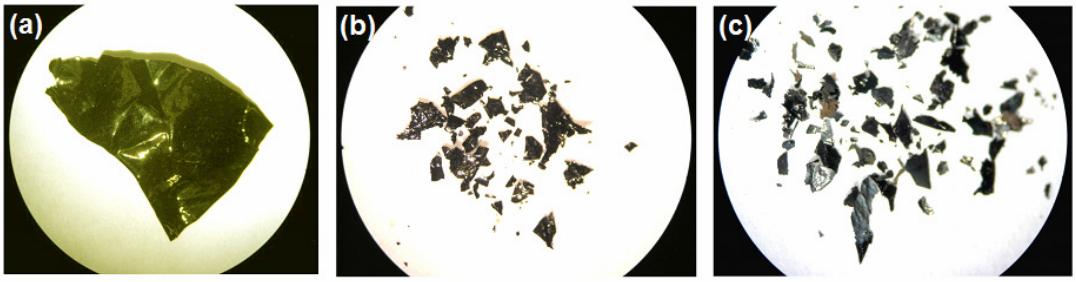

Figure 1 Photograph of (a) Pretreated P3HT at room temperature (b) P3HT collected at 500 °C and (c) P3HT collected at 1050 °C taken by a Nikon Coolpix 8400 digital camera fitted to a Nikon SMZ-645 binocular stereo zoom microscope.

percentages of different possible fragments of 3-hexylthiophene (the monomeric unit of P3HT) are compared with the observed weight losses in our experiment (Table 1). This comparison shows, observed weight loss is always less than the calculated weight loss

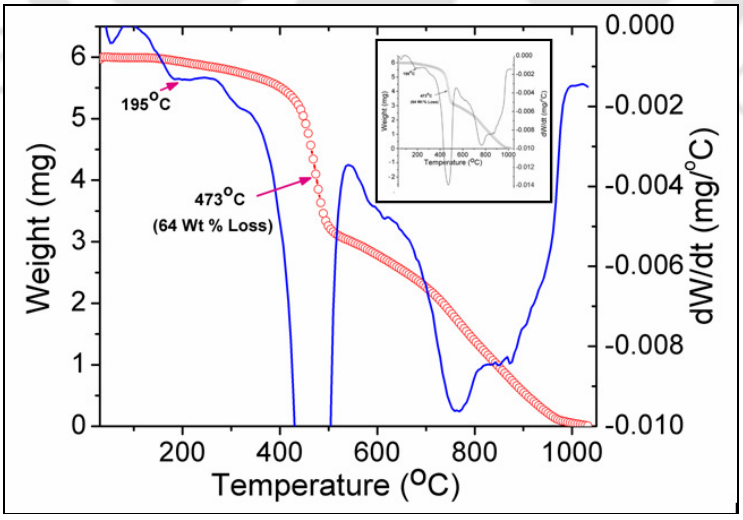

Figure 2 The TGA (red) and DTA (blue) curves (Inset: complete DTA curve) are plotted together to identify the weight loss at different temperatures.

Table 1 Comparison of calculated weight loss with the observed weight losses in TGA experiment.

Fragments	Weight percentage (Calculated) (%)	Observed weight loss in TGA (%)	Temperature range of weight loss in TGA
CS	26.14	21	RT-195 °C
CS+C_6H_{13}	76.64	64	195 °C – 473 °C
CS+ C_6H_{13}+C_2H_2	91.50	90	473 °C – 1050 °C

values. Discrepancy arises as calculated weight loss of monomeric unit is compared with the experimental weight loss of the studied polymer. While the polymer is heated gradually, the heating may not be uniform through out the whole polymer chain.

In this case simultaneous release of the same fragment from all monomeric units of the whole polymer back bone at a certain point of temperature is not a practically possible situation. The first weight loss of 21% at around 195 °C nearly matches with weight loss due to detachment of a CS unit (calculated 26.14%) from the polymer backbone. Studies

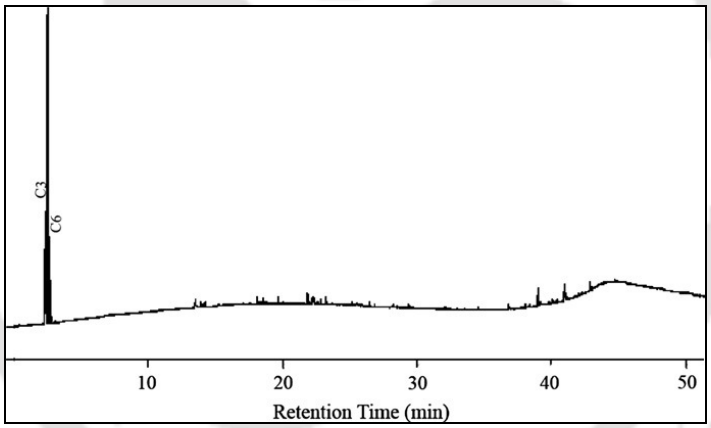

Figure 3 Gas chromatogram observed for gaseous samples collected in the temperature range of 300 °C to 500 °C.

on pyrolysis mass photometry of P3HT also reports CS peak as the base peak which supports the defragmentation of CS unit at the first place at lower temperature [10]. The major weight loss (64% from the original) is predicted as loss of C_6H_{13} fragment, by CS loss. This is further supported by gas chromatograph (Figure 3) obtained for the gaseous samples collected in the temperature range 300 °C to 500 °C. Significant peaks for C_6 fragment along with C_3 fragment is observed in the gas chromatogram. The C_3 fragment may arise due to further fragmentation of the detached C_6 fragments. Moreover, there lies possibility of detachment of only C_3 fragments from some of the monomeric units while maximum of the monomeric units release C_6. This may be the reason for which we observe maximum discrepancy between the calculated and experimentally observed

weight losses in this temperature range. The degradation after 500 °C (total 90 weight % loss up to 1050 °C) may be due to the subsequent loss of C_2H_2 units after detachment of CS and C_6H_{13} from the polymer backbone.

A2.3.2 Electron microscopic analysis

SEM images were recorded for the dark brown smooth films of P3HT and the degraded samples collected at 500 °C and 1050 °C. Pretreated P3HT is very smooth and free of any deformation before decomposition (Figure 4a). P3HT sample collected at 500 °C shows cracking of the polymer film (Figure 4b). Sample collected at 1050 °C (Figure 4c) shows presence of lot of perforations, which indicates the diffusion of volatile species.

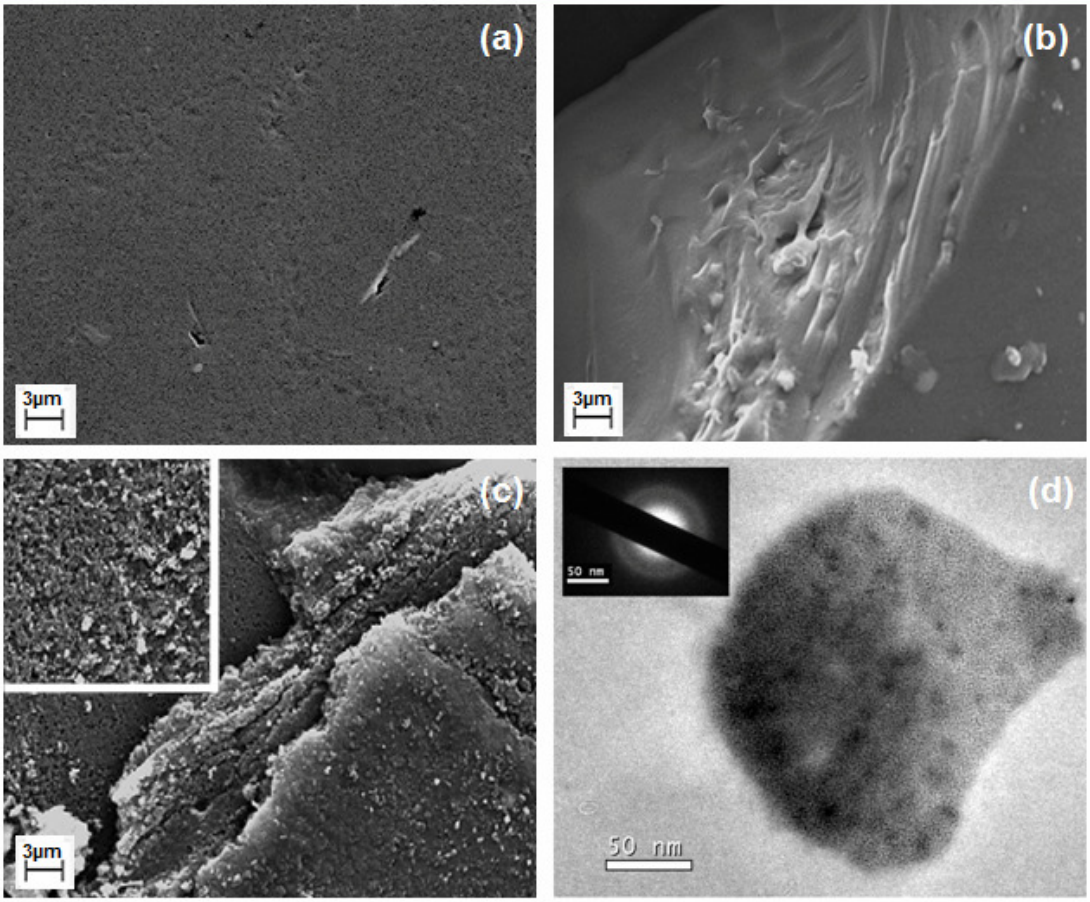

Figure 4 SEM images of (a) pretreated P3HT film (b) sample collected at 500 °C (c) sample collected at 1050 °C (Inset: Enlarged picture of a small portion) from TGA instrument and (d) TEM image of the pretreated P3HT (Inset: SAED pattern of pretreated P3HT)

TEM imaging of the pretreated P3HT film was done which reveals smooth morphology. Amorphous nature of the pretreated P3HT film is confirmed from the SAED pattern (Figure 4d). Sample collected at 1050 °C while analyzed in TEM shows two distinctly

separated phases (Figure 5a and Figure 5b). The bulk residue has many particles, sizes ranging from 3 nm to 27 nm, embedded in it. The SAED pattern collected from these particles shows regular and distinct spots confirming the crystalline nature of this phase (Figure 5c). The d-spacings were measured for the spots arrow marked in the SAED pattern. Measured d-spacings of 7.13 Å and 2.30 Å from this patterns are close to 7.138 Å and 2.18 Å reported for (440) and (111) lattice planes of C_{60} [11]. In some other portions of the TEM image, while seen under higher magnification, some spherical crystalline phases are identified (Figure 5d and Figure 5e). These spherical phases may be some of the individual fullerene molecules. SAED patterns recorded from other portions of degraded P3HT, composing the maximum of the bulk residue, shows circular patterns indicating polycrystalline nature. This may be due to formation of amorphous carbon residue.

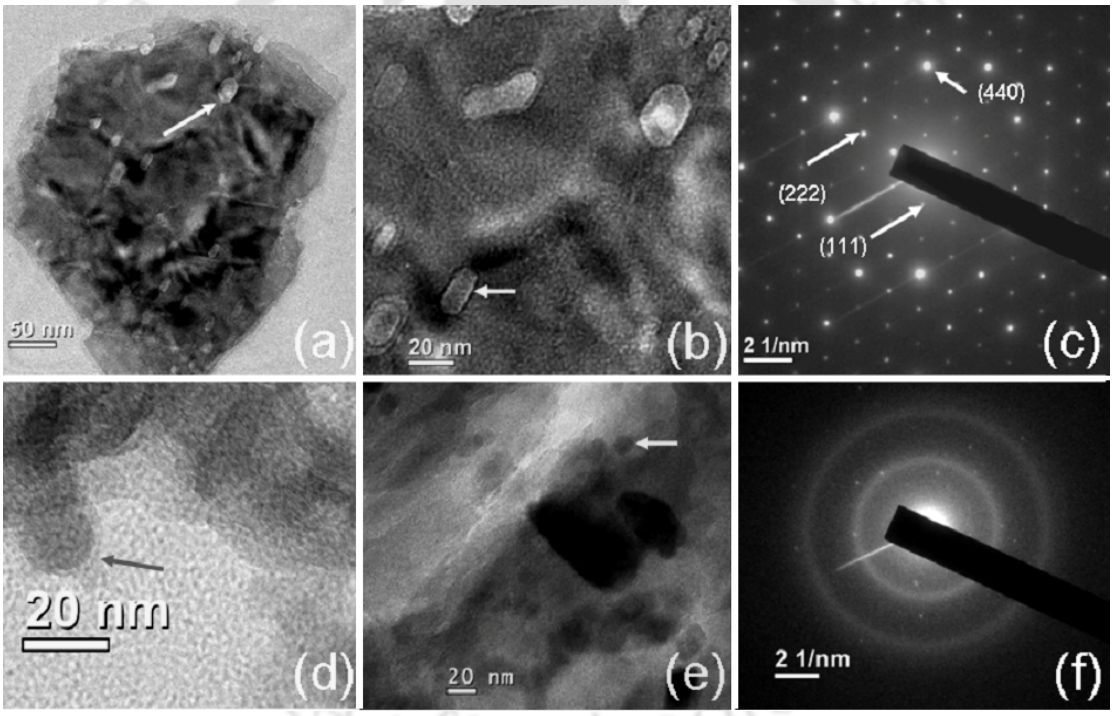

Figure 5 TEM images of P3HT thermally treated at 1050 °C (a) and (b) showing the crystalline phase formed out of film (c) Electron diffraction images of one of these crystallites (d) and (e) showing spherical crystalline higher Fullerenes molecules (f) Electron diffraction image from places other than these crystalline particles.

A2.3.3 Powder XRD spectra

Powder XRD pattern of pretreated P3HT, 500 °C treated P3HT and 1050 °C treated P3HT samples were recorded (Figure 6). Experimentally observed peaks were fitted with Voigt spectral profile for comparative analysis (Table 2). In case of pretreated P3HT we observed a peak at 4.91° along with a broad peak centered at 22.89°. The peak centered at

4.91° corresponds to (100) plane of P3HT having lattice constant 17.99 Å corresponding to lamellar staking of P3HT (interchain distance). The broad peak centered at 22.89° is assigned to interplanar distance between different lamellar stacking with lattice constant 3.88 Å [12-13]. On thermal treatment up to 500 °C, the peak centered at 4.90° almost disappeared. This observation leads to infer that lamellar stacking of P3HT completely breaks of on heating up to 500 °C. This was also evident from the type of surface modification of 500 °C treated P3HT in comparison to the pretreated P3HT as observed

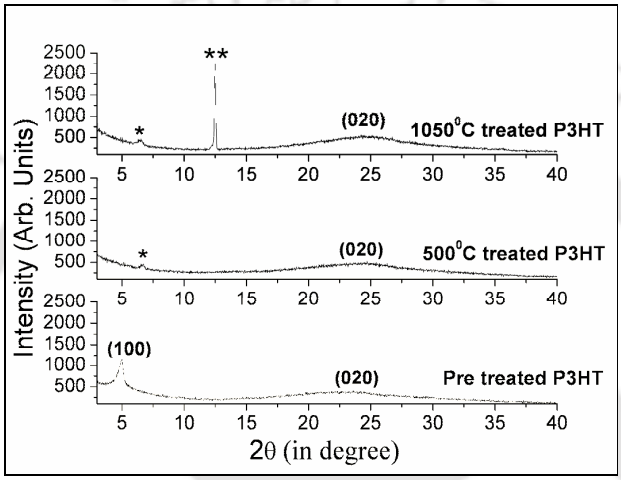

Figure 6 X-ray diffraction of pre treated P3HT, 500 °C treated P3HT and 1050 °C treated P3HT

in SEM images (Figure 4). Cleavage of CS fragments followed by detachment of hexyl side chain of monomeric units at 473 °C contributes to the maximum degradation of P3HT. As discussed earlier, due to inhomogeneous degradation of the polymer, some undegraded thiophene monomeric units may be present till the end of the experiment. The observed small peaks at 6.65° (d-spacing 13.29 Å) and 6.47° (d-spacing 13.66 Å) in 500 °C and 1050°C treated P3HT are close to the interplanar lattice spacing corresponding to repeating unit of thiophene rings (14.8 Å) along the chain of P3HT. This peak has very small spectral intensity compared to (100) peak observed in pre treated P3HT sample referring to small mass fraction responsible for the origin of peak in the thermally treated samples. The shift in 2θ value from 6.65° to 6.47° indicates the loss of regioregularity of the degraded P3HT. Significantly, a very sharp new peak is observed at 12.48° in 1050 °C treated P3HT. This new peak has d-spacing equal to 7.09 Å. Similar peak is found to be reported in literature for amorphous carbon mixed with C_{60} fullerene [45]. This is in good agreement with our observations from TEM micrographs and SAED patterns of the 1050 °C treated P3HT which we could match with the reported d- spacing of 7.14 Å and 2.18 Å for (440) and (111) lattice planes of C_{60}. On thermal treatment, the peak centered at

Table 2 Summary of deconvoluted Powder X-ray diffraction peaks using Voigt spectral function for pretreated and thermally treated samples of P3HT.

Sample	Peak centre (2θ in degree)	Peak amplitude (Arb, Unit)	FWHM Δθ (in degree)	Calculated 'd' Spacing (Å)
Pretreated P3HT	4.91	621.89	0.5107	17.99
	22.89	246.19	12.93	3.88
500 °C treated P3HT	6.65	86.36	0.316	13.29
	24.19	277.49	11.03	3.68
1050 °C treated P3HT	6.47	96.89	0.44	13.66
	12.48	2101.45	0.124	7.09
	24.49	346.8	10.012	3.63

22.89°, in the pretreated P3HT increases to higher 2θ value along with significant increase in intensity and decrease in FWHM. This change is assigned to the formation of amorphous carbon along with crystalline fullerenes on thermal treatment. On increasing the temperature from room temperature (pretreated P3HT) through 500 °C to 1050 °C, 2θ values increases from 22.89° through 24.19° to 24.49° respectively with the reduction of interplanar distance between thiophene chains. This supports gradual formation of amorphous carbon along with formation of fullerenes.

A2.3.4 Raman spectra

Raman spectroscopic analysis of P3HT is reported in literature [14]. Significant peaks at 1502, 1491, 1358 and 832 cm^{-1} are assigned to stretching vibration of thiophene ring. Another peak at around 606 cm^{-1} is assigned to in-plane deformation of the thiophene ring. Stretching vibrational modes of C–H bond are expected to show peaks at 3107, 3084, 3076 and 1081 cm^{-1}. Inplane deformation modes should be observed at 1257, 1085 and 1035 cm^{-1}. The experimentally observed Raman spectra of the pretreated P3HT, 500 °C treated P3HT and 1050 °C treated P3HT (Figure 7) were deconvoluted into Lorentzian components. Different Lorentzian components are tabulated in Table 3 with their respective FWHM and peak intensity values for analysis. Pretreated P3HT (Figure 7 (a)) shows a peak at 1460 cm^{-1} with FWHM value 48.33 cm^{-1}. Other peaks could not be observed due to strong fluorescent background of P3HT polymer. The peak at 1460 cm^{-1}, with increase in temperature, gradually decreases in intensity and frequency shifts towards higher value (Figure 7b and Figure 7c). Raman band assigned to the C=C anti-symmetric stretching vibration shifts up monotonically (6T: 1507 cm^{-1}, 4T: 1519 cm^{-1}, 3T: 1530 cm^{-1}, 2T: 1556 cm^{-1}, where T is thiophene rings conjugated in the chain) with gradual

decrease of intensities [15-16]. In our experiment, stretching C=C asymmetric vibration mode observed at 1460 cm^{-1} shifts through 1540 cm^{-1} to 1635 cm^{-1} as the temperature varies from room temperature (pretreated P3HT) through 500°C (500°C treated P3HT) to 1050 °C (1050°C treated P3HT). Intensity also decreases significantly from 1029 count in pretreated P3HT through 406 counts in 500 °C treated P3HT to 131 counts in 1050 °C

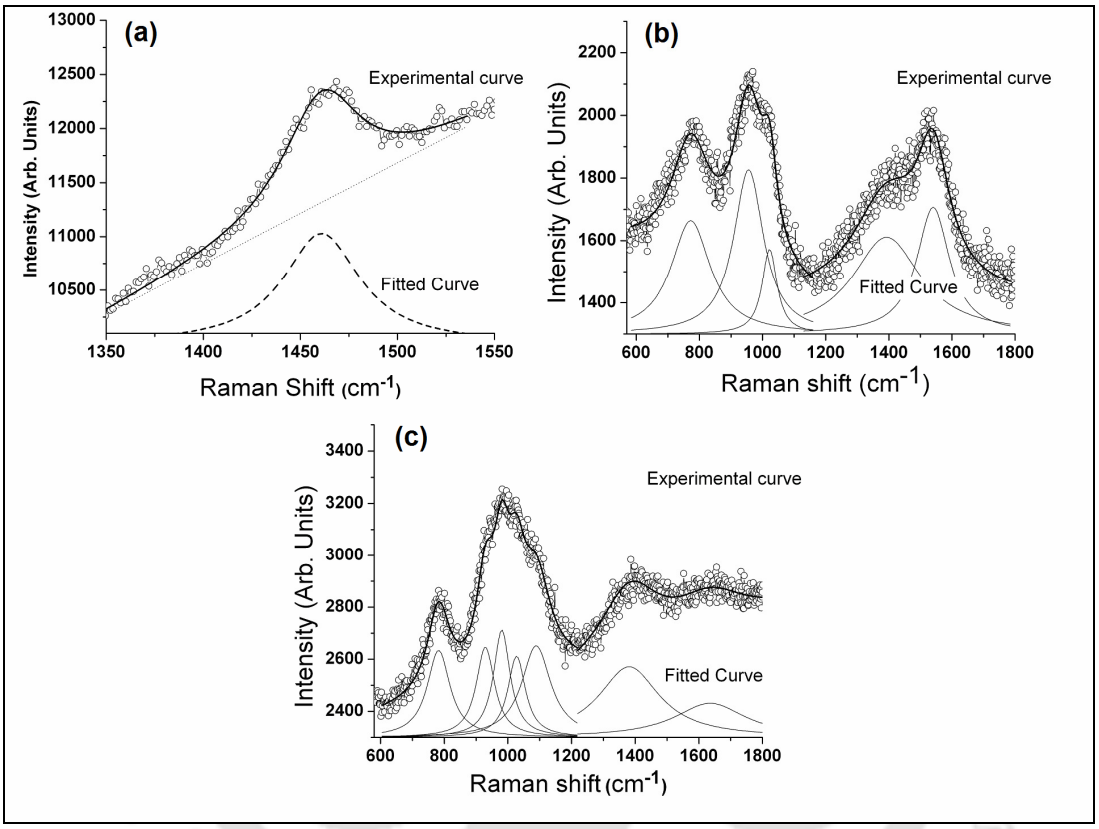

Figure 7 Raman spectra of (a) pretreated P3HT, (b) 500 °C treated P3HT and (c) 1050 °C treated P3HT.

treated P3HT. These observations lead to infer the reduction in the chain length as we gradually increase the temperature. Simultaneously broadening of FWHM of these peaks from 48.33 cm^{-1} in the pretreated P3HT through 126.40 cm^{-1} in 500 °C treated P3HT to 274 cm^{-1} in 1050 °C treated P3HT also in agreement with this inference. A peak at 1392 cm^{-1}, which was not detected in pretreated P3HT, became prominent enough to be observed under the same experimental conditions in the 500 °C treated P3HT. This peak indicates the formation of amorphous carbon. The FWHM of this peak decreases from 263 cm^{-1} in 500 °C treated P3HT to 231 cm^{-1} in 1050 °C treated P3HT. This decrease in FWHM value is indicative of formation of crystalline phase of carbon, namely C_{60} and higher fullerenes, in 1050 °C treated P3HT. This confirms formation of fullerenes at higher temperature after 500 °C. Thus, observations form Raman spectroscopic analysis

regarding formation of fullerenes is in good agreement with results obtained from SEM, TEM, SAED pattern and XRD measurements described earlier. Peak at 1635 cm^{-1}, as observed in 1050 °C treated P3HT (stretching vibration of ring), is of much lower intensity compared to pretreated P3HT indicating almost complete breakage of polymeric structure at this temperature. In case of pretreated P3HT no significant peaks, except the

Table 3 Different Lorentzian components with FWHM with their individual intensities.

Sample	Raman shift ω_0 (cm^{-1})	Intensity (I_0) (Relative counts)	FWHM $\Delta\omega$ (cm^{-1})	Area of the peak
Pretreated P3HT	1460.9	1029.0	48.33	66,509
500 °C treated P3HT	772.2	364.0	151.90	70,956
	955.7	527.0	115.00	82,241
	1022	272.9	57.10	22,395
	1392.8	311.2	263.50	96,447
	1540.3	406.8	126.4	70,350
1050 °C treated P3HT	782	334.2	86.90	40,718
	929.3	347.5	69.80	35,345
	980.9	412.7	63.80	38,508
	1027.4	312.0	66.80	30,115
	1088.9	352.0	111.60	51,423
	1381	271.0	231.00	71,554
	1635.5	131.0	274.00	40,636

one at 1460 cm^{-1}, were observed. After thermal treatment two strong peaks appeared in the region 600–1100 cm^{-1}. Peak centered at around 772 cm^{-1} (500 °C treated P3HT) and 782 cm^{-1} (1050 °C treated P3HT) are assigned to C–S vibration and are of significant intensity in these samples as compared to the pretreated P3HT, where due to high florescent background they were not prominent. Peak centered at around 1022 cm^{-1} in 500 °C treated P3HT and 1027 cm^{-1} in 1050 °C treated P3HT can be assigned to C–H stretching vibration. Peak observed at 955 cm^{-1} in 500 °C treated P3HT and at 929 cm^{-1} and 980 cm^{-1} in 1050 °C treated P3HT are assigned to C–SH deformation mode arising from the degradation residue. The presence of vibrational modes corresponding to C–H,

C–SH and C–S in the thermally treated samples indicates that smaller fragments still remain after degradation, either in the polymer backbone or in the degradation residue, which is indicative of inhomogeneous degradation of the polymer. The fragmented molecules, with C–H, C–SH and C–S bonds, vibrate more freely in comparison while they were in the polymer backbone. This leads to increased intensity of Raman modes of peaks corresponding to C–H, C–SH and C–S bonds in the thermally treated samples.

A2.3.5 FTIR spectra

Gradual decrease in intensities of the FTIR peaks in the finger print region, as literature reports, is a common observation in case of polymer degradation [17]. Experimental observations from FTIR spectra for pretreated P3HT, 500 °C treated P3HT and 1050 °C treated P3HT follows this trend indicating gradual thermal degradation of P3HT with increasing temperature (Figure 8). The peak at 2690 cm^{-1} in the pretreated P3HT, assigned to methyl asymmetric stretching of hexyl side chain, gradually decreases in

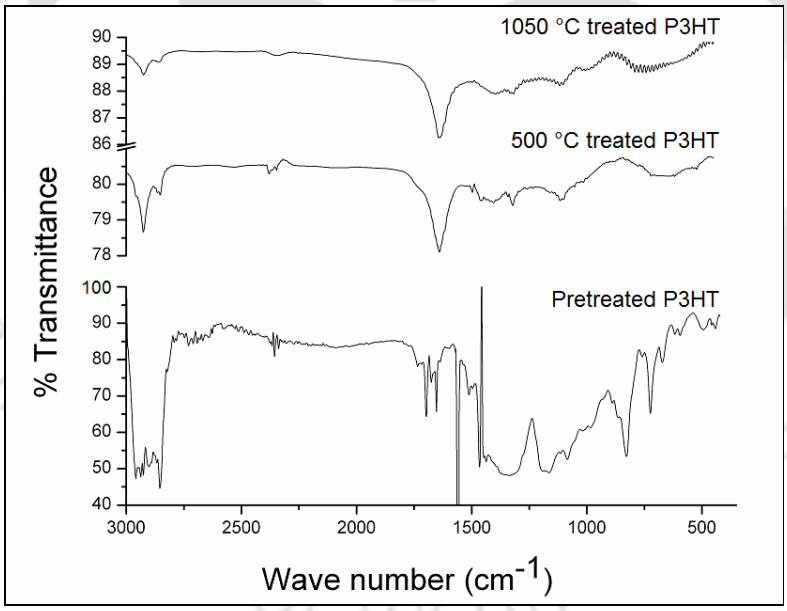

Figure 8 FTIR spectra of Pre treated P3HT, 500 °C treated and 1050 °C treated P3HT.

intensity in the 500 °C treated P3HT and 1050 °C treated P3HT. This implies the detachment of the side chain from the P3HT backbone. Two other peaks centered at 2936 cm^{-1} and 2861 cm^{-1}, corresponding to methylene in phase and out phase vibrations, also decreases in intensity with increase in temperature. Moreover, the wagging and twisting mode of CH_2 group were observed at 1193 cm^{-1} and 1130 cm^{-1} in pretreated P3HT. Absence of these two peaks in 500 °C treated P3HT and 1050 °C treated P3HT is also supportive of detachment of the hexyl side chain at high temperature. P3HT is easily soluble in $CHCl_3$.

The sample collected after 500 °C heat treatment is found to be not well soluble in common organic solvents including $CHCl_3$. Detachment of the hexyl side chain results this decreased solubility of P3HT. The three significant peaks for C2–C3 and C4–C5 anti-symmetric and symmetric stretching modes of thiophene were found at 1560 cm^{-1}, 1511 cm^{-1} and 1464 cm^{-1} in pretreated P3HT. The peak at 1560 cm^{-1} that was very intense in pretreated P3HT, decreases in intensity and becomes negligible at 500 °C. Thus it is supportive of decrease of conjugation with increase in temperature. In pretreated P3HT the peak corresponding to C–C inter ring bond stretching (expected at 1276 cm^{-1}) was found at 1261 cm^{-1}. This shift may be due to steric hindrance of the hexyl side chain [18]. The intensity of this peak decreases becomes negligible above 500 °C implying that thiophene rings get cleaved. The peak at 668 cm^{-1} assigned to C–S stretching in pretreated P3HT disappears after treatment at 500 °C indicating loss of CS units before this temperature.

A2.4 Plausible degradation pathway

Thermal degradation of P3HT, as observed from TGA analysis, starts with release of lighter fragment within 195 °C. The first significant weight loss of ~21% observed experimentally matches nearly to the calculated weight loss for a CS fragment from the polymer backbone. The maximum weight loss observed at 473 °C, indicating a loss of ~64 % from the initial weight, is ascribed to the loss of the C_6H_{13} fragments, and followed by loss of the CS units. Gas chromatographic analysis, Raman, FTIR measurements morphological observations from SEM, powder XRD patterns are all found to supportive

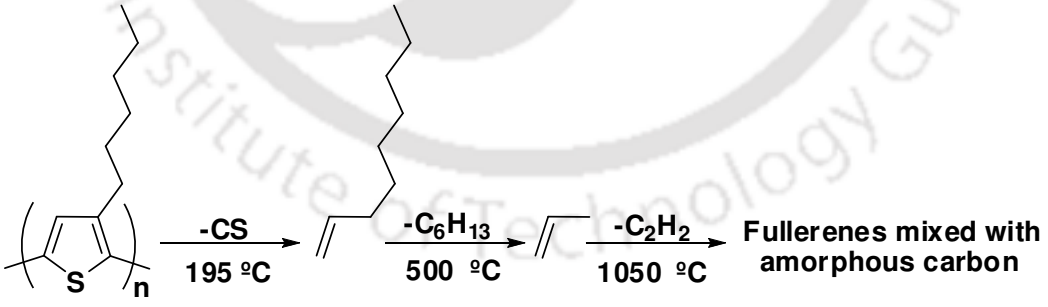

Figure 9 Proposed thermal degradation pathway of P3HT

to this proposed degradation within 500 °C temperature. Decreased solubility of 500 °C treated P3HT is another indication of this detachment. The degradation after 500 °C (total 90% weight loss up to 1050 °C) may be due to the subsequent loss of C_2H_2 units after CS and C_6H_{13} detached from the polymer backbone. The final residue was confirmed to be amorphous carbon and a mixture of fullerenes from the results obtained from TEM,

SAED and powder XRD patterns. Based on these observations, we have proposed a plausible thermal degradation pathway (Figure 9) [19].

A2.5 Concluding Remark

Detailed thermal degradation study of P3HT, an extensively used polymer in optoelectronic devices, is performed (under nitrogen atmosphere) and a thorough understanding on the stability and handling of the polymer are obtained. Results establish that P3HT starts degrading at around 195 °C, with detachment of lighter fragments like CS. Degradation occurring before 500 °C is ascertained to be due to the release of the hexyl side chain. This was confirmed using GC experiment of the gas evolved at particular temperature. Detachment of the hexyl chain makes the polymer insoluble in common organic solvents. Final release of C_2H_2 unit resulted in the formation of both amorphous and crystalline phases of carbon as revealed by SAED analysis. Calculation of d-spacing from TEM data confirms fullerenes mixed with amorphous carbon. To our knowledge this is the first systematic report, where detailed thermal degradation and characterization data for P3HT and its residue are explained. The formation of fullerenes and its detailed characterization also agrees well and supports the proposed degradation mechanism of P3HT.

References

[1] Skotheim, T.; Reynolds, J.; Elsenbamer, R. *Handbook of conducting polymers*, 2nd ed., Marcel Dekker, New York **1998**.

[2] Chiang, C. K.; Fincher, C. R.; Park, Y. W.; Heeger, A. J.; Shirakawa, H.; Louis, E. J.; Gau, S. C.; MacDiarmid, Alan G. *Phys Rev Lett* **1977**, 39(17), 1098.

[3] Reynolds, J.R.; Chien, J. C. W.; Lillya, C. P. *Macromolecules* **1987**, *20*, 1184.

[4] Pyo, M.; Reynolds, J. R. *J Chem Soc Chem Commun* **1993,** 258.

[5] Cirpan, A.; Alkan, S.; Toppare, L.; Hepuzer, Y.; Yagci, Y. *J Polym Sci Part A Polym Chem* **2002**, *40(23)*, 4131.

[6] Yildiz, U. H.; Sahin, E.; Akhmedov, I. M.; Tanyeli, C.; Toppare, L. *J Polym Sci Part A Polym Chem* **2006**, *44(7)*, 2215.

[7] Folch, I.; Borros, S.; Amabilino, D. B.; Veciana, J. *J Mass Spectrom* **2000**, *35*, 550.

[8] Armarego, W. L. F.; Perrin, D. D. *Purification of Laboratory Chemicals*; Butterworth-Heinemann: Burlington, MA, **2002**.

[9] Pomerantz, M.; Liu, L.; Zhang, X. *Arkivoc* **2003**, *12*, 119.

[10] Vatansever, F.; Akbulut, U.; Toppare, L.; Hacaloglu, J. *Polymer* **1996**, *37(7)*, 1103.

[11] JCPDS-00-049-1717, *International Centre for diffraction data*.

[12] Mardalen, J.; Samuelsen, E. J.; Gautum, O. R.; Carlsen, P. H. *Solid State Commun* **1991**, *77(5)*, 337.

[13] Sugiyama, K.; Kojima, T.; Fukuda, H.; Yashiro, H.; Matsuura, T.; Shimoyama, Y. *Thin Solid Films* **2008**, *516 (9)*, 2691.

[14] Dollish, F. R.; Fateley, W. G.; Bentley, F. F *Characteristic Raman frequencies of organic compounds* John Wiley & Sons, **1974**.

[15] Furukawa, Y.; Akimoto, M.; Harada, I. *Synth Met* **1987**, *18(1–3)*,151.

[16] Scott, D. W. *J Mol Spectrosc* **1969**, *31(1–13)* 451.

[17] Gustafsson, G.; Inganas, O.; Nilsson, J. O. *Synth Met* **1989**, *28(c)*, 427.

[18] Somanathan, N.; Wegner, G. *Acta Polymerica* **1999**, *50(4)*, 145.

[19] Reddy, P. K.; Goutam, P. J.; Singh, D. K.; Ghoshal, A. K. Iyer, P. K. *Poly Degrad Stab* **2009**, *94*, 1839.

Chapter A3

PHOTOSTABILITY OF POLY(3-HEXYLTHIOPHENE/ CARBON NANOTUBE COMPOSITE

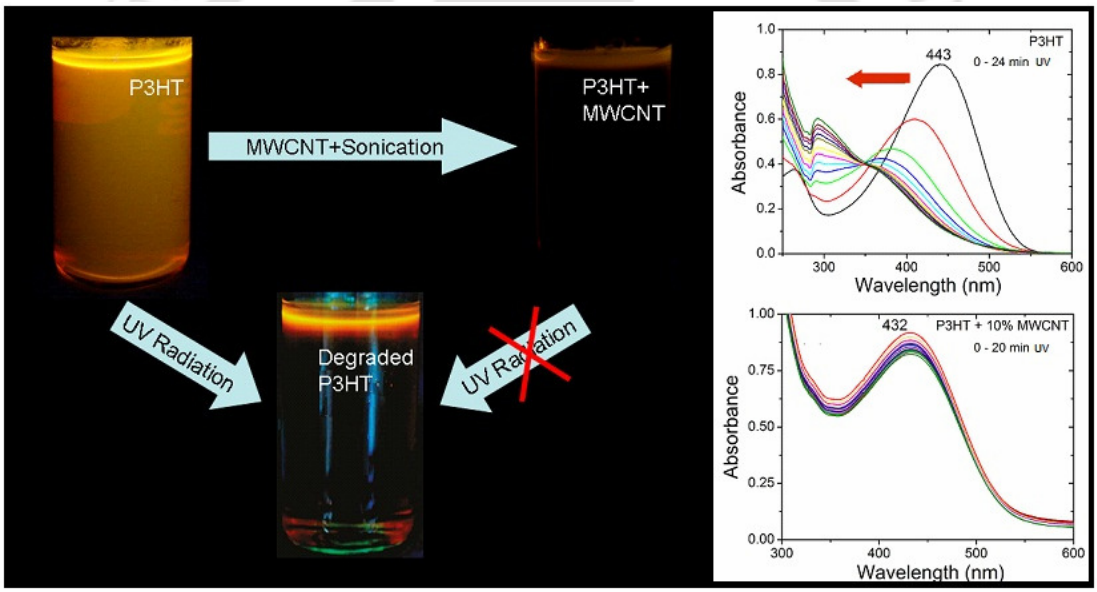

Poly(3-hexylthiophene) (P3HT) degrades in organic solvents containing dissolved molecular oxygen when irradiated with Ultraviolet light. In this chapter, P3HT composite with multiwalled carbon nanotube (MWCNT) is reported to show superior photo stability while similar composite with single walled carbon nanotube (SWCNT) composites does not. UV-visible and fluorescence spectroscopy are used as primary tools for photostability study. Scanning electron microscopy (SEM) and transmission electron microscopy (TEM) reveal coatings of P3HT on the nanotubes. This enhanced photo stability of P3HT-MWCNT composites with its easy processability makes these composites immensely important for optoelectronic applications.

A3.1 Prologue

Despite many promising properties, the stability of poly-3-hexylthiophene (P3HT) in optoelectronic devices has been a challenge due to the degradation it undergoes in presence of light during fabrication and operation. The prime reason for this degradation is the effect of organic / non aqueous solvents while processing and the presence of dissolved molecular oxygen in addition to the exposure or irradiation of UV or visible light [1,2]. This has resulted in device malfunction or inferior quality devices. To overcome this, enormous effort has been devoted to stabilize potentially useful polymers like P3HT. Literature reports various methods to improve the thermal, mechanical, electrical and optical properties of conducting polymers. Introduction of alkyl groups into the main chain, synthesis of soluble precursors, preparation of conducting polymer composites, blending with metal salts/nanoparticles and copolymerization are a few techniques to mention [3,4]. Yet, meager or practically no efforts have been made to prevent the photo degradation of conjugated polymers.

Carbon nanotubes are an important class of organic materials that have fascinating properties, which make them fit for applications in nano-electronics [5]. Boosted by the promising properties of both carbon nanotube (CNT) and conducting polymers, various reports on the polymer/CNTs dispersions based hybrid materials has been published. [6-9] Due to the enhanced conductivity and mechanical properties of P3HT in easily processable nanocomposites of P3HT with multiwalled carbon nanotubes (MWCNT), they are projected as good candidates for possible device fabrication and optoelectronic applications [10].

In the scope of this work, we present a systematic study on enhancement of photo stability of P3HT on preparation of nanocomposites with MWCNT. Irradiation of UV light on this nanocomposite causes no photo degradation to P3HT. We have used UV-Visible absorption spectroscopy, photoluminescence spectroscopy and ESR spectroscopy to understand the photo-degradation behavior of the P3HT and have optimized the percentage of MWCNTs doping required for enhanced photo stability of as synthesized P3HT.

A3.2 Experimental Section

A3.2.1 Chemicals and solvents

Carbon nanotubes (Shenzhen Nanotech, China) were used as received. Solvents, procured from Merck, were used after purification by standard purification techniques [11].

A3.2.2 Instrumentation

Ultrasonications were done in a JAC Ultrasonic 1505 ultrasonicator. UV-Visible spectra were recorded on a Perkin-Elmer Lambda 25 UV-Vis spectrophotometer at room temperature. Photoluminescence studies were done using a Varian photoluminescence spectrophotometer. Scanning electron microscopy images were recorded in a FESEM scanning electron microscope. Samples were prepared on small glass plate wrapped with aluminum foil, on which solution of samples (pristine P3HT and the different composites) were drop casted. Afterwards the samples were dried under vacuum. Before analysis the samples were coated with gold. Tunneling electron microscopic studies were done using a JEOL 2100 tunneling electron microscope. To prepare samples, solutions of pristine P3HT and composite were drop casted on the TEM grid and dried under vacuum before they were analyzed. ESR spectroscopy was done on JEOL JES-FA200 Electron Spin Resonance (ESR) spectrometer.

UV degradation experiments were performed in a Delta Scientific Variable Intensity UV Digester. Degradation chamber which was used contains three Hg discharge lamps (Philips, G6 T5, TUV 6W). We measured the spectral power density at the place where the samples were kept for degradation studies. Emission from Hg vapor lamps primarily consists of three lines 365.4 I-line, 404.7 H-line and 435.8 G-line. The relative intensities of these lines bear a constant ratio at a particular temperature. Optical power meter (ThorLabs Inc) set at 404.7 nm (H-line of Hg vapor) shows radiant power 4.5 mW.

A3.2.3 Synthesis of poly(3-hexylthiophene)

The synthesis and characterization of P3HT is reported in Chapter A2 earlier (Section A2.2.2) [12, 13].

A3.2.4 Preparation of P3HT- MWCNT/SWCNT nanocomposite

A simple sonication technique was adopted for preparation of P3HT-MWCNT/SWCNT nanocomposites. Three different composites with different loading amounts of MWCNT/SWCNTs (5%, 10% and 15% w/w) were prepared. For each preparation, a solution of 0.01 g P3HT in 5 mL dry chloroform, required amount of MWCNT (0.0005 g for 5%, 0.0010 g for 10% and 0.0015 g for 15% composites) were added and the mixture was ultrasonicated for 30 minutes at room temperature. The original P3HT solution, orange red in color under UV light, turns deep brown in the composite solution.

A3.2.5 UV-visible and photoluminescence studies

Stock solutions for UV-visible and photoluminescence studies were prepared maintaining

similar concentration of P3HT, both in pristine P3HT and in composites. Pristine P3HT solution was prepared dissolving 0.01 g of P3HT in 5 mL dry chloroform. Stock solutions of the three different composites were prepared as mentioned above. Necessary equivalent dilutions of both pristine P3HT solution and composite solutions were made using certified micropipettes. All the degradation studies using UV visible and photoluminescence spectrophotometer were done in solution phase taking dry $CHCl_3$ as solvent. The solutions were irradiated in the UV chamber in steps of one minute exposure time and the spectra were recorded after every exposure.

A3.3 Result and discussion

A3.3.1 Electron microscopy

SEM micrograph of pristine P3HT is recorded in lower magnification where the over all morphology is clearly observable. Though the film is full of holes, most of the areas are smooth and of uniform thickness (Figure 1a). Dimension of the pure MWCNT is found to be ~45 nm (Figure 1b). SEM micrographs of composites reveal presence of random networks of interconnected bundles of MWCNT dispersed in the polymer matrix. Micrographs of P3HT+5 % MWCNT composite film (Figure 1c, Figure 1d) showed uniform dispersion of nanotubes within the polymer. In this composite, dimension of the nanotubes increases to ~75 nm. This increase indicates coating of P3HT on the nanotube surfaces. Moreover, the amount of carbon nanotubes is found to be insufficient to interact with all the P3HT present and a major part of P3HT remains exposed as observed. The P3HT+10 % MWCNT composite has well dispersed coated nanotubes (Figure 1e) with dimension ~ 75 nm (Figure 1f) as like P3HT+5 % MWCNT composite. In this case, carbon nanotubes are well coated and neither P3HT nor the MWCNT are found to be excess. This observation indicates that 10% w/w may be the optimum loading amount for coating of the whole amount of nanotubes used. On increasing the quantity of MWCNT to 15% in the composite (P3HT+15 % MWCNT), the amount of polymer becomes insufficient to coat all the nanotubes. Therefore, bundle of nanotubes are coated as a whole by the polymers (Figure 1g) and plenty of uncoated nanotubes (~ 45 nm dimension) are observed lying apart from the composite indicating excess loading of carbon nanotubes (Figure 1h).

Polymer coating on the carbon nanotube surfaces was confirmed by TEM analysis. TEM micrographs of pristine P3HT film (Figure 2a) and P3HT+10 % MWCNT composites (Figure 2b) were recorded along with their respective SAED patterns (insets of Figure 2a and figure 2b). Surface morphology of the pure P3HT film was found to be smooth and SAED pattern shows its amorphous nature. As seen in TEM micrograph of P3HT+10 %

MWCNT composite, a lighter contrast on the tubular dark nanotubes demonstrates the P3HT coatings. SAED pattern from the lighter contrast part is indicative of its amorphous nature and further confirms the coating of P3HT on it.

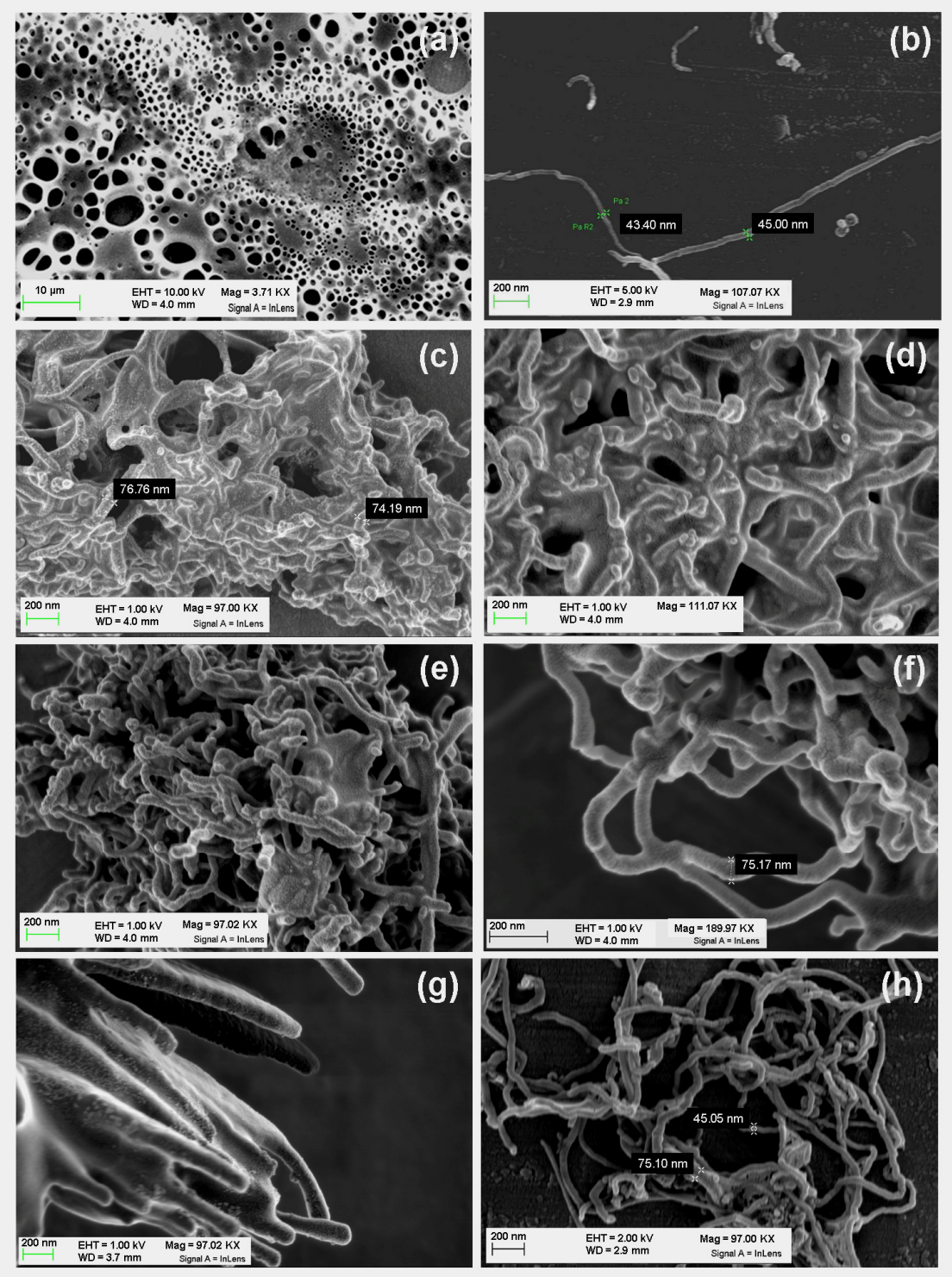

Figure 1 SEM micrographs of (a) as synthesized P3HT (b) pure MWCNT (c), (d) P3HT+5 % MWCNT (e), (f) P3HT+10 % MWCNT and (g), (h) P3HT+15 % MWCNT.

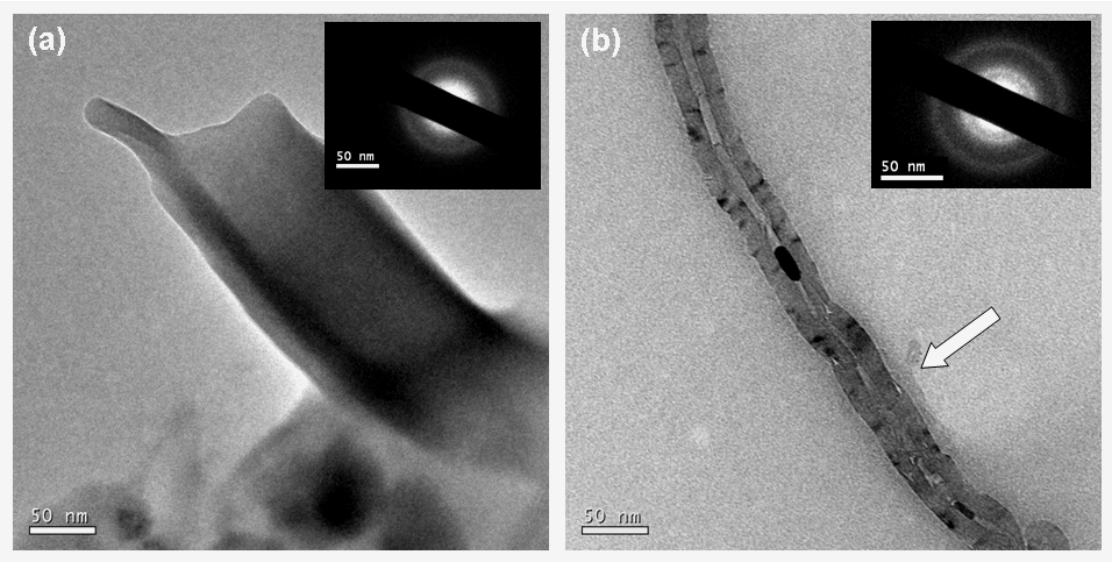

Figure 2 TEM micrographs of (a) as synthesized P3HT (inset: SAED pattern) and (b) P3HT+10 % MWCNT composite (inset: SAED pattern)

Literature survey reveals that dispersion of MWCNT in conjugated polymers has been a well focused problem which affects its processing [14]. Hence, the observed well and uniform dispersion of the carbon nanotubes in our composites is interesting and important from the angle of its applications. It is likely that the interactions between P3HT and MWCNTs *via* π–π and CH-π forces are responsible for uniform dispersion within the solution that stays stable for weeks. Forces of π–π and CH-π interactions probably overcomes the van der waals interaction in between MWCNT which results uniform dispersion of the nanotubes the solution medium [15].

A3.3.2 UV-vis spectroscopy

In conjugated polymers, the extent of conjugation directly affects the observed energy of the π-π* transition which appears as the maximum absorption [16]. The broad absorption spectra of pristine P3HT with absorption maxima at 443 nm is indicative of extensive π-conjugation throughout the polymer backbone (Figure 3a). All the composites showed absorption maxima with minor blue shifts. In case of the P3HT+5 % MWCNT composite, the absorption maxima was observed at 437 nm with a blue shift of 6 nm from the absorption peak of P3HT (Figure 3b). The P3HT+10 % MWCNT composite showed absorption maxima at 432 nm with blue a shift of 11 nm (Figure 3c). P3HT+15 % MWCNT composite also showed absorption maxima at 432 nm (Figure 3d) identical to that with the P3HT+10% MWCNT composite indicating that increasing the loading of carbon nanotubes beyond a certain extent does not alter the absorption behavior of P3HT. Appearance of the absorption maxima at the same position for both P3HT+10 % MWCNT

and P3HT+15 % MWCNT composites implies that 10% w/w is the optimum loading percentage of MWCNT, which is in good agreement with the conclusions from the TEM micrographic analysis. Excess amount of MWCNT, as observed in SEM micrograph for P3HT+15 % MWCNT composite (Figure 1h) remain uncoated by the polymer, and therefore incapable of imparting any further change on the absorption maxima. The minor blue shifts observed for the absorption maxima of the composites are common and are in agreement with earlier reports in literature for composites with P3HT [17-18].

To study the photo degradation behavior, the three carbon nanotube composites with P3HT (P3HT+5 % MWCNT, P3HT+10 % MWCNT and P3HT+15 % MWCNT) were exposed to UV radiation in chloroform solution in steps of one minute exposure time each. Gradual UV irradiation on pristine P3HT solution caused a rapid decrease in absorption intensity

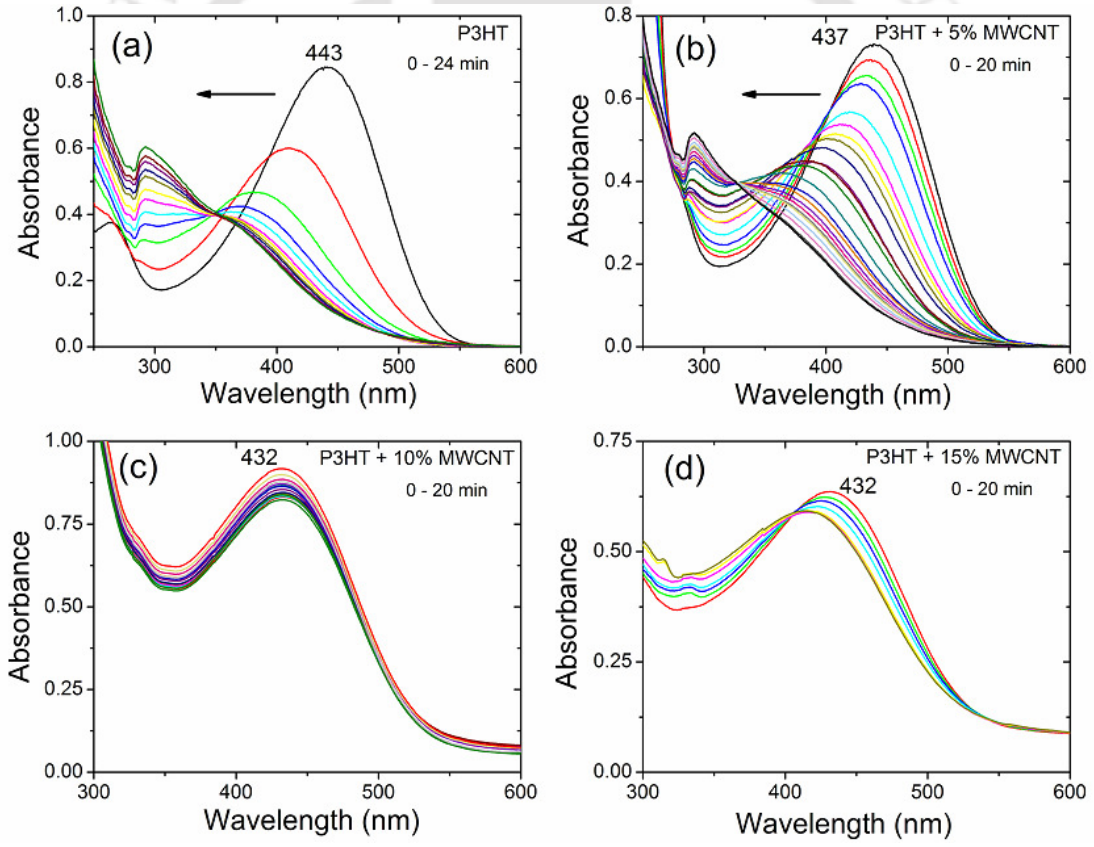

Figure 3 Solution phase UV visible absorptions of (a) Pristine P3HT (0-24 minutes UV exposure) (b) P3HT+5 % MWCNT composite (0-20 minutes UV exposure) (c) P3HT+10 % MWCNT composite (0-20 minutes UV exposure) and (d) P3HT+15 % MWCNT composite (0-20 minutes UV exposure)

with significant blue shifts of the absorption maxima (The plots presented are for 2 minutes irradiation time increment) (Figure 3a). Up to a level of 20 minutes irradiation

time, the entire polymer degraded (absorption spectra recorded till 24 minutes irradiation). This notable change is attributed to the disruption of the π-conjugation and shortening of the conjugated backbone under the influence of UV light. In the case of P3HT+5 % MWCNT composite, the original absorption maxima (437 nm) is blue shifted steadily along with regular reduction in the intensity up to complete degradation of polymer, resulting in disappearance of the peak within 20 minutes of UV-irradiation time (Every plot recorded for one minute irradiation is presented) (Figure 3b). However, presence of 5% MWCNT in the P3HT solution slows down the photo degradation compared to pristine P3HT. Significantly, the P3HT+10 % MWCNT composite does not show any change in absorption maxima (432 nm) even after prolonged irradiation time of 20 minutes (Figure 3c). Again in the case of P3HT+15 % MWCNT composite (absorption maxima at 432 nm), a minor blue shift (7 nm) of absorption maxima with decrease in the absorption intensity was observed (Figure 3d) (Plots are presented for 0, 2, 4, 8, 12, 16 and 20 minutes irradiation only for clarity). Except the minor spectral changes observed initially, the spectra was seen to be static even on irradiation up to the 20th minute. Observations from these UV irradiation results leads to infer that the P3HT+10 % MWCNT composite is best stabilized under UV irradiation. The plausible reason may be that the 10% MWCNT in P3HT is the optimum amount for effective coating of all the nanotubes by the polymer. This is also well established and supported by micrographic analysis using SEM. Loading of lesser amount of carbon nanotubes, like in the case of 5% MWCNT loaded composite, much of the P3HT remains uncoated leaving them exposed to UV irradiation resulting photo degradation. During synthesis and processing of carbon nanotubes, transitional metals such as Fe, Y, Ni, and Co are often used as catalysts. Unavoidably carbon nanotubes are contaminated by these catalyst residues [19]. In case of the P3HT+15 % MWCNT composite, metal impurities may have crossed a threshold helping in minor degradation of composite.

Similar experiments to ascertain photochemical stability of P3HT composites with SWCNT was done. Different weight percentage of SWCNT was loaded in different composites and photo chemical stability was studied exposing to UV radiation in chloroform solution in steps of one minute exposure time each as like we did for P3HT-MWCNT composites and explained above. Here results of UV degradation experiments of three different composites (P3HT+5 % SWCNT, P3HT+10% SWCNT, P3HT+15 % SWCNT) of P3HT with SWCNT are placed (Figure 4a, Figure 4b and Figure 4c). None of the composite showed better stability in comparison to the pristine polymer. In all these composites degradation is fast and within ~5 minute exposure time the λ_{max} in UV visible spectra vanishes almost completely indicating large degradation of the polymer. In these

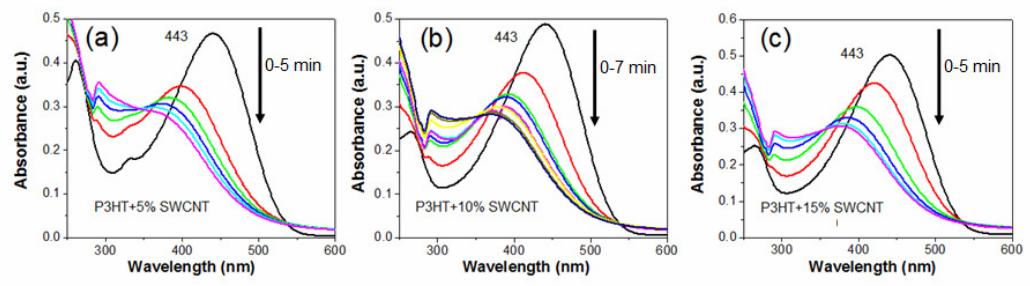

Figure 4 Solution phase UV visible absorptions of (a) P3HT+5 % SWCNT composite (0-5 minutes UV exposure) (b) P3HT+10 % SWCNT composite (0-7 minutes UV exposure) and (c) P3HT+15 % SWCNT composite (0-5 minutes UV exposure)

composites, unlike in case of P3HT composite of MWCNT, no shift of absorption maxima is observed and all composite eventually have the same absorption maxima as like that of the pristine polymer (443 nm). Our observation is supported by literature report where absorption spectra of the P3OT-single-walled carbon nanotubes did not change significantly upon addition of SWCNT indicating insufficient interaction between the two materials [20].

A3.3.3 Photoluminescence spectroscopy

The photoluminescence (PL) spectrum of P3HT sample (Figure 5a) shows an intense emission peak at 575 nm while excited at 443 nm. On exposing the P3HT solution to UV irradiation for one minute, a drastic reduction in the PL intensity is observed. This abrupt reduction of PL intensity indicates that a major part of the polymer backbone has undergone degradation. Further irradiation leads to complete quenching of the PL intensity indicating full degradation of the polymer within 20 minutes of UV exposure time. This degradation behavior observed by PL spectroscopy confirms well the inferences of UV-Visible spectroscopic investigations. Figure 5b, Figure 5c and Figure 5d represent changes in the PL spectra of P3HT+5 % MWCNT, P3HT+10 % MWCNT and P3HT+15 % MWCNT composites. The most significant observation from these spectra is, irrespective of the ratios of MWCNTs used, that intense PL spectrum of the P3HT is quenched heavily upon preparation of composites. The P3HT+5 % MWCNT composite showed emission at 573 nm (437 nm excitation) with diminished intensity (Figure 5b) compared to the pristine P3HT. On exposure to UV irradiation up to 20 minutes, a near total quenching of PL intensity along with a blue shift of ~40 nm is observed. This quenching and modification in the PL intensity may be due to the π-π interaction of the P3HT with carbon nanotubes forming additional decay paths for the excited electrons *via* the MWCNT [10]. The P3HT+10 % MWCNT and P3HT+15 % MWCNT composite also showed similar PL peak at 573 nm (437 nm excitation) (Figure 5c and Figure 5d). Both these

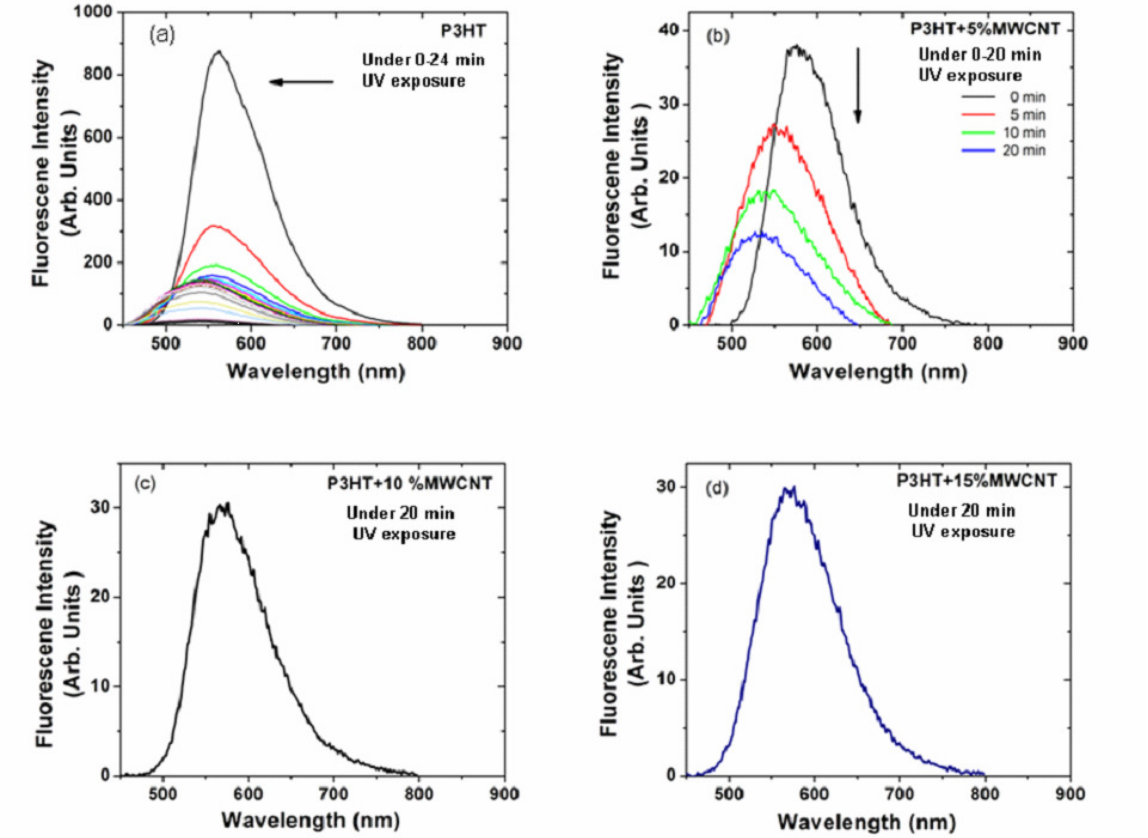

Figure 5 Photoluminescence spectra of P3HT and various composite percentages of MWCNT on UV irradiation (a) Pristine P3HT solution (0-24 minutes) (b) P3HT composite with 5% MWCNT solution (0-20 minutes) (c) P3HT composite with 10% MWCNT solution irradiated with UV light for 20 minutes (d) P3HT composite with 15% MWCNT solution irradiated with UV light for 20 minutes.

samples, with highly quenched PL intensity, showed no further quenching or shift in PL peaks on exposure to UV irradiation for 20 minutes. This indicates higher photo stability of both these composites as compared to pure P3HT and P3HT+5 % MWCNT composite. The clear changes observed in the PL efficiency of P3HT in the presence of MWCNT are perhaps due to acceptance of an electron from the excited state of P3HT by MWCNT. Similar kind of photo induced electron transfer from excited state of a conducting polymer to C_{60} is reported in literature where π-π interactions are dominant [21]. In addition to the π-π interactions, the composites of conjugated polymer with MWCNT are also known to show CH-π interactions [10, 22-23] which may be collectively responsible for the changes in the PL spectra.

A3.3.4 Electron spin resonance spectroscopy

Electron spin resonance (ESR) is a very sensitive probe that provides vital information about the chemical environments associated with unpaired electrons. To follow the

photodegradation of P3HT in solution phase, ESR spectroscopic analyses were done on pure P3HT and UV exposed P3HTs at different time intervals (Figure 6). A significant sharp peak (g = 2.0164) is observed which is close to the free electron g value (g_{th}=2.0023). The deviation of the observed value from the free electron g value is attributed to the coupling of internal molecular magnetic field (arising from unquenched angular momentum) with spin momentum. The deviation of the resonance line position is controlled by the spin orbit coupling parameter λ and the energy difference ΔE, between

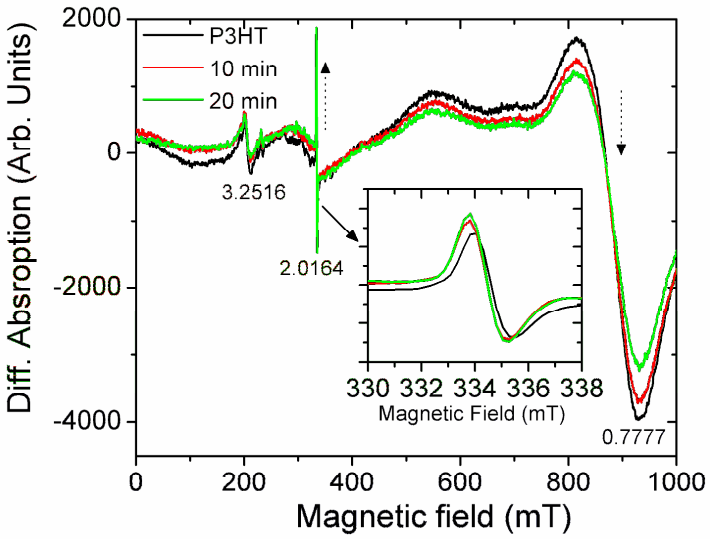

Figure 6 ESR spectra of P3HT exposed till 20 minute irradiation time.

the corresponding electronic levels belongs to the same wave vector (Equation 1) [24].

$$g = g_{th} + \frac{\lambda}{\Delta E} \qquad \text{Equation 1}$$

After UV irradiation, g value shifts from 2.0164 to 2.0172 (inset of Figure 6). Moreover the absorption intensity of this particular peak monotonically increases with increase in UV irradiation time. This sharp peak observed near free electron g value is indicative of delocalization of electrons on the polymer backbone. Another peak with very strong absorption at higher magnetic field (at g = 0.7777) is also observed. After UV irradiation this peak shifts to g value of 0.7787. Intensity of this peak monotonically decreases with increase in UV irradiation time. The line shape of these peaks are asymmetric with asymmetry parameter α= 1.37 for g = 2.0164 peak and and α= 0.42 for g = 0.7777 peak respectively. This asymmetric 'Dysonian line shape' arises due to localization of conduction electrons, and is known as conduction electron spin resonance (CESR). If the length of the sample along the propagation direction of microwaves is larger than the skin depth, then the microwave field would have been damped within the sample. In such

cases the absorption line shape is expressed as a sum of absorption and dispersive components to explain asymmetry observed experimentally [25]. Our studies confirm that the peak at g = 0.7777 arises from P3HT chain, whereas peak at g=2.0164 arises due to the formation of paramagnetic defects. Literature reports such increase in the intensity of ESR peak is observed near free electron *g* value only in the presence of oxygen [26]. Our result supported by literature is also in good agreement with the reported photo oxidative pathway resulting in a P3HT radical [2] that finally leads to the photodegradation of the polymers. Change in the g-value after irradiation indicates modification of internal molecular field due to structural modification along with change in the corresponding energy level, is consistent with changes in the UV visible absorption peak observed experimentally. These conclusions from ESR spectra of P3HT before and after UV exposure are strong evidence of our understanding on the oxygen mediated photo degradation process. Further, attempts to quantitatively measure the relative photo degradation of the three P3HT composites with various percentages of MWCNT using ESR spectroscopic analysis did not give any conclusive result. This may be due to the very low concentration, and percentage of MWCNT in the solution form, showing almost undetectable change of paramagnetic species after UV exposure.

A3.4 Mechanism of enhanced photostability

In an earlier report on photo degradation of P3HT, it was established that both reduced π-conjugation and chain scission are responsible for the degradation process [2]. The reduction of conjugation, manifesting itself as photo bleaching, was reported largely as the product of photosensitization and reaction of singlet oxygen. Hence, in the absence of dissolved oxygen in the solution, no photo chemistry is observed. Chain scissions occur via the classical route of photo oxidation where scission is initiated by unavoidable residual trace of transition metal impurities imparted by the preparative methods of carbon nanotubes. Hence, an optimum of loading amount of MWCNT is important as using higher than this provides lesser stability to P3HT due to higher quantities of metal impurities which further catalyzes the degradation. Based on these observations two plausible mechanisms are proposed by virtue of which enhanced photo stability is achieved in the P3HT+10%MWCNT composite. Firstly, the electron transfer event from the P3HT to the MWCNT, as evident from the high quenching of PL intensity, greatly changes the redox potential of P3HT to oxygen and there by enhances the oxidative stability of P3HT composite with MWCNT compared to the pristine P3HT. Secondly, the π-π interaction between P3HT and carbon nanotubes in composites improves the stability of the π-conjugation system and thereby prevents photosensitization which reduces the

reaction opportunity of singlet oxygen with P3HT. Enhanced photostability, easy processability and excellent film forming property on desired substrates makes them fit for higher efficiency devices [27].

A3.5 Concluding remark

Nanocomposites of P3HT polymer and MWCNT were prepared by ultrasonication technique providing an alternative and easy method of preparing uniform composites from readily available polymeric materials and carbon nanotubes. We have shown that conjugated polymer P3HT degrades rapidly in organic solvents containing dissolved molecular oxygen when irradiated with UV light. The photo degradation of P3HT was characterized by UV visible, PL and ESR spectroscopic techniques. The P3HT+10%MWCNT composite was found to be highly stable for weeks and did not degrade on exposure to UV light [28]. Coating of nanotubes by P3HT polymer was confirmed by SEM and TEM micrographic techniques. Modifications of absorption maxima in the composites compared to the pure polymer along with strong photoluminescence quenching implied π-π interaction between the polymer and the nanotubes. Photo chemical stability of P3HT was confirmed to be significantly enhanced on preparing composite with MWCNT while compared with pure P3HT polymer. The well documented increased electrical conductance with this enhanced photo stability allows these composites for better applications in optoelectronics.

References

[1] Holdcroft, S. *Macromolecules* **1991**, *24*, 4834.

[2] Abdou, M. S. A.; Holdcroft, S. *Macromolecules* **1993**, **26**, 2954.

[3] Skotheim, T.; Reynolds, J.; Elsenbamer, R.; Dekker, M. *Handbook of Conducting Polymers*, 2nd ed.; Marcel Dekker: New York, **1998**.

[4] McCullough, R. D. *Adv. Mater.* **1998**, *10*, 93.

[5] Baughman, R. H.; Zakhidov, A. A.; de Heer, W. A. *Science* **2002**, *297*, 787.

[6] Cochet, M.; Maser, W. K.; Benito, A. M.; Callejas, M. A.; Martinez, M. T.; Benito, J. M.; Schreiber; Chauvet, J. O. *Chem. Commun.* **2001**, 1450.

[7] Dresselhaus, M. S.; Ecklund, G. *Science of Fullerenes and Carbon Nanotubes*: Academic Press: San Diego, CA, **1996**.

[8] Ijima, S. *Nature* **1991**, *354*, 56.

[9] Tamburri, E.; Orlanducci, S.; Terranova, M. L.; Valentini, F.; Palleschi, G.; Curulli, A.; Brunetti, F.; Passeri, D.; Alippi, A.; Rossi, M. Carbon **2005**, *43*, 1213.

[10] Kulia, B. K.; Batabyal, S. K.; Nandi, A. K. *Macromolecules* **2007**, *40*, 278.

[11] Armarego, W. L. F.; Perrin, D. D. *Purification of Laboratory Chemicals; Butterworth-Heinemann*: Burlington, MA, **2002**.

[12] Reddy, P. K.; Goutam, P. J.; Singh, D. K.; Ghoshal, A. K.; Iyer, P. K. *Polym. Degrad. Stab.* **2009**, *94*, 1839.

[13] Pomerantz, M.; Liu, L. M.; Zhang, X. S. *ARKIVOC* **2003**, *xii*, 119.

[14] Bahr, J. L.; Mickelson, E. T.; Bonikowsk, M. J.; Smalley, R. E.; Tour, J. M. *Chem. Commun.* **2001**, *2*, 193.

[15] Geng, J.; Kong, B. S.; Yang, S. B.; Youn, S. C.; Park, S.; Joo, T.; Jung, H. T. *Adv. Funct. Mater.* **2008**, *18*, 2659.

[16] Baskaran, D.; Mays, J. W.; Bratcher, M. S. *Chem. Mater.* **2005**, *17*, 3389.

[17] Kuila, B. K.; Nandi, A. K. *Macromolecules* **2004**, *37*, 8577.

[18] Kuila, B. K.; Nandi, A. K. *J. Phys. Chem. B* **2006**, *110*, 1621.

[19] Ge, C.; Lao,F.; Li, W.; Li, Y.; Chen, C.; Qiu, Y.; Mao, X.; Li, B.; Chai, Z.; Zhao, Y. *Anal. Chem.* **2008**, *80*, 9426.

[20] Kymakis, E.; Amaratunga, G. A. J. *Synth. Met.* **2004**, *142*, 161.

[21] Sariciftci, N. S.; Smilowitz, L.; Heeger, A. J.; Wudl, F. *Science* **1992**, *258*, 1474.

[22] Nishio, M.; Hirota, M.; Umezawa, Y. *CH/pi interaction, evidence, nature and consequences*; Wiley-VCH: New York, **1998**.

[23] Ou, Y. Y.; Huang, M. H. *J. Phys. Chem. B* **2006**, *110*, 2031.

[24] Poole, C.; Farah, H. A. *Handbook of electron spin resonance,* Vol. 2*:* Springer Verlag: New York, **1999**.

[25] Feher, G.; Kip, A. *Phy. Rev.* **1955**, *98*, 337.

[26] Andrews, J.; Keefer, R. M. *Molecular Complexes in Organic Chemistry*: Holden-Day Inc.: San Francisco, CA, **1964**.

[27] Pradhan, B.; Batabyal, S. K.; Pal, A. J. *J. Phys. Chem. B* **2006**, *110*, 8274.

[28] Goutam, P. J.; Singh, D. K.; Giri, P. K.; Iyer, P. K. *J. Phys. Chem. B* **2011**, *115*, 919.

Chapter A4

NATURE OF PHOTOLUMINESCENCE QUENCHING OF POLY(3-HEXYLTHIOPHENE) BY CARBON NANOTUBES

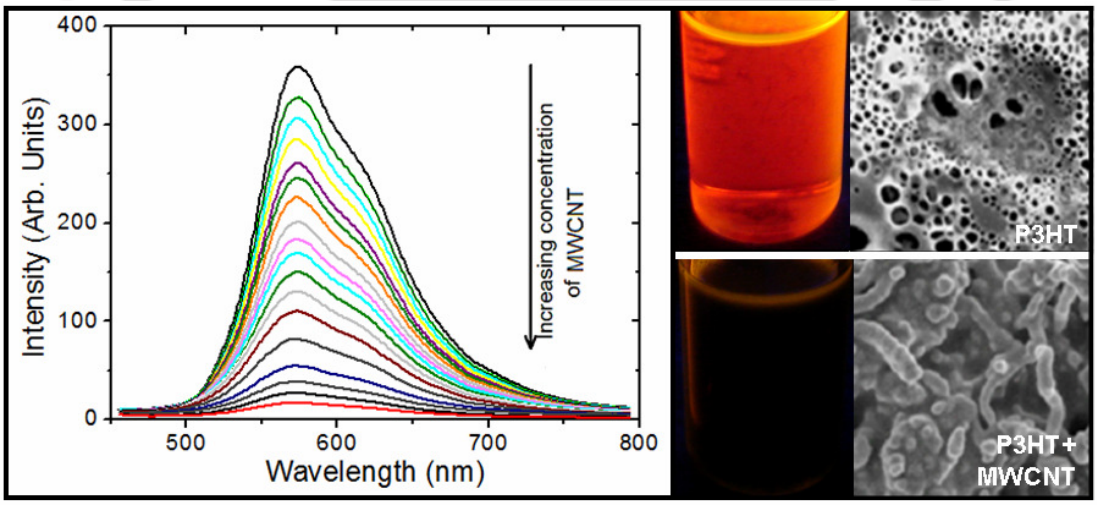

High photoluminescence quenching of poly(3-hexylthiophene) is observed in case of its composites with multiwalled carbon nanotubes and single walled carbon nanotubes even if very minor quantities of carbon nanotube is blended. With the experimental findings of UV-visible spectroscopy, photoluminescence spectroscopy and time resolved photoluminescence spectroscopy the nature of this photoluminescence quenching has been confirmed as static quenching.

A4.1 Prologue

Photoluminiscence (PL) quenching has been a subject of great interest due to its potential use in many material science and biomedical applications. Specific DNA/RNA detection [1] and gas sensing [2] are some recent examples to mention where the detection techniques are based on photoluminescence quenching of some florescent materials. Variety of molecular interactions like molecular rearrangements, excited-state reactions, energy transfer, ground-state complex formation and collisional quenching are responsible for PL quenching [3]. Highly fluorescent poly(3-alkylthiophenes) (P3ATs) are conjugated polymers with good solubility, processability, and environmental stability. Regioregular poly(3-hexylthiophene) (P3HT) is used as electron donor in bulk heterojunction solar cells with record power conversion efficiencies up to 5% [4-6]. The most efficient organic photovoltaic solar cells to date utilize a bulk heterojunction of conjugated polymer (electron donor) and fullerene derivative (electron acceptor) with solar power conversion efficiencies of nearly 8%. Electron mobility in these materials, however, depends strongly on fullerene clustering and hopping transport [7-9]. Carbon nanotubes (CNTs) tout several unique properties that nominate them as intuitive and possibly superior candidates to replace the electron accepting and transport fullerene phase in bulk-heterojunction organic photovoltaic systems. Recent studies on blends of conjugated polymers and single walled carbon nanotubes (SWCNTs) suggest that efficient exciton quenching occurs at these interfaces [10]. Although there is still some uncertainty regarding precise values, estimates of the ionization potential and electron affinity for P3HT and various SWCNTs suggest that a type II band offset should be formed at the interface between the two materials. Indeed, several spectroscopic studies on polymer - SWCNT systems have concluded that photoinduced interfacial charge separation occurs in these systems. However, it should be noted that quenching of the polymer photoluminescence or a faster PL decay is often cited as an indication of photoinduced electron transfer [11]. A fast transfer of photoinduced charges from donor to acceptor is very essential for an efficient photovoltaic device. If the electron is not transferred within a few femto seconds, the photo generated exciton will decay to ground state emitting PL resulting in an inefficient photovoltaic device. Hence, composites which show high photoluminescence quenching are in focus for applications in solar cell construction. Thus, preparation of composite materials, using conducting polymers as donor and carbon nano materials as acceptor is a recent well focused area of research.

Composites of P3HT with multiwalled carbon nanotube (MWCNT) [12] and SWCNT [13] are well characterized in literature. In these composites high photoluminescence

quenching of P3HT occurs even if a small amount of carbon nanomaterial is blended. In our work on enhancement of photostability of P3HT in Chapter A3, we also observed very high quenching of photoluminescence on addition of very low amount of MWCNT to P3HT. However, despite this observation of significant quenching behavior, the nature of this photoluminescence quenching (static or dynamic) has not yet been reported. In this chapter, we have studied the photoluminescence quenching of P3HT in the presence of MWCNT and SWCNT to ascertain its nature of photoluminescence quenching.

A4.2 Experimental Section

A4.2.1 Chemicals and Solvents

MWCNT and SWCNT (Shenzhen Nanotech, China) were used as received. All solvents were used after purifications by standard purification techniques [14].

A4.2.2 Instrumentation

Scanning electron microscopic images were recorded in a Carl Zeiss SIGMA field emission scanning electron microscope. Samples were prepared on small glass plates wrapped with aluminum foil and solution of samples (pristine P3HT and the different composites) were drop casted. Afterwards the samples were dried under vacuum. Before analysis, the samples were coated with gold. Ultrasonications were done in a JAC Ultrasonic 1505 ultrasonicator. UV-Visible spectra were recorded on a Perkin-Elmer Lambda 25 UV-Vis spectrophotometer at room temperature. Photoluminescence studies were done using a Varian photoluminescence spectrophotometer. Time resolved photoluminescence spectra were recorded in a Lifespect spectrometer (Edinburgh Instruments).

A4.2.3 Preparation of composite

MWCNT-P3HT and SWCNT–P3HT composite stock solutions were prepared by ultrasonication technique. Concentrations of the composites were maintained in micro molar to reduce the possibility of quenching effect arising due to molecular aggregation. In each case 1.0×10^{-4} g of nanotube was added to 25 mL micromolar solution of P3HT (1.2×10^{-6} M) in chloroform. Then the solution was sonicated for 30 mins. The original red orange colour of P3HT solution turns dark brown in the composites (P3HT- MWCNT composite is shown in Figure 1). To follow the gradual change in photoluminescence of P3HT upon addition of nanotubes, photo luminescence of 3 mL of 1.2×10^{-6} M polymer solution is recorded first. Gradually, nanotubes were added by adding the composite solutions in steps of 40 μL per addition. Every time, to maintain same concentration

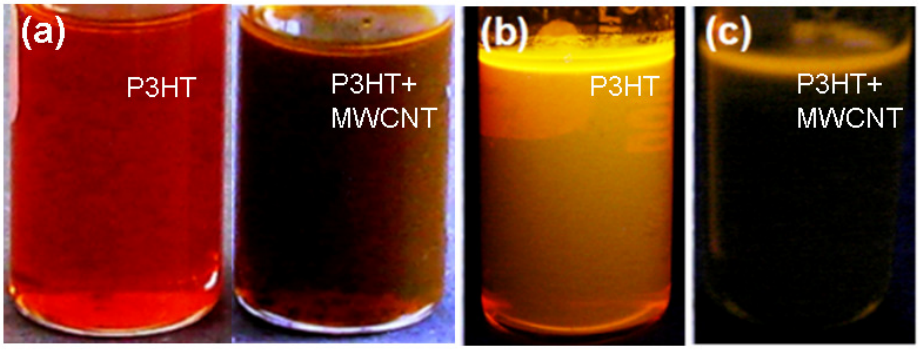

Figure 1 Photograph of chloroform solution of (a) P3HT and P3HT-MWCNT composite under white light (b) P3HT under UV light and (c) P3HT-MWCNT composite under UV light.

of the P3HT, 40 µL of P3HT solution is thrown and 40 µL of composite solution was added and spectra were recorded till we get maximum quenching.

A4.3 Result and discussion

A4.3.1 Morphological characterization of P3HT nanotube composites

SEM micrographic analyses were done to characterize the composites. SEM micrograph of pristine P3HT (Figure 2a) is recorded in lower magnification (3.71 kX) where the over all morphology is clearly observable. Due to fast evaporation of casting solvent, holes are formed. Uniform thickness is observed in high magnification (inset, Figure 2a) .

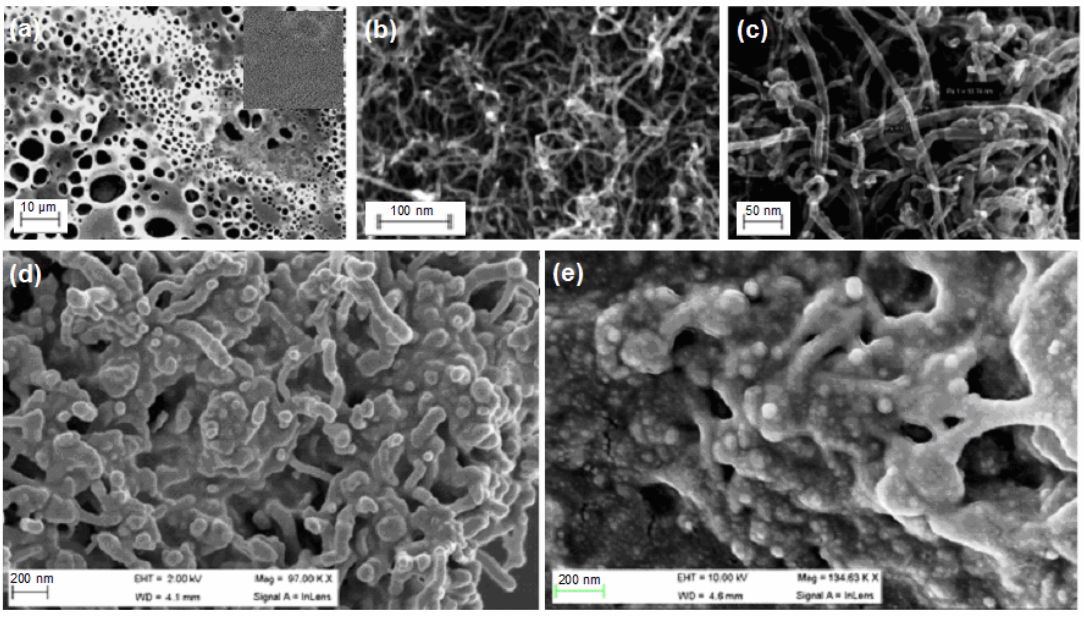

Figure 2 FESEM micrographs of (a) pristine P3HT, (b) Pure MWCNT (c) Pure SWCNT (d) P3HT-MWCNT composite (e) P3HT-SWCNT composite

Micrographs of pristine MWCNT (Figure 2b) and pristine SWCNT (Figure 2c) were also recorded. Diameter of MWCNT is ~45 nm and that of SWCNT used is ~14 nm. High magnification FESEM images of P3HT-MWCNT (97 kX) (Figure 2d) and P3HT-SWCNT (134 kX) (Figure 2e) were recorded from the samples, where we got the maximum quenching at the end of photoluminescence spectroscopic measurement experiment. In the P3HT-MWCNT composites (Figure 2d) the nanotubes are mostly observable very clearly. The MWCNTS in the composites are increased by size (~74 nm) indicating covering of the nanotube surfaces by P3HT coating. Similar observation was found in P3HT-MWCNT composites prepared in Chapter A3 [15]. However, in P3HT-SWCNT composites, the distinct shapes of nanotubes were not clearly seen (Figure 2e).

A4.3.2 UV-visible and photoluminescence spectroscopy

The changes in the absorption spectra of P3HT with increasing concentration of MWCNTs were recorded (Figure 3a) carefully. These experimental absorption curves were deconvoluted using Gaussian lineshapes to exactly determine the peak position, line width and intensity. Figure 3b shows deconvoluted spectra of pristine P3HT solution (i.e. before addition of MWCNTs). Two distinct peaks, with absorption maxima 373.85 nm (assigned as Peak-1) and 443.56 nm (assigned as Peak-2) respectively could be deconvoluted. Variation in the absorption maxima with increasing MWCNTs concentration in the P3HT solution is shown in Figure 3c. Absorption peak position is found to be monotonically blue shifted with increasing concentration of MWCNTs. This indicates the increase in the band-gap with addition of MWCNTs. More interestingly a systematic shift in the absorption peak position indicates interaction between P3HT and MWCNTs. Figure 3d shows change in the absorbance of P3HT with increasing concentration of MWCNTs. Absorbance intensity of Peak-1 does not show appreciable change, while that of Peak-2 gets monotonically decreased.

PL intensity of P3HT is found to monotonically decrease with addition of MWCNTs (Figure 4a). To estimate the quenching efficiency of MWCNTs for P3HT and investigate the mechanism of photoluminescence quenching, these PL spectra were deconvoluted using Gaussian line profile, typically shown for P3HT alone in Figure 4b. PL spectra of P3HT is found to consist of three peaks at wavelengths 569.0 (Peak-1), 616.5 (Peak-2) and 622.9 nm (Peak-3) on the deconvoluted spectra (Figure 4b). Figure 4c shows the Stern-Volmer plot corresponding to these three components. Figure 4d shows the Stern-Volmer plot corresponding to the total intensity observed experimentally at integrated peak position. The Stern-Volmer plot follows linear behavior except at the very high concentration where it shows exponential nature. The inset of the Figure 4d shows the

linear fit for lower concentration ranges given by $F_0 / F = 1 + \alpha_1 x$, where α_1 equals to 0.0005974 ± 0.000368. The combined region could be fitted with $F_0 / F = 1 + \alpha_2 x + \beta_2 \exp(\gamma_2 x)$. Where, $\alpha_2 = 0.0005974$, $\beta_2 = 0.02896$ and γ_2 is 0.0005974. Separate fit for lower concentration region with only linear curve shows

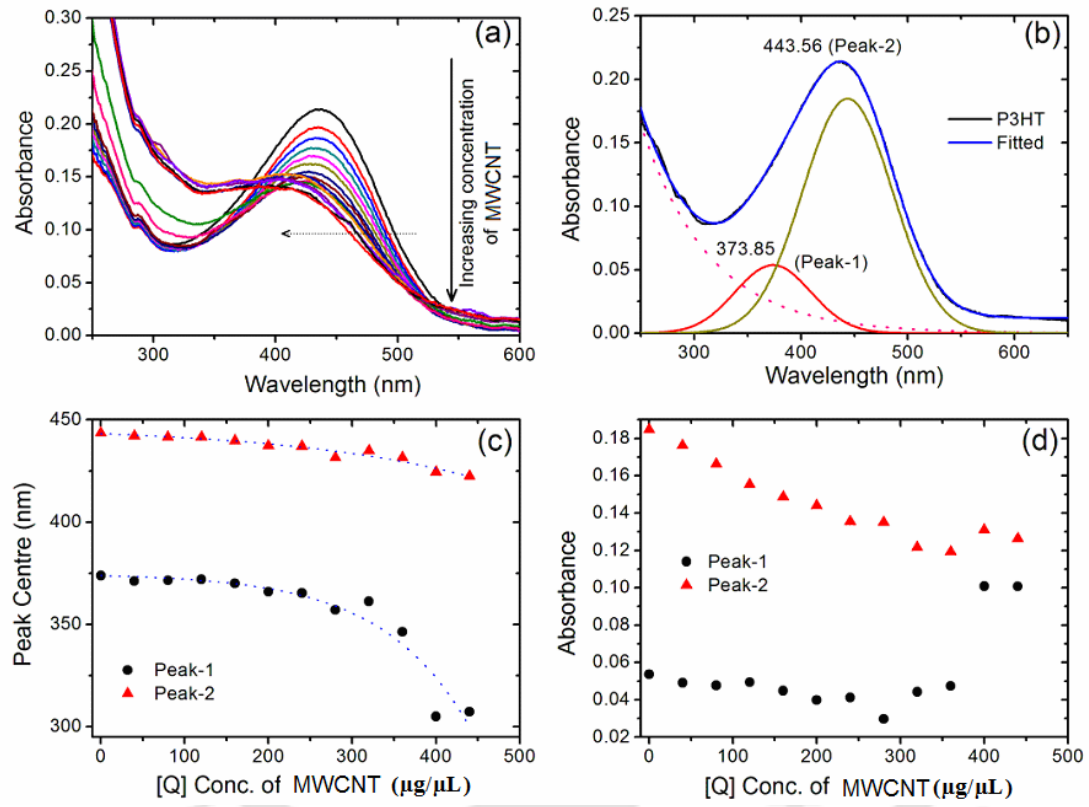

Figure 3 UV visible spectra of (a) P3HT upon addition of MWCNT (b) deconvoluted peaks (c) change in peak center and (d) changes in absorption.

better fit as shown in the inset of Figure 4d. Positive deviations from the Stern-Volmer equations have been observed when the extent of quenching is large. Such a situation is usually interpreted in terms of a "sphere of action" within which the probability of quenching is unity. The "modified form of the Stern-Volmer equation" [3] expressed by $F_0 / F = (1 + K_D[Q]) \exp([Q]VN/1000)$ does not give a good fit in this case. Where V is the volume of the sphere. This equation modifies to purely exponential growth when contribution of dynamic quenching is negligible, i.e., $K_D \approx 0$.

The linear nature of Stern-Volmer plot indicates that either of the two possible mechanisms of PL quenching, static or dynamic quenching, is involved in this process. Shift in the UV-Vis absorption maxima indicates a strong probability of static quenching

i.e. through the formation of non-fluorescent complex. When such a complex absorbs light, it returns to the ground state without the emission of a photon. This is further confirmed through time resolved photoluminescence spectroscopy (TRPL).

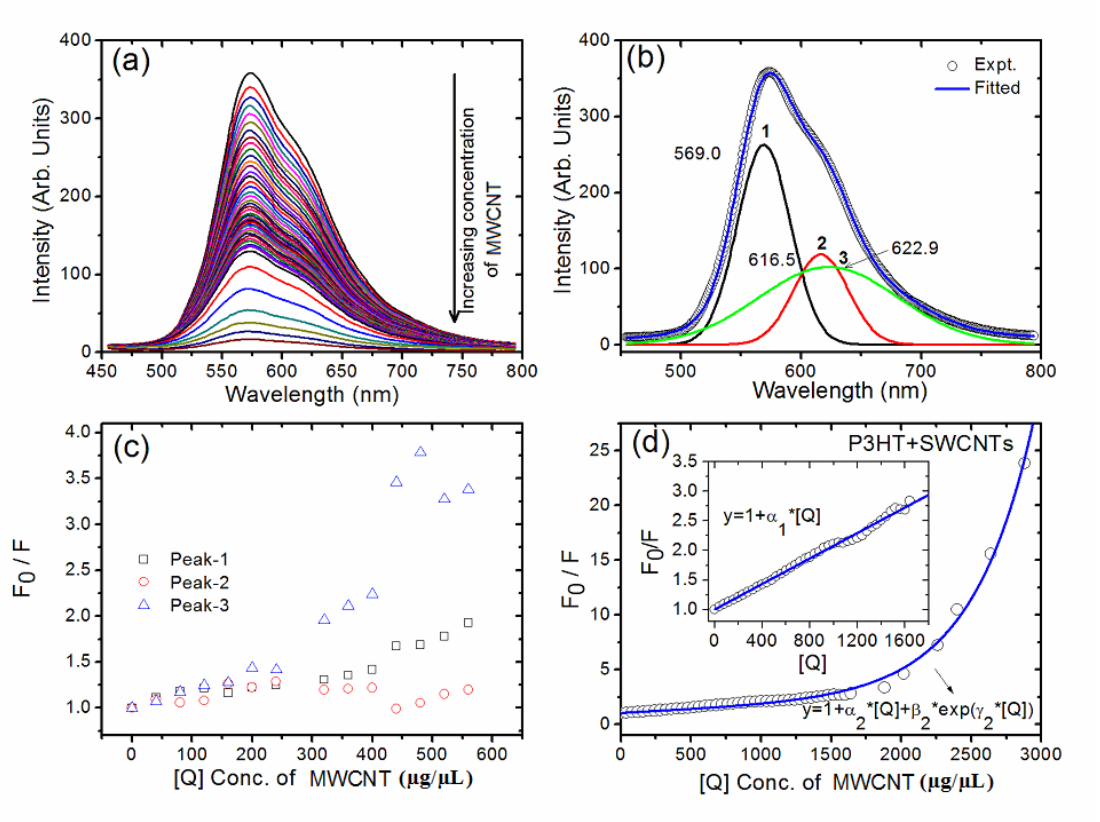

Figure 4 Photoluminescence quenching of P3HT upon addition of MWCNT (a), deconvoluted peaks (b), Fo/ F for the three peaks at different concentrations and SV plot (d)

Figure 5 shows the TRPL spectra of P3HT when excited with 475 nm diode laser and emission is monitored at 569 nm. With continuous addition of MWCNTs, the TRPL spectra have been recorded for various concentrations of MWCNTs (not plotted here for clarity). Visibly all the spectra lie over one another. These spectra were deconvoluted using exponential decay profile to estimate the PL life time, typically shown for P3HT alone in Figure 5a indicating presence of two decay channels with 140.14 ± 2.96 ns (τ_1) and 555.97 ± 1.86 ns (τ_2) responsible for 25.12 and 74.88 % of the decay process respectively. Figure 5b and Figure 5c shows the variation in (τ_0/τ) for the decay channels τ_1 and τ_2 respectively with increasing concentration of MWCNTs. This figure clearly shows that ratio of PL decay time before and after addition of MWCNTs remains constant nearly at 1. This eradicates any possibility of existence of dynamic quenching contribution, since such process would lead to decrease in the PL excited state lifetime. These TRPL results are in agreement with linear SV plot and peak position shift observed in the absorption

spectra indicating “Static quenching” to be only responsible for the process.

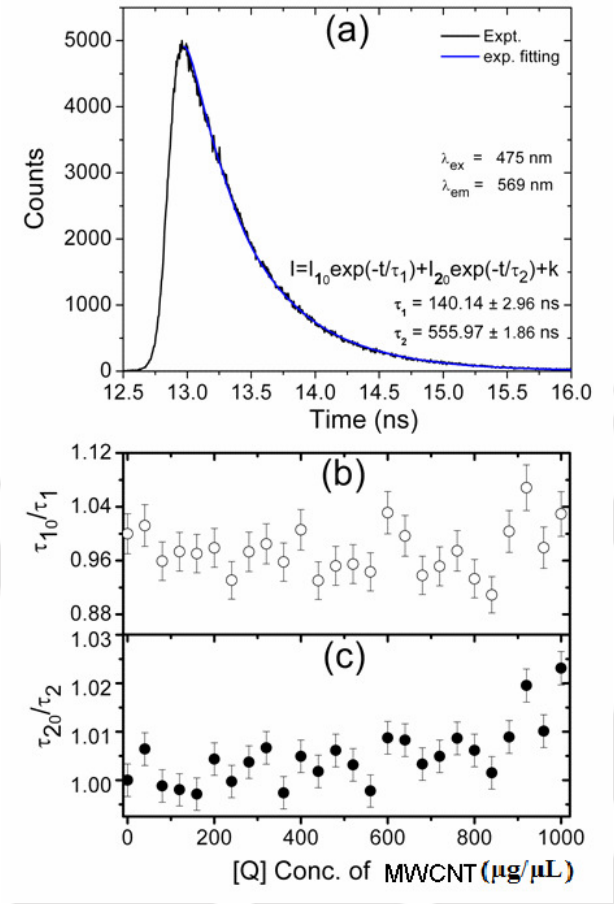

Figure 5 Life time results for P3HT -MWCNT nanocomposites.

Further, experiments have been carried out with SWCNTs to estimate the relative quenching efficiency of MWCNTs and SWCNTs. Figure 6a shows the change in the UV visible absorption spectra with increasing concentration of SWCNTs. Unlike MWCNTs, visibly little change in the absorption spectra appears with addition of SWCNTs. Similar to the MWCNTs, these spectra were deconvoluted using a combination of two Gaussian peaks. The variation in the peak position and intensity of these two components are shown in Figure 7b-e. Similar to MWCNTs, with addition of SWCNTs to P3HT the absorption maxima monotonically shifts to the lower wavelengths. But in case of SWCNTs, change is relatively weak and follows a linear trend for the similar concentration. In case of SWCNTs, the absorbance do not show appreciable change in comparison to MWCNTs as shown in Figure 6d and Figure 6e respectively for peak-1 and peak-2. This observation is supported by literature report where absorption spectra of the P3OT-SWCNT did not change significantly upon addition of SWCNT indicating insufficient interaction between the two materials [16].

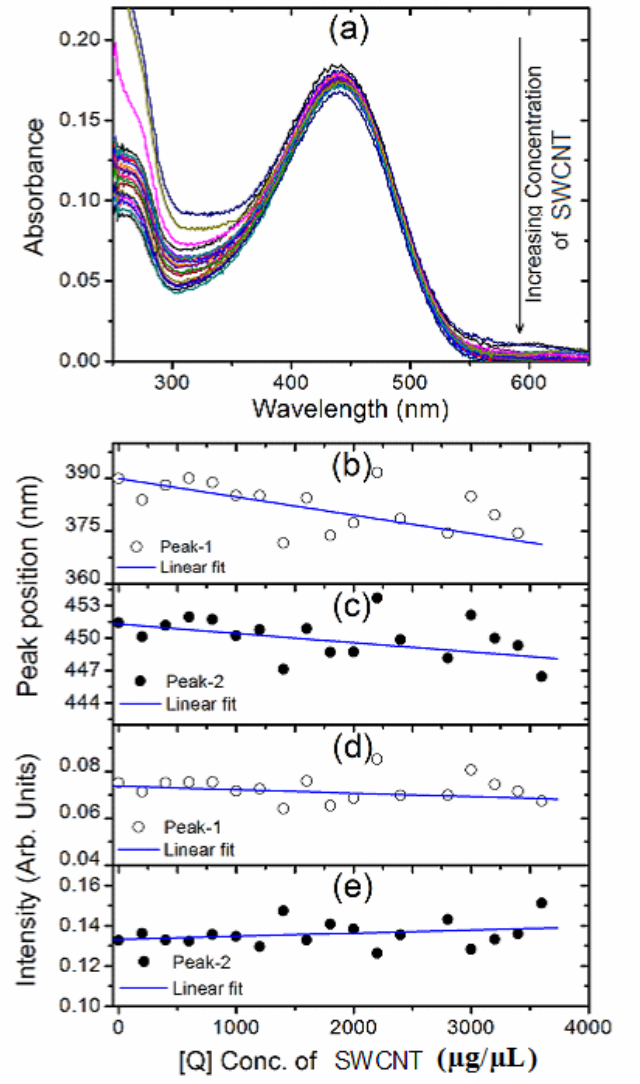

Figure 6 UV visible studies for P3HT SWCNT nanocomposites.

Figure 7a shows the change in the photoluminescence of P3HT with increasing concentration of SWCNTs. Corresponding Stern-Volmer plot is shown in Figure 7b. Stern-Volmer plot is linear for lower concentration and shows positive curvature at higher concentrations. Non-linear curvature may arise either due to a number of factors like combined effect of static and dynamic quenching, limited accessibility of quenchers or due to very large extent of quenching. Presence of dynamic quenching in our case is eliminated through time resolved studied presented later, while the limited accessibility of quenchers to the nanotubes due to bundling effect would lead to negative curvature in contrast to the observed upward curvature.

Similar to the case of MWCNTs, with continuous addition of SWCNTs to P3HT at various concentrations, the change in the photoluminescence lifetime has been monitored.

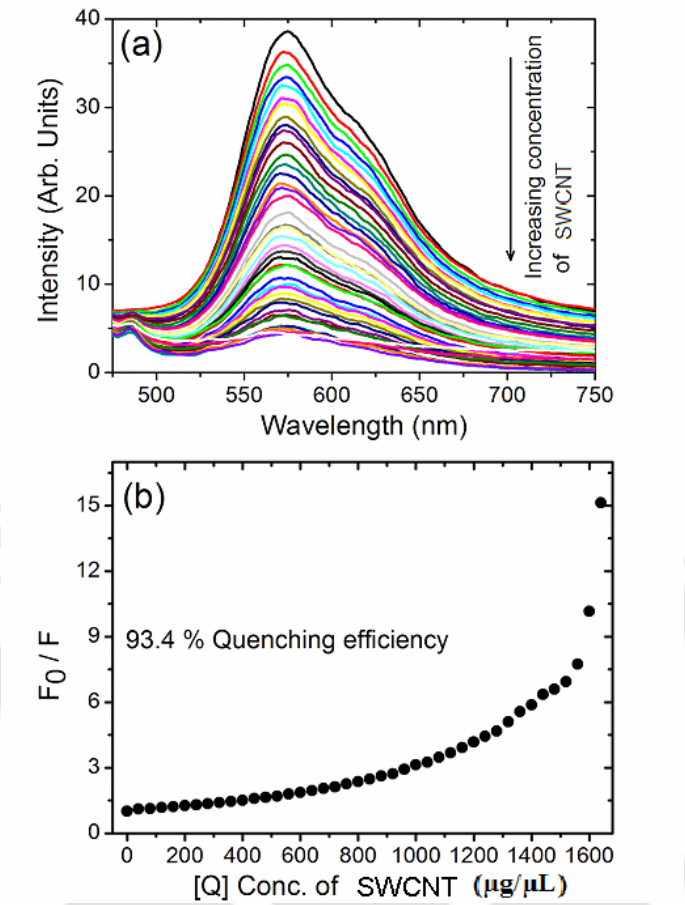

Figure 7 Photoluminiscence quenching of P3HT upon addition of (a) SWCNT and (b) SV plot

Similar to MWCNTs these spectra were fitted with a combination of two exponential decay components. The change in the decay time for these two components τ_1 and τ_2 are

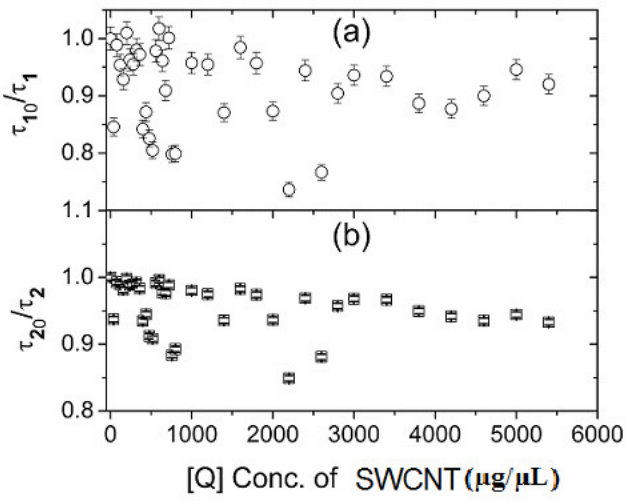

Figure 8 Time resolved spectroscopic results for P3HT-SWCNT composites

shown in Figure 8a and Figure 8b respectively. The ratios τ_{10}/τ_1 and τ_{20}/τ_2 remains nearly constant at 1. This strongly indicates the absence of any contribution from dynamic quenching. Thus the positive deviation observed in Stern-Volmer plot arises from large extent of quenching to be explained using 'Sphere of action model'.

A4.4 Concluding remark

From the experimental results of UV visible and photoluminescence spectroscopic studies, photoluminescence quenching observed in P3HT and carbon nanotube composites are confirmed to be "static quenching". Positive deviation observed in Stern-Volmer plot arises from large extent of quenching to be explained using "Sphere of action model". Quenching of photoluminescence of P3HT by MWCNT is more efficient in comparison to SWCNT.

References

[1] Kurata, S.; Kanagawa, T.; Yamada, K.; Torimura, M.; Yokomaku, T.; Kamagata, Y.; Kurane, R. *Nucleic Acid Research* **2001**, *29(6)*, 1.

[2] Anni, M.; Rella, R. *J. Phys. Chem. B* **2010**, *114*, 1559.

[3] Lakowicz, J. R. *Principles of fluorescence spectroscopy, Third Edition*; Springer: New York, **2006.**

[4] Chirvaze, D.; Chiguvare, Z.; Knipper, M.; Parisi, J.; Dyakonov, V.; Hummelen, J. C. *J. Appl. Phys.* **2003**, *93*, 3376.

[5] Chirvaze, D.; Parisi, J.; Hummelen, J. C.; Dyakonov, V. *Nanotechnology* **2004**, *15*, 1314.

[6] Günes, S.; Neugebauer H.; Sariciftci N. S. *Chem. Rev.* **2007**, *107*, 1324.

[7] Liang, Y.; Xu, Z.; Xia, J.; Tsai, S.-T.; Wu, Y.; Li, G.; Ray, C.; Yu, L. *Adv. Mater.* **2010**, *22*, 1.

[8] Green, M. A.; Emery, K.; Hishikawa, Y.; Warta, W. *Prog. Photovolt: Res. Appl.* **2010**, *18*, 346.

[9] Grzegorczyk, W. J.; Savenije, T. J.; Dykstra, T. E.; Piris, J.; Schins, J. M.; Siebbeles, L. D. *J. Phys. Chem. C* **2010**, *114*, 5182.

[10] Holt, J. M.; Ferguson, A. J.; Kopidakis, N.; Larsen, B. A.; Bult, J.; Rumbles G.; Blackburn J. L. *Nano Lett.* **2010**, *10*, 4627.

[11] Ferguson, A. J.; Blackburn, J. L.; Holt, J. M.; Kopidakis, N.; Tenent, R. C.; Barnes, T. M.; Heben, M. J.; Rumbles, G. *J. Phys. Chem. Lett.* **2010**, *1*, 2406.

[12] Kuila, B. K.; Malik, S.; Batabyal, S. K.; Nandi, A. K. *Macromolecules* **2007**, *40*, 278.

[13] Zhang, Z. B.; Li, J.; Qu, M.; Cabezas, A. L.; Zhang, S. L. *IEEE Electron Device Letters* **2009** , *30(12)*, 1302.

[14] Armarego, W. L. F.; Perrin, D. D. *Purification of Laboratory Chemicals*; Butterworth-Heinemann: Burlington, MA, **2002**.

[15] Goutam, P. J.; Singh, D. K.; Giri, P. K.; Iyer, P. K. *J. Phys. Chem. B* **2011**, *115*, 919.

[16] Kymakis, E.; Amaratunga, G. A. J. *Synth. Met.* **2004**, *142*, 161.


भारतीय प्रौद्योगिकी संस्थान गुवाहाटी
Indian Institute of Technology Guwahati

Part B

Chapter B1

INTRODUCTION

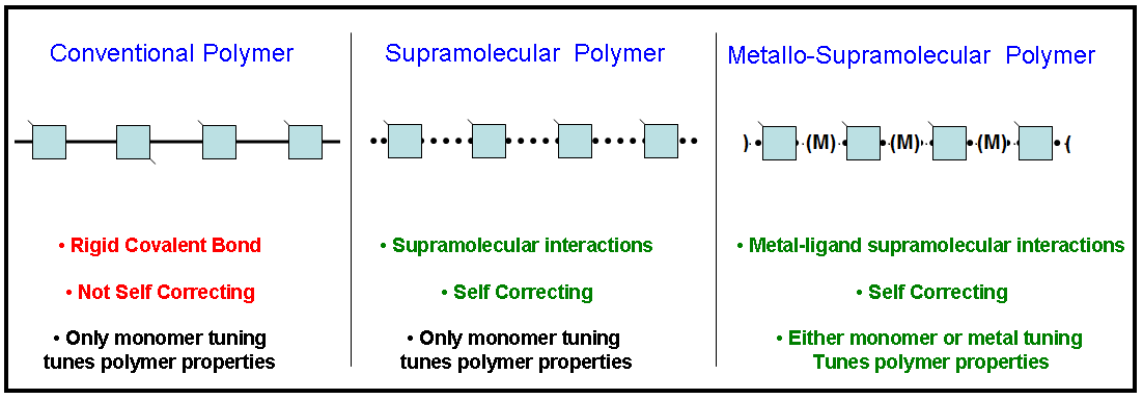

Metallopolymers are organic-inorganic hybrid materials featuring metal complexes within a polymeric system. They are attractive because of the common advantages of polymers like their low cost, ease of processing, good mechanical properties along with the unique tunable properties of metal complexes (optical, magnetic, electronic, catalytic). One important subset of these materials is the class of metallosupramolecular polymers, where the metal-ligand interaction is dynamic in nature and thus acts as the supramolecular motif. In this chapter, emergence, advantages and need based importance for further research in this area are highlighted with the help of available literature reports.

B1.1 Supramolecular polymers

B1.1.1 Supramolecular chemistry

The development of supramolecular chemistry added a new perspective to modern chemistry by non covalent interaction to organize molecular building blocks and thus enabling 'chemistry beyond molecule' [1]. Self assembly and host-guest chemistry are the two broad categories of supramolecular chemistry. The former describes the building up of non covalent arrays of defined geometry from specifically engineered molecular components. The latter involves the combination of small molecules, comprising a host that specifically accommodates a guest, thus leading to molecular recognition. The forces involved in supramolecular chemistry are hydrogen bonding, electrostatic interactions, van der Waals forces, π-π stacking, charge transfer interactions etc. [2-7]. Unlike covalent bond, these forces are weaker and easily disrupted. Self assembly shows the spatial confinement through spontaneous connection of a few or many components, which result in discrete or extended entities at molecular or supramolecular level. Meanwhile, it has been demonstrated that the use of non covalent interactions offers a fantastic opportunity for synthesis of large, complex structures such as receptors, devices and catalysts [8].

Modern society substantially depends on polymers due to the vast variety of their physical and chemical properties as well as their wide spread commercial application [9]. Traditional polymers are covalently formed polymers, where the monomers are linked by covalent bonds [10]. So formed covalently bonded polymers have well defined (static) molecular weight distributions that define their physical properties. Interest in supramolecular polymers has been stimulated to a great extent by the impressive progress made in supramolecular chemistry in general [11-14], and in the field of synthetic self assembling molecules in particular. Here, self-assembly has been adopted for the synthesis of different polymers [15]. According to Sijbesma et al. [16] "Supramolecular polymers are defined as polymeric arrays of monomeric units that are brought together by reversible and highly directional secondary interactions, resulting in polymeric properties in dilute and concentrated solutions, as well as in the bulk. The monomeric units of the supramolecular polymers themselves do not possess a repetition of chemical fragments. The directionality and strength of the supramolecular bonding are important features of systems that can be regarded as polymers and that behave according to well-established theories of polymer physics".

B1.1.2 Types of supramolecular polymers

During the last few years, considerable efforts have been made in the direction of self

assembling and supramolecular polymers as novel materials with 'intelligent' and tunable properties [17]. Three different types of supramolecular polymers are generally mentioned in literature. The first type is formed by the reversible association of bifunctional monomers. In this class the average degree of polymerization (DP) is determined by the strength of the end group interaction [18]. Second type of supramolecular polymers can be formed by planar structures that have the possibility to assemble on both sides of the plane. Here, the DP is completely governed by the association constant and the concentration. In the third category, supramolecular polymers are based on the reversibility of metal coordination bonding between a ligand and metal ions. Eventually, they are referred as metallo-supramolecular polymers or coordination polymers. These polymers are the closest analogues to conventional macromolecules, because most of the polymers mentioned make use of strong bonding, in which the reversibility can be tuned by chemical means only. The DP of the polymers in case of the coordination polymers is similar to that of the condensation polymers, and achieving exact stoichiometry is also of importance here[19].

In the scope of this thesis, the third type of supramolecular polymers, which are constructed from an alternating incorporation of metal ions and organic ligand molecules will be discussed (Figure 1).

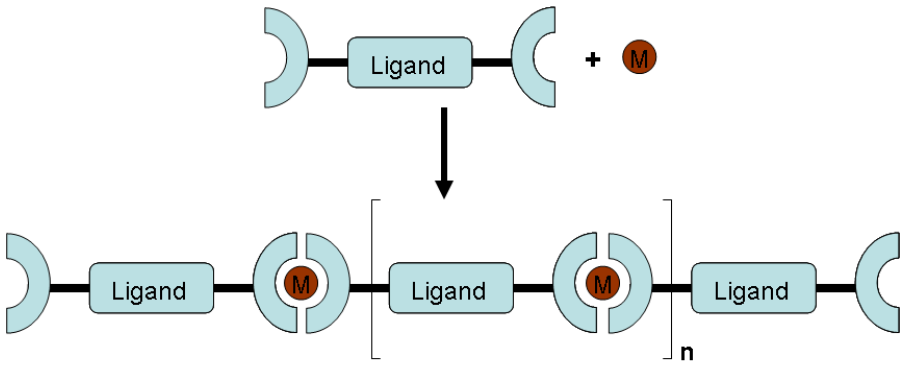

Figure 1 Representation of a typical metallo-supramolecular polymer of a ditopic ligand with two receptor units and metal M

B1.2 Metallo-supramolecular polymers: Features, applications and examples

Many researchers have already reported on the formation and application of supramolecular polymers in detail [20-24]. Metallo-supramolecular polymers potentially offer the functionality of the metal ion along with the processability of the polymer [25].

Metal-ligand coordination provides an excellent means for the synthesis of supramolecular systems as the coordination bond is highly directional, the ligand structures can be varied in a desired manner by established organic chemistry techniques, and the thermodynamic and kinetic stability can be fine tuned with the appropriate ligand types and metal ions [26, 27]. There has been a lot of contemporary interest in the use of metal-ligand binding as the thermodynamic driving force for self assembly of ditopic ligands into metallo- supramolecular polymers [28]. These metal containing polymers in which the metal-ligand interaction is dynamic in nature can thus act as supramolecular motifs [29].

Consideration of literature referred above suggests that metallo-supramolecular polymeric-materials have better potential to be used in light emitting diodes and light harvesting materials when compared to pure inorganic materials or organic polymeric materials. The reason behind the same are due to the following features.

- The use of noncovalent metal-ligand binding as the driving force for the self assembly of ditopic ligand offers a facile route to preparation of coordination polymers.
- For reversible coordination polymers, the DP and temperature dependence binding constant (K) are related as DP ~ $(K[M])^{1/2}$. According to this, higher DP is achieved at higher monomer concentration ([M]). Hence, sufficient optimization is possible by tuning the binding constant and the monomer concentration.
- Inorganic materials consist of covalent or ionic bonds or atoms over the entire expanse of solids. Synthesis, purification and characterization of organic molecules (ligand part in coordination polymer) are much simpler as compared to inorganic materials.
- Band gap tuning by chemical structure modification of the spacer part and using different metal ions along with self-organization behavior attracted tremendous attention both for basic scientific research and technological advances over inorganic materials. High thermal stability with excellent luminescence is some of the other important properties of metallo-supramolecular polymers.
- Self error correction and thermodynamically favored structure are great advantages in case of reversible coordination polymers.
- Coordination polymers offer considerable processing advantages over inorganic materials, device fabrication is easier and they can be generated by solution deposition techniques even on flexible substrates.

In fact, due to their potential usefulness in a plethora of applications like catalysis, light-

emitting devices and sensory materials, metallopolymers have become a prominent research theme at the interface of metal-organic chemistry and polymer science. Utilizing a variety of non-covalent interactions, several recent studies have demonstrated that different types of building block can be assembled with supramolecular motifs, yielding polymer materials that span a broad range of structures and properties [20-22, 30-32]. By varying metal–ligand binding motifs different types of binding characteristics [26-27, 33-35] (e.g., thermodynamic and kinetic stabilities) can be obtained, which in turn can be utilized to tune the nature of the resulting supramolecular materials [36-41].

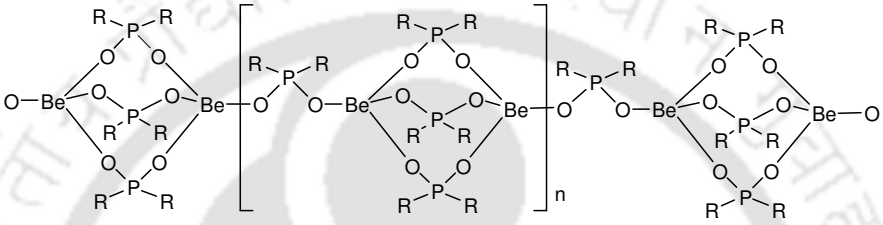

Figure 2 The first reported coordination polymer

In 1968, A. Ripamonti and coworkers first reported the soluble coordination polymers beryllium phosphinates (Figure 2) [42]. They studied the solution properties which indicated that these compounds are linear polymers which undergo a reversible

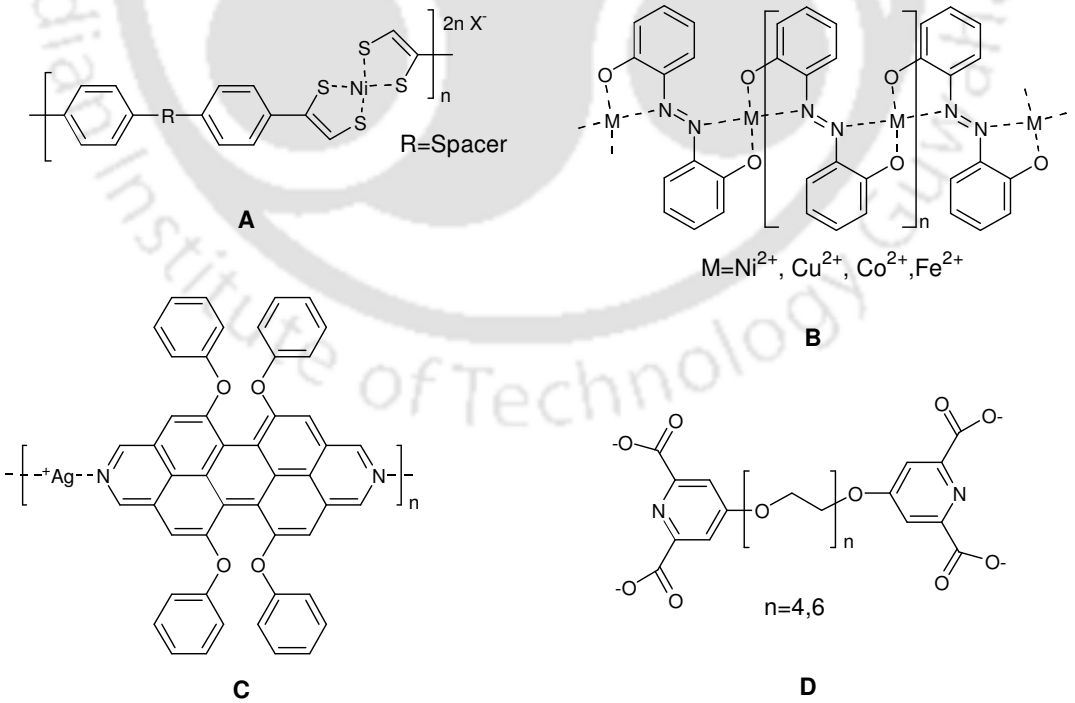

Figure 3 Different building blocks of metallo-supramolecular polymers

degradation influenced by the nature of the solvent, concentration and temperature. With

the advancement of metal ligand coordination chemistry, various metal-ligand system based coordination polymers are developed recently by different groups. Wang and Reynolds [43] reported soluble and electroactive nickel bis(dithiolene) polymers (A in Figure 3). Dihydroxy-functionalized azobenzene was applied by the group of Suh [44] for the construction of coordination polymeric systems with transition metals ions like Ni^{2+}, Cu^{2+}, Co^{2+} and Fe^{2+} (B in Figure 3) which have been named polyazometals. Pyridine-Metal Coordination based metallo-supramolecular polymers had also been reported by several other groups [45-46]. Würthner and Sautter reported formation of metallo-supramolecular polymer by a pyridine based dye with Ag^{+} (C in Figure 3) [47]. Vermonden and coworkers utilized oligoethylene glycol spacered pyridine-2,6-dicarboxylic acid receptors and could synthesize water soluble coordination polymers with Zn^{2+} ions (D in Figure 3) [48].

B1.3 Chelating complexes: An effective way to obtain metallo-supramolecular polymer with high binding constants

The coordination of pyridine ligands to metal ions being linear in manner, most of the reported polymers had low binding constant. To overcome this shortcoming attempts to design new ligands capable of forming coordination polymers with high binding constant were made. This involved addition of chelating moieties within the ligand system. Rehahn et al. reported the first coordination polymer utilizing kinetically labile metal complexes and with high binding constant. This polymer had a phenanthroline based ditopic ligand capable of forming chelate (Figure 4). Later, many literatures came up, where phenathroline and/or bipyridine based building blocks were involved in polymer preparation [49-54].

Octahedral coordination by three phenanthroline or 2,2'-bipyridine ligand give rise to enantiomers. The 2,2':6',2''-terpyridine (tpy) ligand is ideally suited as a ligand for coordination polymers as 2:1 ligand-metal complexes does not give rise to enantiomers which has advantage over 2,2'-bipyridine [27]. Terpyridine ligands bearing flexible oligomeric and polymeric spacers have been reported by the group of Schubert (A in Figure 5) [36, 55-56]. Beck and Rowan synthesized a terpyridine type ditopic ligand with 2,6-bis(1-methylbenzimidazolyl)-4-hydroxypyridine based binding site and pentaethylene glycol as a spacer, which forms metallo-supramolecular polymers that are photoactive mechanoresponsive gels (B in Figure 5) [57]. In another communication Rowan and co

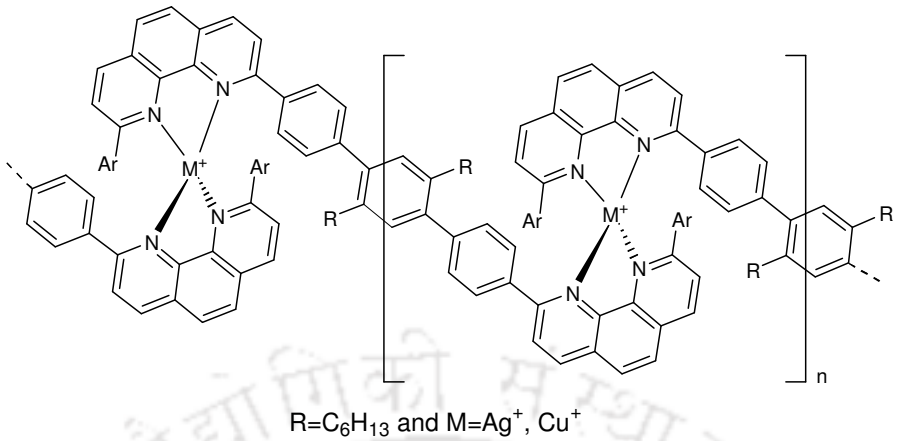

Figure 4 First coordination polymer utilizing kinetically labile metal complexes and with high binding constant.

workers reported a metallo-supramolecular polymeric system with similar binding site but with a different rigid spacer unit (C in Figure 5) [58].

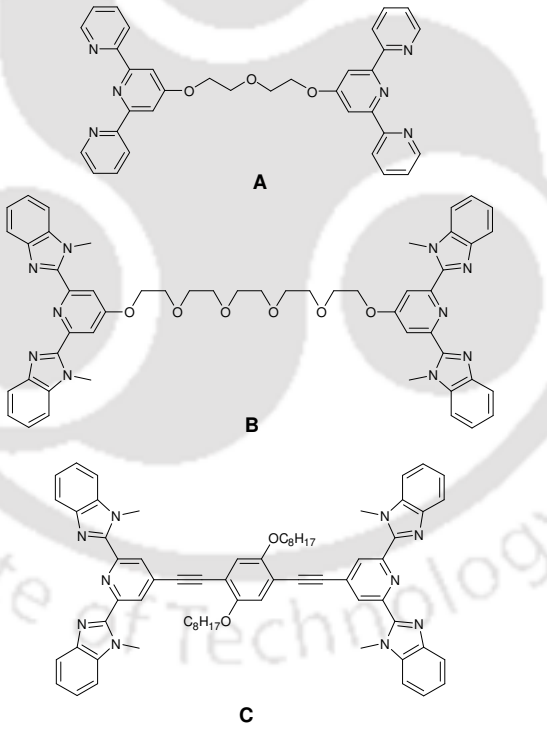

Figure 5 Terpyridine based ditopic ligands for metallo-supramolecular polymer formation

To summarize, many literature are appearing in the area of design and development of supramolecular polymers where attempts to tune the properties of the polymeric system by varying the binding site, spacer part and the metal ion have been shown. Literature survey suggests that metallo-supramolecular polymeric-materials have better potential to be used in light emitting diodes and light harvesting materials in comparison to pure

inorganic materials or organic polymeric materials and hence this area is focused as a need based research area.

B1.4 Supramolecular receptors and guest selective recognition

As described earlier in this chapter, host-guest chemistry is another important area under supramolecular chemistry. Supramolecular receptor molecules can form supramolecules by selectively binding guest molecules like ionic or molecular substrates (or both) by means of various intermolecular interactions. Molecular recognition, i.e. the ability of molecules and functional groups to recognize and interact with each other, is fundamentally important for understanding many chemical phenomena, e.g., drug–receptors, enzyme–substrate recognition, adhesion of molecules to surfaces, self-assembly of molecules etc. The recognition is binding with a purpose and the process occurs through a set of structurally well-defined intermolecular interactions. Thus, molecular recognition implies the storage and read out of molecular information. Although, the term recognition was initially used in connection with biological systems, in the beginning of the 1970's it was used in the selective complexation of metal ions [59]. Pedersen [60], who discovered the crown ethers and later received the Nobel Prize for it in 1987, mentioned the use of the compound for the recognition of ammonium ions [61].

Cram [62] and co-workers concluded that two factors are important to achieve high binding constants, [63] firstly the principle of complementary binding sites must be fulfilled. Receptor and guest binding sites should be in close proximity geometry, they should be complementary and they should fit without generating steric strain. Secondly, receptors which are suitably pre-organized for guest binding will lead to the more stable

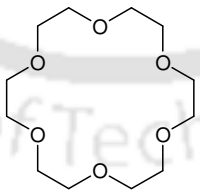

Figure 6 Crown ether 18-crown-6

complex. Crown ether ammonium ion binding occurs by hydrogen bonding between oxygen atoms (or nitrogen, sulfur or other free electron pair in hetero crown ethers) and N^{+}–H bonds. The cyclic arrangement leads to a pre-organization of the host, whereby selectivity is determined by the ring size. Primary ammonium ions are complexed with highest affinity by 18-crown-6 derivatives (Figure 6) [64].

Achievements of molecular recognition depend on the design of molecular receptors so that it can create numerous non covalent binding interactions with the guest molecule and sense its molecular size, shape, and architecture. Receptors should contain some intramolecular cavities, clefts or pockets to which guest molecule can fit in, which is known as concave receptors. Another significant point is the flexibility of supramolecular systems which is of great importance in biological receptor-substrate interactions. In last decades, this field is receiving importance because of their significance in intermolecular chemistry and in chemical selectivity. This receptor chemistry is extending to all types of substrates: cationic, anionic, or neutral molecules of organic, inorganic, or biological nature[65]. Noteworthy progress made in order to design and synthesize novel receptors capable of recognizing chemical and biological guest molecules has contributed greatly in the development of supramolecular chemistry [66-69]. Major challenges that need attention are the development of structurally simple and stable receptors that would have

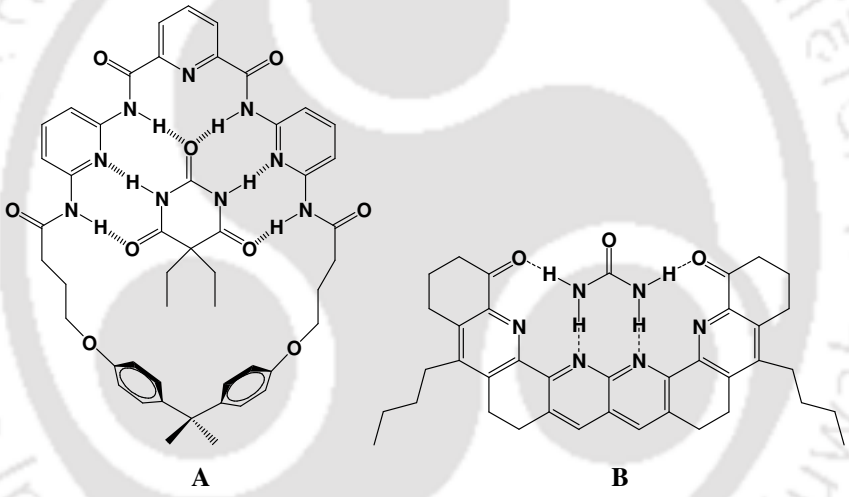

Figure 7 Barbituric acid receptor by Hamilton (A) and Urea receptor by Bell and co workers (B)

better utility and much wider applicability. There were many receptors which are capable of recognizing neutral molecules. Hamilton [70] reported a macrocyclic receptor which form complex with barbituric acid through hydrogen bonding (Figure 7a). Bell [71] and co-workers designed a series of heterocyclic receptor for urea (Figure 7b).

Recently, Chetia et al. reported simple 2,6-bis (2-benzimidazolyl) pyridine as urea receptor and toxic benzene metabolites receptor (Figure 8) [72, 73].

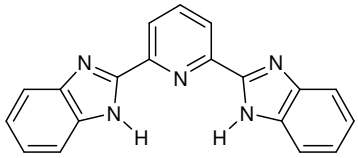

Figure 8 2, 6-bis (2-benzimidazolyl) pyridine as receptor for urea and benzene metabolites

B1.5 Scope of the work

It is important to mention that benzimidazole and its derivatives promote intra and inter-molecular interactions, such as hydrogen bonding and π-stacking, providing scope to the formation of molecular aggregates. Coordination behavior of benzimidazole, 2-substituted benzimidazoles and benzothiazoles, towards transition metal ions are well established in literature [74]. Looking into the important biological activities of the benzothiazole nucleus [75], and its similarities in binding modes with benzimidazole as well as availability of easy synthetic methods [76], we pursued the synthesis of ditopic monomers with it and used it for supramolecular polymer formation.

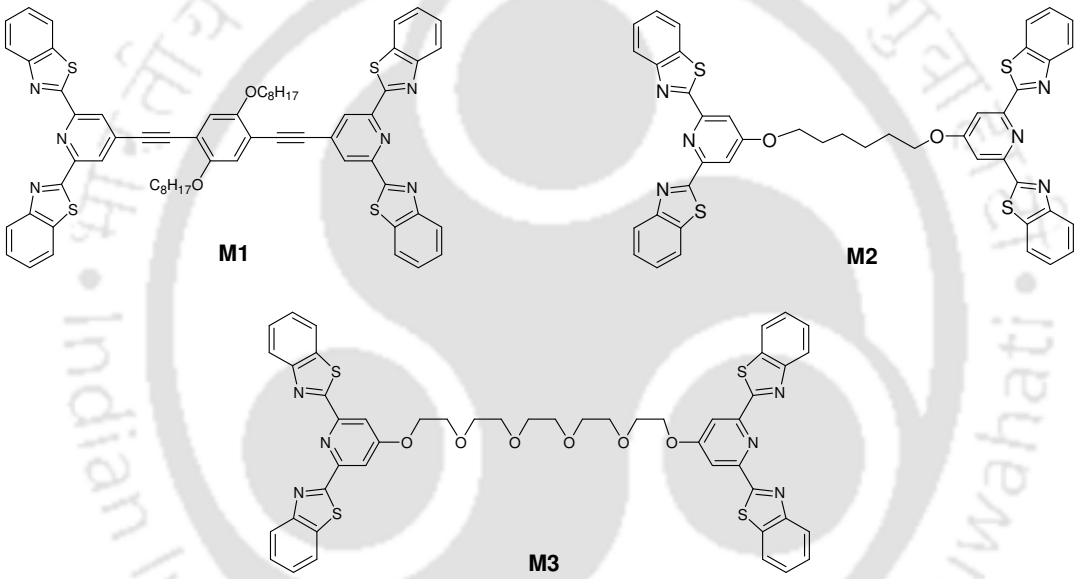

Figure 9 New ditopic monomers which contains 2,6-bis(benzthiazolyl)pyridine ligand as the binding unit

In the scope of our work, synthesis of new ditopic monomers which contains 2,6-bis(benzthiazolyl)pyridine ligand as the binding unit were planned (Figure 9). Literature reports motivated us to apply them for supramolecular polymer formation with Zn^{2+} ion. In Chapter B2, two ditopic ligands, one with rigid spacer 1,4-diethynylbenzene (M1) and other with a flexible hexyl chain (M2) are taken up for supramolecular polymer formation with Zn^{2+} ion. In Chapter B3 another ligand with a pentaethylene glycol chain as spacer (M3), which eventually folds on addition of K^{+} ion, is taken up for supramolecular polymer formation. In Chapter B4, use of M2 is taken up as guest selective supramolecular receptor for resorcinol from other benzene metabolites.

References

[1] Lehn, J.M. *Science* **2002**, *295*, 2400.

[2] Rebek Jr, J. *Angew. Chem. Int. Ed. Eng.* **1990**, *29*, 245.

[3] Vögtle, F. *Suparmolecular Chemistry* John Wiley & Sons: New York, **1991**.

[4] Amabilino, D. B.; Stoddart, J. F. *Chem. Rev.* **1995**, *95*, 2725.

[5] Fyfe, M. C. T.; Stoddart, J. F. *Acc. Chem. Res.* **1997**, *30*, 393.

[6] Harada, A.; Li, J.; Kamachi, M. *Nature* **1992**, *356*, 325.

[7] Harada, A.; Li, K.; Kamachi, M. *Nature* **1994**, *370*, 126.

[8] Reinhoudt, D.N. ; Crego-Calama, M. *Science* **2002**, *295*, 2403.

[9] Heeger, A.J. *Angew. Chem. Int. Ed. Eng.* **2001,** 40, 2591.

[10] Marvel, C.S. *J. Chem. Educ.* **1965**, *42 (1)*, 3.

[11] Cram, D. J.; Cram, J. M. *Science* **1974**, *183*, 803.

[12] Pedersen, C. J. *J. Am. Chem. Soc.* **1967**, *89*, 7017.

[13] Pedersen, C. J. *Angew. Chem., Int. Ed. Eng.* **1988**, *27*, 1053.

[14] Lehn, J. M. *Makromol. Chem., Macromol. Symp.* **1993**, *69*, 1.

[15] Friese, V. A.; Kurth, D. G. *Coordination Chemistry Reviews* **2008,** *252*, 199.

[16] Brunsveld, L.; Folmer, B. J. B.; Meijer, E. W.; Sijbesma R. P. *Chem. Rev.* **2001**, *101*, 4071.

[17] Schubert, U. S.; Eschbaumer C. *Angew. Chem. Int. Ed.* **2002**, *41*, 2892 .

[18] Martin, B. *R. Chem. Rev.* **1996**, *96*, 3043.

[19] Archer, R. D. *Coord. Chem. Rev.* **1993**, *128*, 49.

[20] Ciferri, A. *Macromol Rapid Commun* **2002**, *23*, 511.

[21] Hofmeier, H.; Schubert, S. *Chem. Commun.* **2005**, 2423.

[22] Hofmeier, H.; Hoogenboom, R.; Wouters, M.E.L.; Schubert, U.S. *J. Am. Chem. Soc.* **2005**, *127*, 2913.

[23] Dobrawa, R.; Wurthner F. *Journal of Polymer Science: Part A: Polymer Chemistry* **2005,** *43*, 4981.

[24] Gerhardt, W. W.; Zucchero, A. J.; Wilson, J.N.; South, C.R.; Bunz, U. H. F.; Weck, M. *Chem. Commun.* **2006**, 2141.

[25] Rowan, S. J.; Beck, B. *Faraday Discuss.* **2005**, *128*, 43.

[26] Holder, E.; Langeveld, B. M. W.; Schubert, U. S. *Adv. Mater.* **2005**, *17*, 1109.

[27] Schubert, U. S.; Eschbaumer, C *Angew Chem. Int. Ed.* **2002**, 41, 2892.

[28] Holliday, B. J.; Swager, T. M. *Chem. Commun.* **2005**, 23.

[29] Schubert, U.S.; Newkome, G.R.; Manners, I. *Metal Containing and Metallosupramolecular Polymers and Materials*, ACS:Washington, D.C. **2006**.

[30] Brunsveld, L.; Folmer, B. J. B.; Meijer, E. W.; Sijbesma, R. P. *Chem. Rev.* **2001**, *101*, 4071.

[31] Meier, M. A. R.; Wouters, D.; Ott, C.; Guillet, P.; Fustin, C.-A.; Gohy, J.-F.; Schubert, U. S. *Macromolecules* **2006**, *39*, 1569.

[32] Gerhardt, W. W.; Zucchero, A.J.; Wilson, J. N.; South, C. R.; Bunz, U. H. F.; Weck, M. *Chem. Commun.* **2006**, 2141.

[33] Nguyen, P.; Gomes-Elipe, P.; Manners, I. *Chem. Rev.* **1999**, *99*, 1515.

[34] Wolf, M. O. *Adv. Mater.* **2001**, *13*, 545.

[35] Holliday, B. J.; Swager, T. M. *Chem. Commun.* **2005**, 23.

[36] Schmatloch,S.; Gonzalez, M. F.; Schubert, U. S. *Macromol. Rapid Commun.* **2002**, *23*, 957.

[37] Yount, W. C.; Juwarker, H.; Craig, S. L. *J. Am. Chem. Soc.* **2003**, *125*, 15302.

[38] Vermonden, T.; van der Gucht, J.; de Waard, P.; Marcelis, A. T. M.; Besseling, N. A. M.; Sudho¨lter, E. J. R.; Fleer, G. J. and Stuart, M. A. C. *Macromolecules*, **2003**, *36*, 7035.

[39] Loveless, D. M.; Jeon, S. L.; Craig, S. L. *Macromolecules* **2005**, *38*, 10171.

[40] Yount, W. C.; Loveless, D. M. and Craig, S. L. *J. Am. Chem. Soc.* **2005**, *127*, 14488.

[41] Schmittel, M.; Kalsani, V.; Kishore, R. S. K.; Colfen, H.; Bats, J. W. *J. Am. Chem. Soc.* **2005**, *127*, 11544

[42] Gemiti, F.; Giancotti, V.; Ripamonti. A. *J. Chem. Soc. A*, **1968**, 763.

[43] Wang, F.; Reynolds, J. R. *Macromolecules* **1990**, *23*, 3219.

[44] Suh, J.; Oh, E.; Kim, H. C. Synth. Met. **1992**, *48*, 325.

[45] Yount, W. C.; Juwarker, H,; Craig, S. L. *J. Am. Chem. Soc.* **2003**, *125*, 15302.

[46] Khlobystov, A. N.; Blake, A. J.; Champness, N. R.; Lemenkovskii, D. A.; Majouga, A. G.; Zyk, N. V.; Schröder, M. *Coord. Chem. Rev.* **2001**, *222*, 155.

[47] Würthner, F.; Sautter, A.; Thalacker, C. *Angew. Chem. Int. Ed.* **2000**, *39*, 1243.

[48] Vermonden, T.; van der Gucht, J.; de Waard, P.; Marcelis, A. T. M.; Besseling, N. A. M.; Sudhölter, E. J. R.; Fleer, G. J.; Cohen Stuart, M. A. *Macromolecules* **2003**, *36*, 7035.

[49] Phillips-McNaughton, K.; Groves, J. T. *Org. Lett.* **2003**, *5*, 1829.

[50] Knapp, R.; Schott, A.; Rehahn, M. *Macromolecules* **1996**, *29*, 478.

[51] Kelch, S.; Rehahn, M. *Macromolecules* **1997**, *30*, 6185.

[52] Kelch, S.; Rehahn, M. *Macromolecules* **1998**, *31*, 4102.

[53] Chen, J.; MacDonnell, F. M. *Chem. Commun.* **1999**, 2529.

[54] Cassagneau, T.; Fendler, J. H.; Johnson, S. A.; Mallouk, T. E. *Adv. Mater.* **2000**, *12*, 1363-1366.

[55] Schmatloch, S.; van den Berg, A.; Alexeev, A. S.; Hofmeier, H.; Schubert, U. S. *Macromolecules* **2003**, *36*, 9943.

[56] Hofmeier, H.; Schmatloch, S.; Wouters, D.; Schubert, U. S. *Macromol. Chem. Phys.* **2003**, *204*, 2197.

[57] Beck, J. B.; Rowan, S. J. *J. Am. Chem. Soc.* **2003**, *125*, 13922.

[58] Iyer, P. K. Beck, J. B.; Weder, C.; Rowan, S. J. *Chem. Commun.*, **2005**, 319.

[59] Lehn, J. M. *Struct. Bonding*, **1973**, *16*, 1.

[60] Pedersen, C. J. *Angew. Chem., Int. Ed. Eng.* **1988**, *27*, 1021.

[61] Pedersen, C. J. *J. Am. Chem. Soc.* **1967**, *89*, 7017.

[62] Cram, D. J. *Angew. Chem., Int. Ed. Eng.* **1988**, *27*, 1009.

[63] Timko, J. M.; Moore, S. S.; Walba, D. M.; Hiberty, P. C.; Cram, D. J. *J. Am. Chem. Soc.* **1977**, *99*, 4207.

[64] Rüdiger, V.; Schneider, H. J.; Solov'ev, V. P.; Kazachenko, V. P.; Raevsky, O. A. *Eur. J. Org. Chem.* **1999**, 1847.

[65] Lehn, J. M. *Perspecitives in Coordination Chemistry*, (Eds.: Williams, A. F.; Floriani, C. and Merbach, A. E.), VHCA, Basel, and VCH:Weinheim, **1992.**

[66] Martinez-Máñez, R.; Sancenón, F. *Chem. Rev.* **2003**, *103*, 4419.

[67] Sessler, J. L.; Camiolo, S.; Gale, P. A. *Coord. Chem. Rev.* **2003**, *240*, 17.

[68] Beer, P. D.; Gale, P. A. *Angew. Chem., Int. Ed.* **2001**, *40*, 486.

[69] Lehn, J. M. *Supramolecular Chemistry, Concepts and Perspectives*; VCH: Weinheim,Germany, **1995**.

[70] Hamilton, A. D. *Bioorg. Chem. Frontiers* **1991**, *2*, 115.

[71] Bell, T.W.; Liu, J. *J. Am. Chem. Soc.* **1988**, *110*, 3673.

[72] Chetia, B.; Iyer, P. K. *Tetrahedron Lett.* **2006**, *47*, 8115.

[73] Chetia, B.; Iyer, P. K. *Tetrahedron Lett*. **2007**, *48*, 47.

[74] Téllez, F.; López-Sandoval,H.; Castillo-Blum, S. E. ; Barba-Behrens N. *ARKIVOC* **2008**, *V*, 245.

[75] Rana, A.; Siddiqui, N.; Khan, S. A. *Indian Journal of Pharmaceutical Sciences* **2007**, *69 (1)*, 10.

[76] Drew M. G. B.; Hill C.; Hadson M. J.; Iveson P. B.; Madic C.; Vaillant L.; Youngs T. G. A. *New J. Chem*. **2004**, *28*, 462.

Chapter B2

SYNTHESIS AND OPTICAL PROPERTIES OF 2,6-BIS(BENZOTHIAZOLYL)PYRIDINE BASED METALLO-SUPRAMOLECULAR POLYMERS

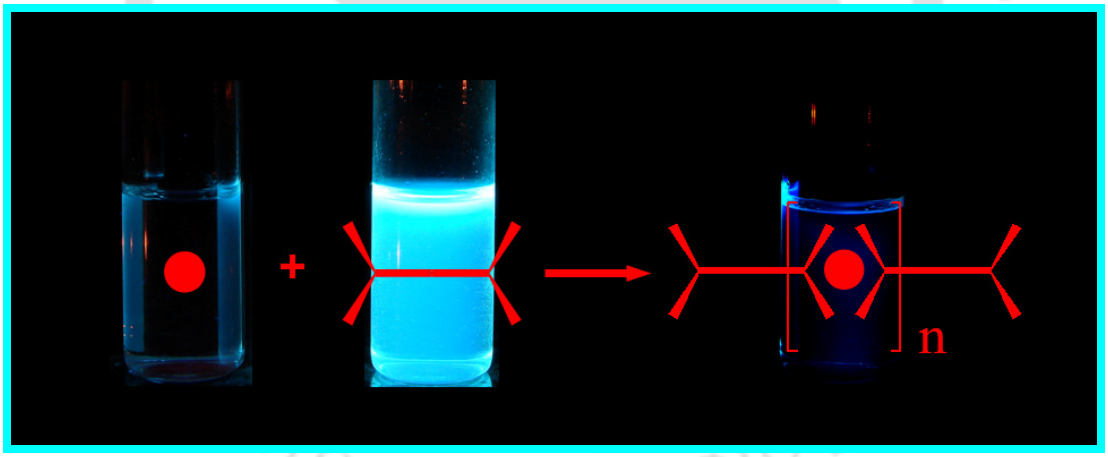

Two new ditopic monomers that contain 2,6-bis(benzothiazolyl)pyridine ligand as the binding moiety were synthesized. One monomer with a 1,4-diethynylbenzene as spacer leads to the formation of supramolecular conjugated polymers with Zn^{2+} metal ion. The other monomer with a simple hexyl chain also forms supramolecular polymeric system with Zn^{2+} ion but with less efficiency in comparison to the earlier one. UV visible and phtoluminescence spectroscopy along with viscosity measurements were used to follow the supramolecular polymer formation. Structure optimization of the binding moiety, in free monomer and in complex with Zn^{2+} ion form were done by DFT method.

B2.1 Prologue

Many recent literatures report the synthesis, characterization and applications of various metallo-supramolecular polymers with different properties [1-5]. Recently, interest has been developed in synthesizing terpyridine ligand based metallo-supramolecular polymers since they form chelate with metal ions which increase the stability of the polymeric systems. Schubert [6-8] as well as Rowan and Weder [9-10] are pioneers in this area with their significant contribution leading to a wide variety of structures and applications. Benzothiazole is an important molecule and this simple nucleus is present in compounds that possess interesting biological activities, such as in antitumor, antimicrobial, anthelmintic, antileishmanial, anticonvulsant and anti-inflammatory processes [11]. Even though benzothiazole based binding site synthesis is as easy as that based on benzimidazole, very few literatures are available where the use of former two as bonding site in supramolecular polymer formation are reported. We adopted a simple methodology [12] to synthesize bis(2-benzothiadazolyl) pyridine based binding site to extend the idea of formation of metallo-supramolecular polymers constructing ditopic monomers out of it.

In this chapter, synthesis of two new ditopic monomers M1 and M2 (Figure 1) which contains 2,6-bis(benzothiazolyl)pyridine ligand as the binding moiety will be highlighted. Metallo-supramolecular polymer formation by these two monomers upon self-assembly with Zn^{2+} ion will be discussed. Experimental results of UV-visible spectroscopy,

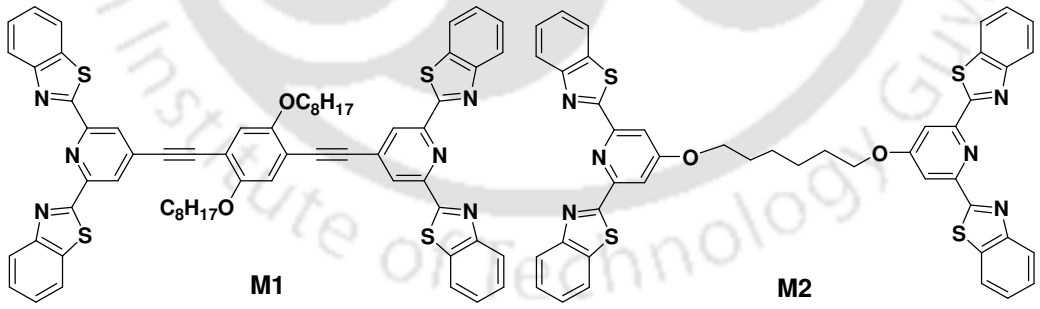

Figure 1 Two diatopic monomers containing contains 2,6-bis(benzothiazolyl)pyridine as biniding moiety

photoluminescence spectroscopy and viscosity measurements were analyzed to follow the supramolecular polymer formation. Moreover, structure optimization of the binding moiety, in free monomer and in complex with Zn^{2+} ion are discussed supportive DFT calculations.

B2.2 Experimental section

B2.2.1 Chemicals and solvents

All chemicals unless otherwise mentioned were used as received. All solvents were used after purification by standard purification techniques [13]. Other chemicals were used as received.

B2.2.2 Instrumentation

UV visible spectra were recorded on a Perkin-Elmer Lambda 25 UV-Vis spectrophotometer at room temperature. Photoluminescence studies were done using a Varian photoluminescence spectrophotometer. Viscosity measurements were done in micro molar concentration using a m-VROC RheoSense, Inc. viscometer.

B2.2.3 Preparation of 2,6-bis-benzothiazol-2-yl-pyridin-4-ol ligand

The 2,6-bis-benzothiazol-2-yl-pyridin-4-ol ligand has been prepared by using known route reported in the literature method (Scheme 1) [14-15].

Chelidamic acid (1.8 g, 9.83 mM) and 2-aminothiophenol (2.99 g, 23.89 mM) were dispersed in 20 mL orthophosphoric acid. The mixture was stirred and refluxed at 220°C for 14 hrs. After cooling to about 100°C, the hot mixture was poured to ice cold water and stirred for half an hour. The precipitate formed was filtered off and poured to hot 10 % Na_2CO_3. The reaction mixture was stirred for 10 mins. The filtered product was acidified to a pH value of 4. Precipitate was again filtered, washed with water and recrystalised from methanol to yield a greenish powdery compounds (> 90% yield).

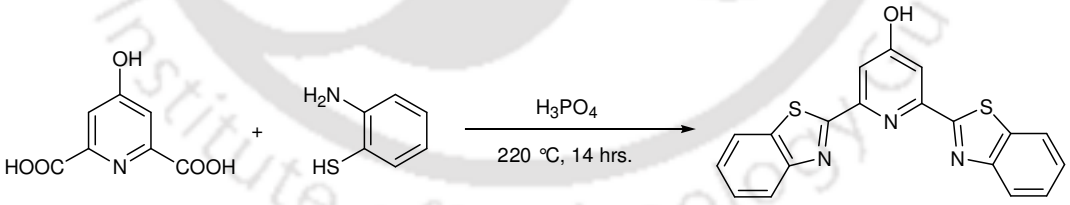

Scheme 1

B2.2.4 Synthesis of 2,6-bis(benzothiazolyl)-4-bromopyridine

2,6-bis-benzothiazol-2-yl-pyridin-4-ol (1.0 g, 2.77 mM) was added to a round bottom flask attached with a reflux condenser (Scheme 2). A large excess of phosphorous oxybromide was added to the flask and the reaction was mixture was heated at 140 °C for 16 hrs under a nitrogen atmosphere. The homogenous solution was then poured hot into water and the pH was adjusted to 8.0 by addition of 10 % NaOH solution. The mixture was stirred for an hour and the organic layer was separated out. The aqueous layer was

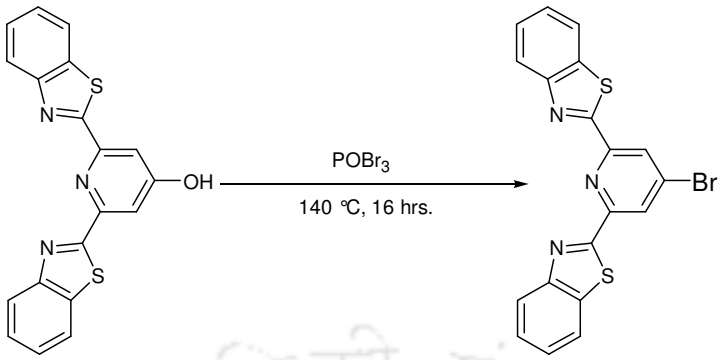

Scheme 2

extracted with dichloromethane. Solvent was evaporated to yield the solid product (1.06 g, 75 %).

^{1}H NMR (400 MHz, DMSO): δ 8.32 (s, 2H), 7.80 (m, 4H), 7.53-7.32(m, 4H)

^{13}C NMR (400 MHz, DMSO): δ 158.20, 155.40, 152.00, 135.40, 133.65, 126.30, 125.62, 123.30, 123.70, 118.18.

B2.2.5 Synthesis of 2,6-bis(benzothiazolyl)-4-trimethylsilylethynyl pyridine

2,6-bis(benzimidazolyl)-4-bromopyridine (1.0 g, 2.36 mM), $Pd(PPh3)_2Cl_2$ (0.08 g, 0.12 mM), CuI (0.02 g, 0.12 mM), triethylamine (15 mL) and dimethylformamide (10 mL) were added to a flask with a reflux condenser and were purged with nitrogen for 30 mins (Scheme 3). The reaction mixture was heated to 55 °C and trimethylsilylacetylene (0.84 mL, 5.90 mM) was added. Stirring was continued for an hour and the hot reaction mixture was poured into a saturated aqueous EDTA solution (100 mL) to which chloroform (20 mL) was added. After stirring for an hour the organic layer was separated out and the aqueous layer extracted with chloroform. The solvent was evaporated to give a brown solid.

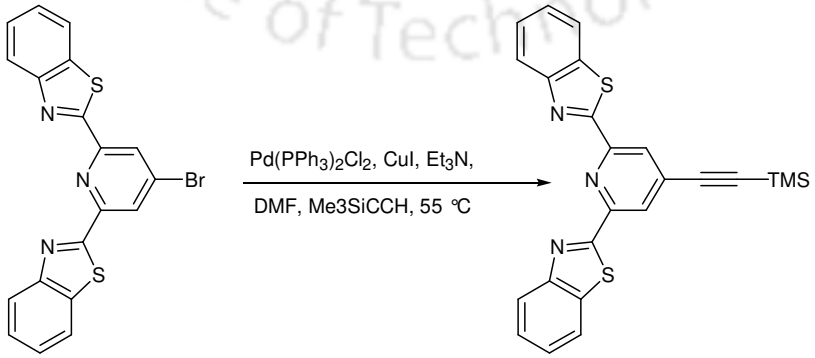

Scheme 3

Purification was carried out by chromatography using a silica gel column with chloroform as the eluent, to yield a white yellow solid (1.005 g, 96.3 %).

^{1}H NMR (400 MHz, CDCl3): δ 8.23 (s, 2H), 8.12-7.70 (m, 4H), 7.50 (m, 4H), 0.26 (s, 9H)
^{13}C NMR (400 MHz, CDCl3): δ 156.20, 155.70, 147.56, 142.33, 138.84, 132.44, 128.79, 127.95, 125.30, 115.69, 107.58, 106.98, -0.34.

B2.2.6 Synthesis of 2,6-bis(methyl-benzothiazolyl)-4-ethynylpyridine

2,6-bis(benzothiazolyl)-4-trimethylsilylethynylpyridine (0.75 g, 1.70 mM), aqueous KOH (25 mL, 20 %), tetrahydrofuran (25 mL, freshly distilled) and methanol (25 mL) were stirred at room temperature for 4 hours (Scheme 4). The organic layer was separated out and the aqueous layer was extracted with chloroform. The solvent was evaporated to give a brown solid. Purification was carried out by chromatography using a silica gel column with chloroform as the eluent, to yield a white solid (0.542 g, 80.5 %).

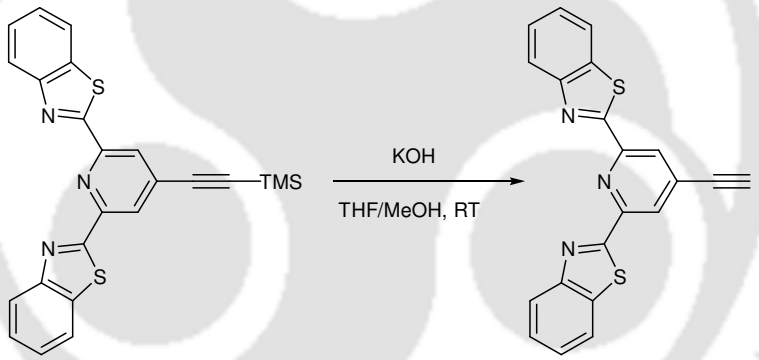

Scheme 4

^{1}H NMR (400 MHz, CDCl3): δ 8.26 (s, 2H), 8.02-7.52 (m, 4H), 7.43 (m, 4H), 3.3 (s, 1H)
^{13}C NMR (400 MHz, CDCl3): δ 156.43, 155.98, 147.78, 142.67, 138.38, 132.89, 128.99, 128.15, 125.67, 115.93, 89.17, 86.10.

B2.2.7 Synthesis of Monomer M1

2,6-bis(benzothiazolyl)-4-ethynylpyridine (0.190 g, 0.51 mM), 1,4-diiodo-2,5-dioctyloxybenzene (0.147 g, 0.25 mM), $Pd(PPh_3)_4$ (0.018 g, 0.015 mM), CuI (0.003 g, 0.015 mM), toluene (8 mL) and diisopropylamine (3 mL) were added to a flask with a reflux condenser and the mixture was stirred at 70 °C for 22 hrs under nitrogen (Scheme 5). The hot reaction mixture was subsequently poured into saturated aqueous EDTA solution (100 mL) to which chloroform (20 mL) was added. After stirring for an hour the

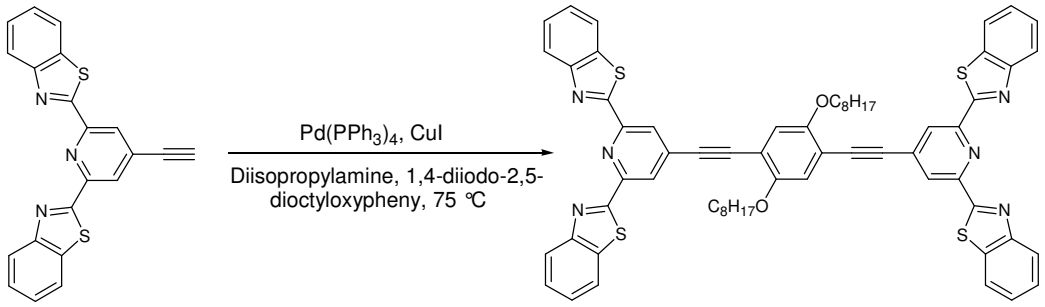

Scheme 5

the organic layer was separated out and the aqueous layer was extracted with chloroform. The solvent was evaporated to give an orange solid. Purification was carried out by chromatography using a silica gel column with 0.5 % methanol in dichloromethane as the eluent, to yield M1 as a yellow solid (0.220 g, 82 %).

^{1}H NMR (400 MHz, CDCl3): δ 8.63 (s, 4H), 8.12-7.99 (m, 8H), 7.71-7.46 (m, 8H), 7.26(s, 2H), 4.29 (t, 4H, J=6Hz), 1.73-0.75 (m, alkyl chain)
^{13}C NMR (400 MHz, CDCl3): δ 155.03, 154.53, 129.62, 129.33, 126.64, 123.66, 122.27, 117.88, 113.85, 80.06, 69.98, 32.02-14.31 (alkyl chain)

HR-MS(ESI): 1068.3207 Analysis: C, 73.02; H, 5.12; N, 8.02; S, 11.08 λ_{max}: 326 nm $\lambda_{Emission\ Max}$: 466 nm (ex. 336 nm)

B2.2.8 Synthesis of Monomer M2

2,6-bis-benzothiazol-2-yl-pyridin-4-ol ligand (2.0 g, 5.5 mM), 1,6-dibromohexane (0.19 mL, 1.26 mM) and Na_2CO_3 (4.1 g) were dissolved into a 10 mL solution of DMSO and stirred at 90°C for 24 hrs (Scheme 6). After removing the heat, the mixture was poured

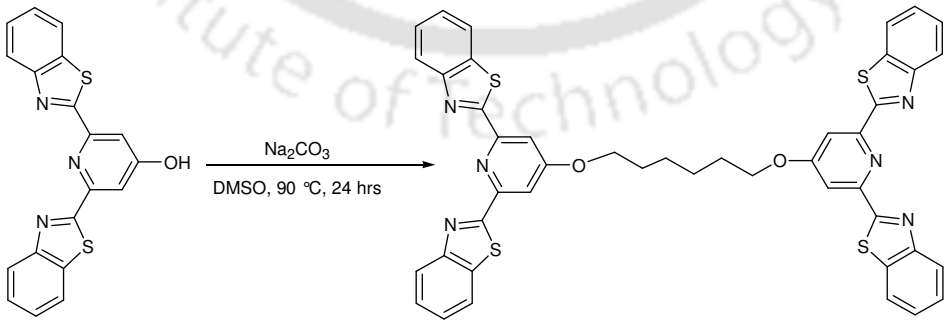

Scheme 6

into 200 mL of half-saturated NH_4Cl and washed with 100 mL of chloroform. The organics were collected and extracted again from a mixture of water and chloroform. The

organics were evaporated and the residue dried under vacuum. The material was purified via column chromatography (100:0 $CHCl_3$:MeOH, 97:3 $CHCl_3$:MeOH) to yield 0.8 g of product as a solid. (68% yield)

^{1}H NMR (400 MHz, $CDCl_3$): δ 8.06 (d, 4H, J=8 Hz), 7.88 (s, 4H), 7.36-7.43 (m, 8 H), 4.24 (t, 4H, J=6.1 Hz), 3.67-3.69 (m, 4H)
^{13}C NMR (400 MHz, $CDCl_3$): δ 166.89, 151.25, 150.64, 142.66, 137.35, 123.72, 122.99, 120.34, 112.06, 110.10, 68.71, 29.43, 25.85

HR-MS(ESI): 804.1502 Analysis: C, 67.42; H, 4.80; N, 9.53; S, 13.78 λ_{max}: 320 nm $\lambda_{Emission\ Max}$: 378 nm (ex. 330 nm)

B2.2.9 Metal titration studies

UV visible spectra and photoluminescence spectra were recorded in solution phase at room temperature using 1:9 acetonitrile chloroform mixed solvent. $Zn(ClO_4)_2$ was as Zn^{2+} slat. For both UV visible and photoluminescence studies, solution of monomers in a mixture of $CH_3CN/CHCl_3$ (1: 9 v/v) was titrated with aliquots of Zn^{2+} in increment of 0.1 equivalents until 1:2 ratio of Monomer: Zn^{2+} where complex was formed and gradual spectral changes were observed.

B2.2.10 Computational work for structural optimization

There are two binding sites in each of the monomers M1 and M2. At one end, there are three possible orientations of the binding atoms in the binding site as a result of rotation of C-C single bond between the benzothiazole and pyridine aromatic rings (Figure 2). The three probable binding site orientations (I, II, III in Figure 2) were optimized by density functional theory [16-17] using Becke's three-parameter hybrid functional with nonlocal correlation of Lee-Yang-Parr [18-19]. Pople's basis set 6-31+G(d) was used for the calculations where diffuse function was added to the heavier atoms i.e. C, N and S to

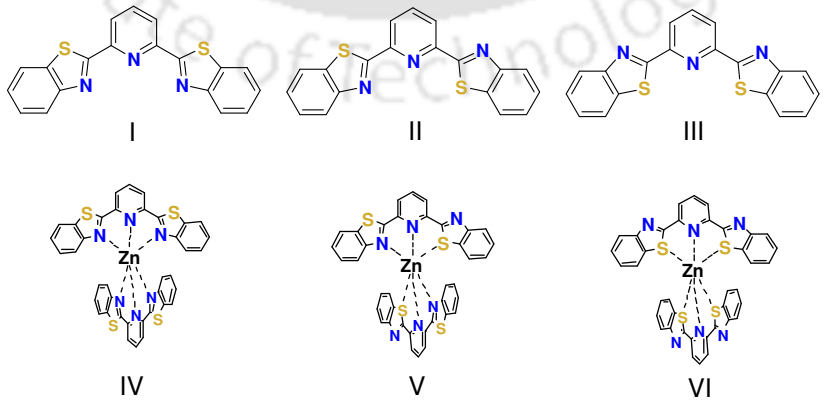

Figure 2 Orientations of binding atoms in structures considered for optimization.

account for the lone pair interactions which affect the dihedral angle between the aromatic rings. Frequency calculations using the same method and basis set were performed. All the calculations were performed without any symmetry constrains. To find out how Zn^{2+} binds, we considered the three orientations (IV, V, VI in Figure 2) of the binding site. Other possible structures should logically have intermediate energies between the two extreme cases of (IV) and (VI) while coordinating to Zn^{2+}. We have also considered one intermediate case (V) for comparison. Following the same method of optimization, as described above, 1:2 stoichiometric complexes of Zn^{2+} ions with the three probable binding site orientations were calculated. All the calculations were carried out using Gaussian 03W program [20].

B2.3 Result and discussion

B2.3.1 UV-visible studies

Stages of the self-assembly could be followed by UV visible spectra. Metallo-supramolecular polymer formation by ditopic M1 and M2 were studied by titrating 0.1 equivalent of Zn^{2+} aliquots per addition into a solution of the monomer in mixed solvent (1:9 acetonitrile/chloroform) and recording the changes in UV-visible spectra.

B2.3.1.1 Titration of M1 with Zn^{2+} ion

In case of M1, increasing concentration of the metal ion progressively decreased the intensity of the absorption band at 326 nm (λ_{max}) (Figure 3). Another two shoulders were

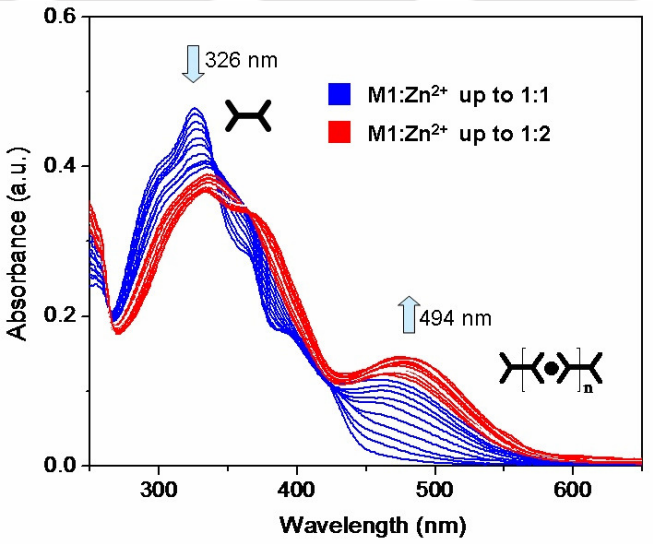

Figure 3 Family of UV visible spectra recorded upon titration of M1 (1 μM) in CH_3CN/ $CHCl_3$ (1:9 v/v) with 0 to 2 equivalents Zn^{2+}

observed at 364 nm and 398 nm that appeared to originate from the chromophore constituted by the 2,6-bis(benzothiazolyl)pyridine moiety and the 1,4-diethynylphenylene spacer. The peak at 326 nm got gradually red shifted, which is due to the formation of stable supramolecular complex between M1 and Zn^{2+}. One new peak at around 494 nm was growing up gradually with additions of Zn^{2+} ion. The family of spectra clearly showed formation of an isosbestic point at 340 nm indicating the presence of species at equilibrium. It was observed that the spectral features reached a limiting value (where the spectral lines started to overlap on each other) around 2.0 equivalents of metal ions. It was noticeable that changes observed in the spectra from 1.1 to 2.0 equivalents metal were less compared to the initial ten additions. Significantly, one shoulder peak of M1 initially present at 364 nm gradually shifted to 374 nm while metal ion was added gradually from 1.1 to 2.0 equivalents. This might have resulted due to the growth of distinct 1:2 complex of M1:Zn^{2+} by dissociation of the 1:1 complexes formed earlier. Thus, the gradual decrease in the band intensity at 326 nm and formation of a new higher intensity band at 494 nm with a clear isosbestic point led us to infer the supramolecular association M1 with Zn^{2+}.

B2.3.1.2 Titration of M2 with Zn^{2+} ion

Similar to M1, binding ability of the ditopic ligand M2 was evaluated by titrating 0.1 equivalent of Zn^{2+} aliquots per addition into a solution of M2 in 1:9 acetonitrile and chloroform solvent mixture and the changes in UV-visible spectra were recorded. On increasing the concentration of the metal ion, the initial absorption band with λ_{max} at 320

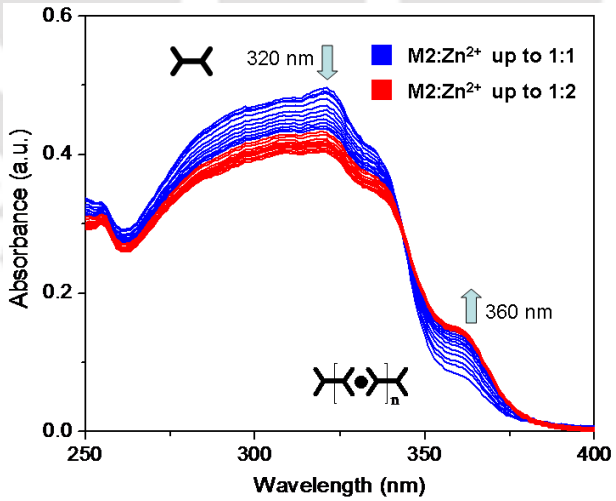

Figure 4 Family of UV visible spectra recorded upon titration of M2 (1 μM) in CH_3CN/ $CHCl_3$ (1:9 v/v) with 0 to 2 equivalents of Zn^{2+}

nm showed gradual decrease in absorption (Figure 4). This family of spectra showed formation of an isosbestic point at 343 nm indicating the presence of at least one species

at equilibrium. It was observed that the spectral features reached a limiting value only around 2.0 equivalents of metal ions (the changes observed in the spectra on addition of 1.1 to 2.0 equivalents metal were very minor compared to the initial ten additions). Thus the gradual decrease in the band intensity at 320 nm and formation of a new higher intensity blue-shifted band at 360 nm with a clear isosbestic point was proof for the formation of metallo-supramolecular complex between monomer M2 and Zn^{2+}.

B2.3.2 Fluorescence Spectroscopy

The metallo-supramolecular polymer formation by ditopic ligand M1 and M2 were studied by titrating 0.1 equivalent of Zn^{2+} aliquots per addition into a solution of the monomer in 1:9 acetonitrile and chloroform mixed solvent and recording the changes in photoluminescence spectra.

B2.3.2.1 Titration of M1 with Zn^{2+} ion

The changes observed in the fluorescence spectra of a solution of M1 in acetonitrile and chloroform solvent mixture on adding up to 2.0 equivalents of Zn^{2+} showed a large

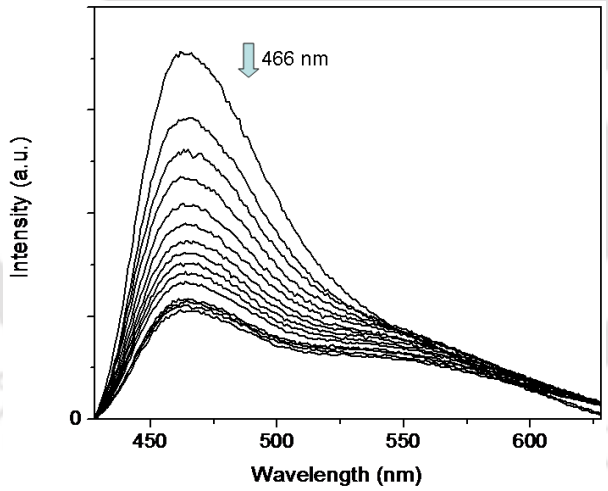

Figure 5 Family of photoluminescence spectra recorded upon titration of M1 (1 μM) in $CH_3CN/CHCl_3$ (1:9 v/v) with 0 to 2 equivalents of Zn^{2+}

quenching in intensity of the 466 nm band (Figure 5). This indicated interaction between M1 and Zn^{2+} by formation of metallo-supramolecular complex. The excited state was modified significantly leading to visual change resulted from high quenching of fluorescence (Figure 6). The spectra showed a significant gradual broadening. The changes observed in the fluorescence spectra on adding more than 1 equivalent of $Zn(ClO_4)_2$ aliquots to M1 were less insignificant, which is in good agreement with the results of UV visible titration results.

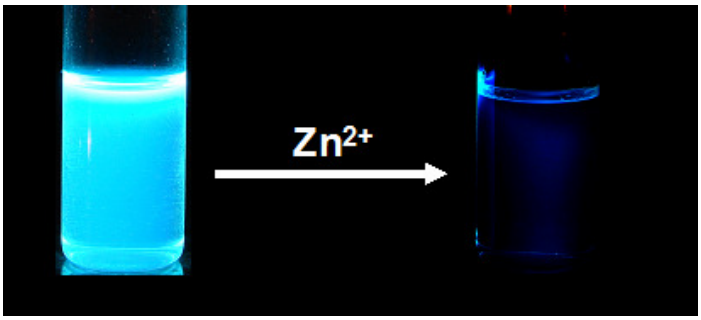

Figure 6 Visual changes observed under UV light while 2 equivalents of Zn^{2+} is added to M1

B2.3.2.2 Titration of M2 with Zn^{2+} ion

Fluorescence spectra of a solution of M2 in 1:9 acetonitrile and chloroform solvent mixture on addition Zn^{2+} ion up to 2.0 equivalents showed a large quenching in intensity of the 378 nm band (Figure 7). This quenching indicates interaction between M2 and Zn^{2+} ion. With gradual addition of the metal ions, the excited state was modified considerably leading to the quenching of fluorescence. The changes observed in the fluorescence spectra on adding more than 1 equivalent of Zn^{2+} aliquots to M2 were less significant, which is in good agreement with the results of UV visible titration.

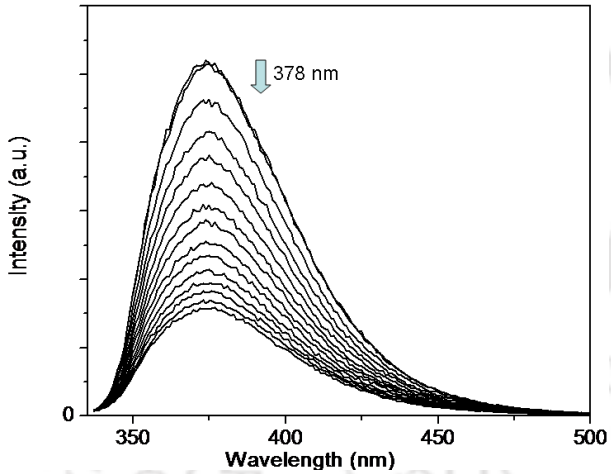

Figure 7 Family of photoluminescence spectra recorded upon titration of M2 (1 μM) in $CH_3CN/CHCl_3$ (1:9 v/v) with 0 to 2 equivalents of Zn^{2+}

B2.3.3 Viscosity measurements

Viscosity changes, on addition of Zn^{2+} ion, were measured for both M1 and M2 at low concentrations (1 μM). Acetronitrile and chloroform mixture solution (1:9) of M1 showed initial viscosity of 0.563 mPa s (Figure 8) . On gradual addition of Zn^{2+} ions, viscosity gradually increased. At 1:1 ratio of M1 : Zn^{2+}, the viscosity reached a maximum value of 1.12 mPa s. Increase of viscosity value was supportive of supramolecular polymer

formation by M1 upon addion of Zn^{2+} ion. On further addition of Zn^{2+} ion, the viscosity started decreasing from the maximum value. At 1:2 ratio of M1 : Zn^{2+}, the viscosity found to decrease up to 0.743 mPa s. This observation led to comment that, at 1:1 ratio of M1:Zn^{2+}, supramolecular polymer was formed which on further addition of metal ions dissembled and reached a minimum at 1:2 ratio. This is in good agreement with the changes observed in UV visible spectroscopy. Similar experiments with M2 resulted in similar trend. The viscosity of pure monomer solution increased to 0.660 mPa s in its 1:1 complex with Zn^{2+} ion from original 0.532 mPa s value. Again, like in the case of M1, on

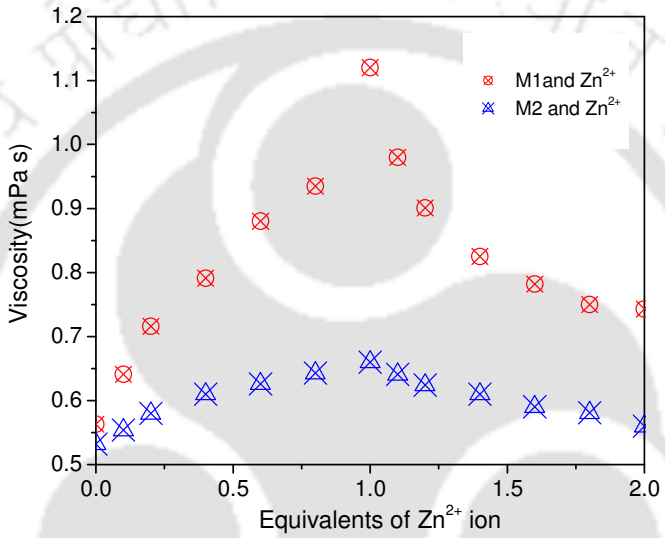

Figure 8 Gradual change in viscosity while M1 (red) and M2 (blue) were titrated with Zn2+ ion from 0 to 2 equivalents

further addition of Zn^{2+} ion, the viscosity decreased to 0.560 mPa s in the 1:2 complex. But significantly, the increase in viscosity at 1:1 complex in much less in this case while compared with M2. This observation lead to think that due to the flexible spacer in M2, it

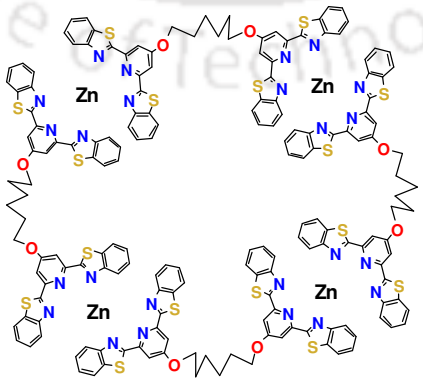

Figure 9 Possible cyclic association of M2 with Zn^{2+} ion

was not much effective in forming one dimensional polymeric system in comparison to M1. May be the flexible spacer helps in bending of the monomer M2 and reduces the number of possible monomer addition by formation of cyclic associations with less number of constitutional units (Figure 9).

B2.3.4 Computational work for structural optimization

The optimized structures of binding moiety with three different binding atom orientations and its 2:1 complex were found to be as shown in Figure 10. Geometry optimizations showed that in the free monomer, both the S atoms were present inside the binding site of the binding moiety and lead to minimum energy (III in Figure 10). This might be because of minimization of repulsion of the bigger S atoms with the π electron cloud of the pyridine ring while they were present inside the binding site. But in case of the 2:1 complex of the binding moiety with Zn^{2+}, the lowest energy orientation was found to be one, where all the N atoms are inside the binding site (IV in Figure 10) and coordinated to the metal ion. If smaller N atoms were present inside the binding site, Zn^{2+} ion got less hindrance and hence could approach maximum into the binding site. While bigger S atoms were present inside the binding site, maximum repulsion took place between the electron cloud of the metal ion and the electron clouds of the S atoms (VI in Figure 10).

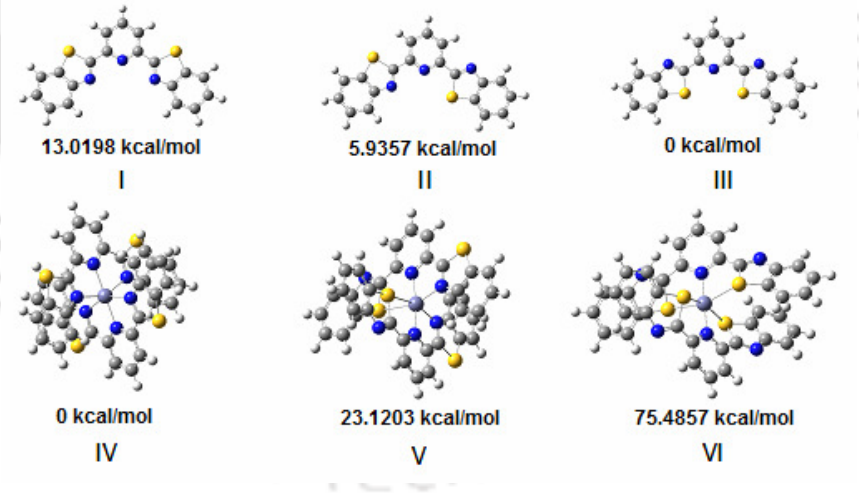

Figure 10 Optimized structures of binding moiety and Zn^{2+} complex of binding moiety with their respective relative energies

This resulted in high energy situation and the binding moiety in complex VI is twisted where the dihedral angles between the aromatic rings found to be in the range from 28.92 to 30.36°. In case of one intermediate situation (V in Figure 10), from among the other possible structural orientations, showed intermediate energy value as expected. Now it is evident that even though monomers M1 and M2 in its free states have the S atoms inside the binding site at both the ends of the monomer, they cannot involve

in complexation in this way. While forming polymer by metal mediation, the binding atom orientations in side the binding site must be as shown in VI. (Add. Data 1-6, incorporated in the CD attached)

B2.4 Concluding remark

Two new monomers, M1 and M2 with benzothiazole based binding sites were synthesized and characterized. Both the monomers were found to self assemble in solution with Zn^{2+} ion forming metallo-supramolecular polymers. Experimental results showed that M1 was more effective in forming long supramolecular associations compared to M2. This difference in polymer forming ability was predicted to be due to the flexibility of the hexyl spacer part in M2 which might have led to cyclic associations of smaller numbers of monomers. The bis-benzthiazole based binding moiety on energy optimization showed that in uncomplexed free state, the bigger S atoms oriented inside the binding site. While they formed complex with metal ion, the smaller N atoms oriented inside.

References

[1] Brunsveld, L.; Folmer, B. J. B.; Meijer, E. W.; Sijbesma, R. P. *Chem. Rev.* **2001**, 101, 4071.

[2] Ciferri, A. *Macromol. Rapid Commun.* **2002**, 23, 511.

[3] Hofmeier, H.; Schubert, S. *Chem. Commun.* **2005**, 2423.

[4] Hofmeier, H.; Hoogenboom, R.; Wouters, M. E. L.; Schubert, U. S. *J. Am. Chem. Soc* **2005**, 127, 2913.

[5] Gerhardt, W.W.; Zucchero, A. J.; Wilson, J. N.; South, C. R.; Bunz, U.H. F.; Weck, M. *Chem. Commun.*, **2006**, 2141.

[6] Schmatloch, S.; González, M.; Schubert, U. S. *Macromol. Rapid Commun.* **2002**, 23, 957.

[7] Schmatloch, S.; van den Berg, A.; Alexeev, A. S.; Hofmeier, H.; Schubert, U. S. *Macromolecules* **2003**, 36, 9943.

[8] Hofmeier, H.; Schmatloch, S.; Wouters, D.; Schubert, U. S. *Macromol. Chem. Phys.* **2003**, 204, 2197.

[9] Beck, J. B.; Rowan, S. J. *J. Am. Chem. Soc* **2003**, 125, 13922.

[10] Iyer, P. K.; Beck, J. B.; Weder, C.; Rowan, S. J. *Chem. Commun.* **2005**, 319.

[11] Rana, A.; Siddiqui, N.; Khan, S. A. *Indian Journal of Pharmaceutical Sciences* **2007**, 69 (1), 10.

[12] Drew, M. G. B.; Hill, C.; Hadson, M. J.; Iveson, P. B.; Madic, C.; Vaillant, L.; Youngs, T. G. A. *New J. Chem* **2004**, *28*, 462.

[13] Armarego, W. L. F.; Perrin, D. D. *Purification of Laboratory Chemicals; Butterworth-Heinemann*: Burlington, MA, **2002**.

[14] Addison, A. W.; Burke, P. J. *J. Heterocycl. Chem.* **1981**, 18, 803.

[15] Addison, A. W.; Rao, T. N.; Wahlgren, C. G. *J. Heterocycl. Chem.* **1983**, 20, 1481.

[16] Hohenberg, P.; Kohn, W. *Phys. Rev. B* **1964**, 136, 864.

[17] Kohn, W.; Sham, L. *J. Phys. Rev. A* **1965**, 140, 1133.

[18] Becke, A. D. *J. Chem. Phys.* **1993**, 98, 5648.

[19] Lee, C.; Yang, W.; Parr, R. G. *Phys. Rev. B*, **1988**, 37, 785.

[20] Frisch, M. J.; Trucks, G. W.; Schlegel, H. B.; Scuseria, G. E.; Robb, M. A.; Cheeseman, J. R.; Montgomery, J. A.; T. Vreven; Kudin, K. N.; Burant, J. C.; Millam, J. M.; Iyengar, S. S.; Tomasi, J.; Barone, V.; Mennucci, B.; Cossi, M.; Scalmani, G.; Rega, N.; Petersson, G. A.; Nakatsuji, H.; Hada, M.; Ehara, M.; Toyota, K.; Fukuda, R.; Hasegawa, J.; Ishida, M.; Nakajima, T.; Honda, Y.; Kitao, O.; Nakai, H.; Klene, M.; Li, X.; Knox, J. E.; Hratchian, H. P.; Cross, J. B.; Bakken,

V.; Adamo, C.; Jaramillo, J.; Gomperts, R.; Stratmann, R. E.; Yazyev, O.; Austin, A. J.; Cammi, R.; Pomelli, C.; Ochterski, J. W.; Ayala, P. Y.; Morokuma, K.; Voth, G. A.; Salvador, P.; Dannenberg, J. J.; Zakrzewski, V. G.; Dapprich, S.; Daniels, A. D.; Strain, M. C.; Farkas, O.; Malick, D. K.; Rabuck, A. D.; Raghavachari, K.; Foresman, J. B.; Ortiz, J. V.; Cui, Q.; Baboul, A. G.; Clifford, S.; Cioslowski, J.; Stefanov, B. B.; Liu, G.; Liashenko, A.; Piskorz, P.; Komaromi, I.; Martin, R. L.; Fox, D. J.; Keith, T.; Al-Laham, M. A.; Peng, C. Y.; Nanayakkara, A.; Challacombe, M.; Gill, P. M. W.; Johnson, B.; Chen, W.; Wong, M. W.; Gonzalez, C.; Pople, J. A. *Gaussian 03*, *Revision E.01*, Gaussian, Inc., Wallingford CT, **2004**.

Chapter B3

GUEST SELECTIVE RECOGNITION OF RESORCINOL BY 1,6-BIS(2,6-BIS(BENZOTHIAZOL-2-YL)PYRIDINE-4-YLOXY)HEXANE

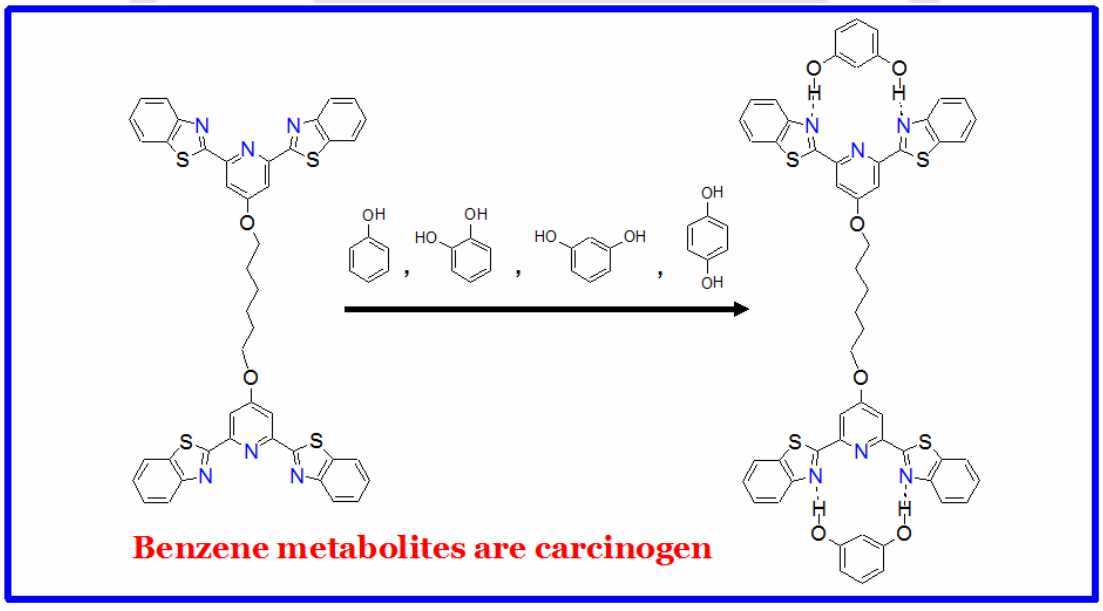

Benzene and its metabolites induce breakage and rearrangement of chromosomes in human, animal and yeast cells leading to cancer. In this chapter, monomer 1,6-bis(2,6-di(benzo[d]thiazol-2-yl)pyridin-4-yloxy)hexane is shown to be capable of selectively recognizing resorcinol from the other benzene metabolites like phenol, hydroquinone and catechol. Results of UV visible, photoluminescence and NMR spectroscopic techniques are discussed to establish this guest selective recognition.

B3.1 Prologue

Molecular receptors can be defined as organic structures which can bind selectively ionic or molecular substrates (or both) by means of various intermolecular interactions to form a supramolecule. Receptor chemistry extends to all types of substrates: cationic, anionic, or neutral molecules of organic, inorganic, or biological nature [1]. Receptors recognize a guest by various supramolecular interactions [2-7]. Unlike covalent forces, these forces are weaker and are easily disrupted. Achievements of molecular recognition depend on the design of molecular receptors so that it can create numerous non-covalent binding interactions with the guest molecule and sense its molecular size, shape and architecture. Receptor should contain some intramolecular cavities, clefts or pockets to which guest molecule can fit in, which basically acts as the binding site to the guest molecule. Another significant point is the flexibility of supramolecular systems which is of great importance in biological receptor-substrate interactions. More selective a receptor for a particular guest, more useful for its application in separations. Therefore, designing receptors which selectively recognize toxic molecules is an important area of research.

Benzene and its metabolites are carcinogens, known to cause the breakage and rearrangement of chromosomes in human, animal and yeast cells. Besides their carcinogenic properties, these metabolites of benzene are present in several naturally occurring biomolecules such as Coenzyme Q (CoQ), in the form of hydroquinone or quinone fragments in their structures, due to which they are able to undergo redox interconversions in the living cells [8]. In spite of their important relevance to biology, there are very few synthetic receptors that form supramolecular adducts with all these small phenolic compounds [9-10]. Synthetic receptor, 2,6-bis(benzimidazol-2-yl)pyridine,

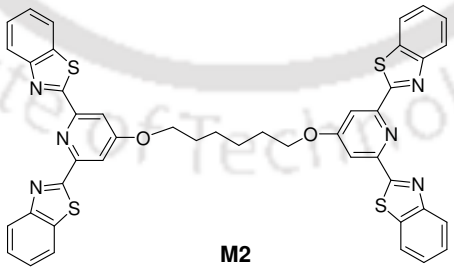

M2

Figure 1 1,6-bis(2,6-di(benzo[d]thiazol-2-yl)pyridin-4-yloxy)hexane ligand

capable to recognize phenol, catechol, hydroquinone and resorcinol was reported [11]. Here we report that ligand 1,6-bis(2,6-di(benzo[d]thiazol-2-yl)pyridin-4-yloxy)hexane (M2) (Figure 1) which contains 2,6-bis(benzothiazolyl)pyridine moiety as the binding unit and a aliphatic hexyl chain as the spacer is capable of recognizing resorcinol

(guest) selectively among the other benzene metabolites like phenol, hydroquinone and catechol. Simple spectroscopic techniques such as UV-visible and photoluminescence spectra are used as tools to follow the selective recognition process.

B3.2 Experimental Section

B3.2.1 Chemicals and solvents

All reagents were used as received without further purification unless otherwise mentioned. Solvents were used after purifications by standard purification techniques [12].

B3.2.2 Preparation of ditopic ligand M2

Ditopic ligand M2 has been prepared by a method as described in Chapter B2 (B2.2.8) of this thesis from 2,6-bis-benzothiazol-2-yl-pyridin-4-ol ligand prepared by a known literature method [13-14].

B3.2.3 Instrumentation

UV visible spectra were recorded on a Perkin-Elmer Lamda 25 UV-Vis spectrophotometer at room temperature. Photoluminescence studies were done using a Varian Cary Eclipse Fluorescence Spectrophotometer. NMR experiments were done using a Varian Mercury 400 MHz NMR spectrometer.

For both UV visible and florescence studies, solution of M2 was made in 1:1 acetonitrile and chloroform mixed solvent. Concentration of monomer was maintained at 6.67×10^{-5} M for UV visible studies, and it was maintained at around 6.90×10^{-7} M for photoluminescence studies.

B3.3 Result and discussion

B3.3.1 UV visible spectroscopy

The binding ability of receptor M2 was evaluated by titrating 0.1 equivalents of resorcinol aliquots into a solution of the receptor in dry acetonitrile/chloroform (1:1) at regular intervals and recording the changes in UV visible spectra. It was observed that on increasing the concentration of resorcinol, progressive decrease of intensity in the initial absorption band having λ_{max} at 320 nm associated with the π-π^* transition resulted. Concurrently, with gradual addition of the guest, a new peak at 282 nm with its shoulder at 277 nm developed gradually. The intensity of the peak positioned at 282 nm gradually increased and its shoulder finally came up as a distinct peak at 277 nm. This family of

spectra, as a result of addition of guest to the receptor, showed clear formation of an isosbestic point at 287 nm indicating the presence of at least one species at equilibrium.

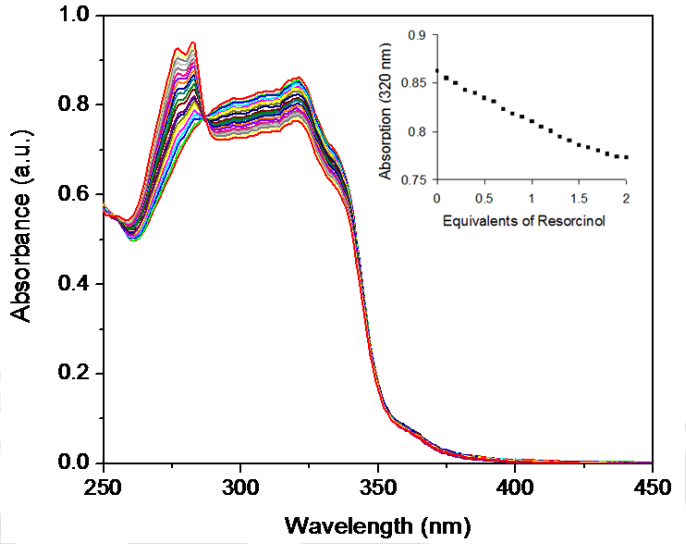

Figure 2 UV visible spectra of M2 during titration with resorcinol from 0-2 equivalents (v/v). Inset shows the titration profile of the band at 320 nm corresponding to M2: resorcinol H-bonded complex.

This is well indicative for the formation of stable complex between receptor M2 and resorcinol. The inset in Figure 2 shows the changes in titration profile of the band at 320 nm corresponding to M2:Resorcinol complex. Thus, the gradual decrease in the band intensity at 320 nm and formation of a new higher intensity blue-shifted band at 282 nm with a clear isosbestic point is proof for the formation of hydrogen-bonded complex between M2 and resorcinol. The association constant (K_a) for the 1:2 complex was calculated to be 617 M^{-1} using Eq. 1, [15] where A_o is the absorbance of the monomer, A is the absorbance of the monomer-resorcinol complex, C_M is the concentration of the monomer, C_C is the concentration of the monomer-resorcinol complex and C_g is the concentration of the guest (resorcinol).

$$\frac{A_0}{A - A_0} = \left(\frac{C_M}{C_C - C_M}\right)\left[\frac{1}{K_a C_g} + 1\right] \quad (1)$$

These observations indicate that there were interactions between the resorcinol and the receptor M2. The lower concentrations at which these spectroscopic changes were observed clearly reveal that receptor M2 possesses excellent properties as a host material for recognizing phenolic guests with high affinity.

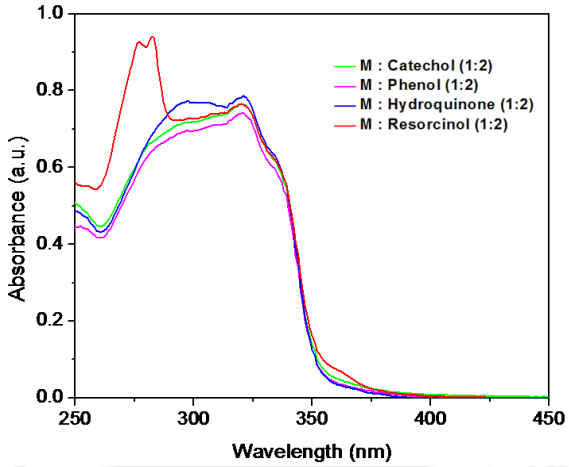

Figure 3 UV visible spectra of 1: 2 complex of M with catechol, phenol, hydroquinone and resorcinol.

Similar UV visible titration experiments of M2 were also performed with phenol, catechol and hydroquinone. Figure 3 shows the titration curves of 1:2 complex of receptor M2 with phenol, catechol and hydroquinone. Titration curve of M2 with resorcinol is also placed for comparison. Except in the case for resorcinol, other benzene metabolite neither showed formation of new peaks nor do they show decrease of absorption intensity upon addition to M2. While all (catechol, phenol, hydroquinone and resorcinol) were added together, change observed in UV- visible spectra was similar to the change as observed for only resorcinol. This clearly reveals selective binding of only resorcinol among the other benzene metabolites.

B3.3.2 Photoluminescence spectroscopic studies

Fluorescence titration is an easy method to monitor the supramolecular host guest complexation. On gradual addition of resorcinol to a solution of M2 in acetronitrile and

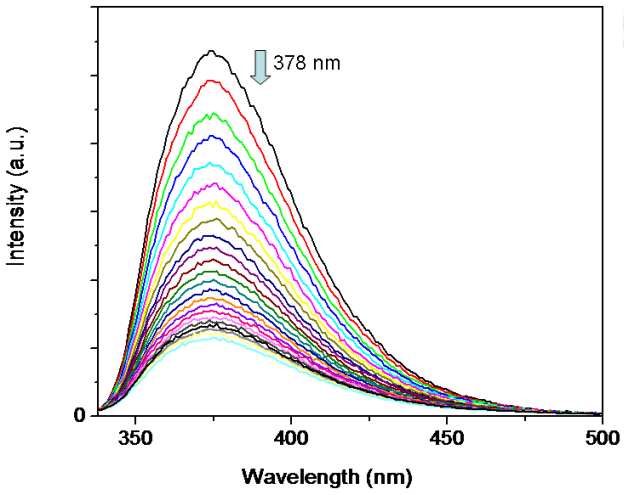

Figure 4 Emission spectra of M2 during the titration with resorcinol from 0-2 equivalents (v/v).

chloroform (1:1) mixed solvent up to 2 equivalents of resorcinol shows significantly large quenching in fluorescence intensity of the 378 nm band (Figure 4). This indicates formation of the donor-acceptor complex between resorcinol and M2, where the excited state is modified leading to the quenching of fluorescence.

The changes in the fluorescence spectra on adding further aliquots of resorcinol to M2 were very minor. Therefore, formation of donor-acceptor supramolecular complex modifies the optical properties of M2 in solution and could be employed for probing neutral guests.

B3.3.3 NMR spectroscopy

NMR spectroscopic studies were performed to follow the supramolecular recognition process. NMR spectra were recorded in solution phase using 1:9 acetonitrile and chloroform mixed solvent. The receptor M2 originally contains peaks at δ 8.06 (d, 4H), 7.88 (s, 4H) and 7.36-7.43 (m, 8H) in the aromatic region (Figure 4). Moreover, it contains two other significant peaks at δ 4.24(t, 4H) and 3.67-3.69 (m, 4H)) resulting from the two different types of -CH_2 protons nearer to the aromatic rings. While M2 titrated with resorcinol, the peak at δ 8.06 (benzene ring proton nearest to N atom) started shifting gradually towards up field and at 1:2 ratio of M1:resorcinol it finally reached a value of δ 8.00. One other aromatic multiplet also shifted to δ 7.20-7.36 form its original value of δ 7.36-7.43. The O-CH_2 peak at δ 4.24 shifted towards maximum and reached δ 4.03. The CH_2 present next to this, initially showing a multiplet at δ 3.67-3.69 also got modified significantly by shifting itself to δ 3.58-3.59 upon addition of 2 equivalents of

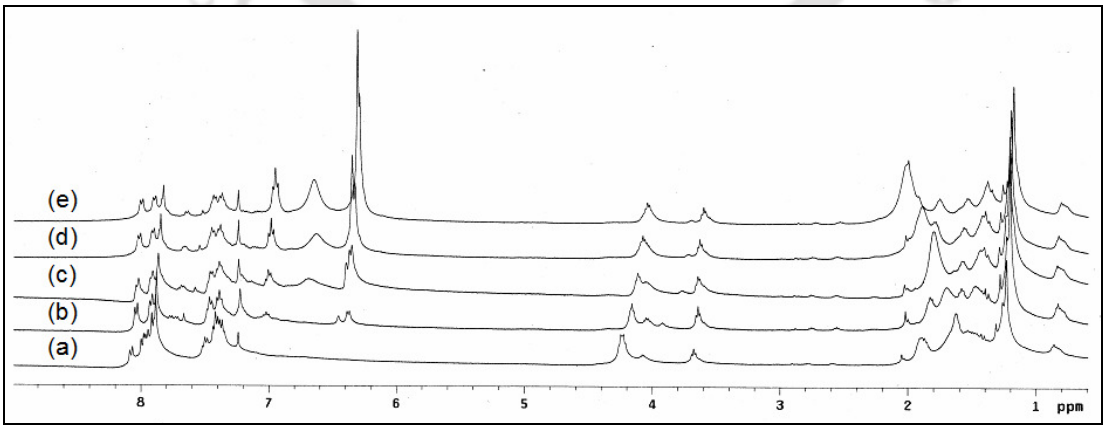

Figure 4 Changes in NMR spectra of (a) M2 (b) M2 with 0.5 equivalent of Resorcinol (c) M2 with 1.0 equivalent of Resorcinol (d) M2 with 1.5 equivalent of Resorcinol and (e) M2 with 2.0 equivalent of Resorcinol

resorcinol. Another new peak at δ 6.64, which was initially absent in the M2 spectra, started growing with gradual addition of resorcinol. This peak showed a regular broadening with an increase in its area. This is supportive of the formation of H-bonds between the monomer and the guest molecule. These changes in the spectral pattern, as observed clearly in the NMR titrations, definitely confirms association of resorcinol with M2 via hydrogen bonding interactions.

B3.3.4 Plausible binding mechanism

Chetia et al. [11] reported that 2,6-Bis(2-benzimidazolyl)pyridine (Figure 5a) has the ability to detect toxic benzene metabolites such as phenol, hydroquinone, resorcinol, catechol and p-benzoquinone from solution of acetonitrile. They also reported that the ligand was the highest affinity receptor which bonded hydroquinone solely through

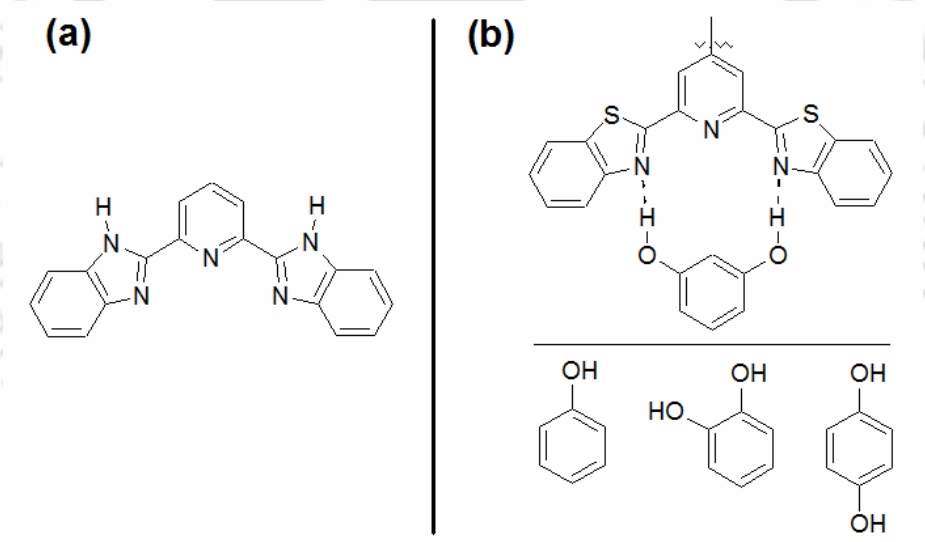

Figure 5 (a) Ligand reported by Chetia et al. (b) Selective binding of resorcinol by of M3 at binding sites.

Hydrogen bonds (binding constant, 441 M^{-1}). In our case, the two binding sites of the monomer M2 is much similar to that of the reported ligand (Figure 5b). M2 binds only with resorcinol selectively as confirmed by our spectroscopic measurements. Moreover, binding constant value (617 M^{-1}) observed in this case is much higher. We propose that the two OH hydrogen of the resorcinol may be at a distance that may be appropriate to form a chelate complex by two hydrogen bonds with the two N atoms of the binding site of M2 (Figure 5b). In earlier chapters also, we have seen that while forming metal complexes, the orientation of the N atoms preferably becomes inside the binding site.

Here, in the M2-resorcinol complexation, a similar orientation may be possible. This type of orientation will lead to stable supramolecular complex with M2 by virtue of its chelate formation. Hydroquinone and catechol, even though have two OH hydrogens, does not form such stable supramolecular complexes as the distance of the OH hydrogen atoms may restrict formation of chelate rings. Phenol, on the other hand, has only one OH group and therefore is incapable to form chelate ring type complex. Ligand M2 has the advantage of having at least two binding sites in it which can bind two resorcinol molecules simultaneously. Moreover, the parent ligand of monomer M2 (2,6-bis-benzothiazol-2-yl-pyridin-4-ol ligand) had problem with solubility in common organic solvents. It may be due to presence of two S atoms in the big aromatic system. Therefore we could not apply the parent compound for similar recognition studies. The hexyl spacer in M2 increases its solubility in common organic solvents enabling screening of the other benzene metabolites other than resorcinol.

B3.4 Concluding remark

In summary, M2 ligand has been shown as a guest selective receptor, capable of selectively recognizing resorcinol from among all the other toxic metabolites of benzene with high sensitivity and selectivity. Binding constant calculation shows M2 has high affinity for resorcinol due to chelate ring formation via hydrogen bonds. Simple method of preparation, selectivity with high sensitivity, significant binding strength and ease in molecular recognition makes M2 and exclusive and extremely efficient receptor for the detection of resorcinol.

References

[1] Lehn, J.-M. *Perspecitives in Coordination Chemistry*, (Eds.: Williams, A. F.; Floriani, C. ; Merbach, A. E.), VHCA, Basel, and VCH: Weinheim **1992**.

[2] Rebek Jr, *J. Angew. Chem. Int. Ed. Engl.* **1990**, *29*, 245.

[3] Vögtle, F. *Suparmolecular Chemistry*,John Wiley & Sons: New York **1991**.

[4] Amabilino, D. B.; Stoddart, J. F. *Chem. Rev.* **1995**, *95*, 2725.

[5] Fyfe, M. C. T.; Stoddart, J. F. *Acc. Chem. Res.* **1997**, *30*, 393.

[6] Harada, A.; Li, J.; Kamachi, M. *Nature* **1992**, *356*, 325.

[7] Harada, A.; Li, K.; Kamachi, M. *Nature* **1994**, 370, 126.

[8] Ramasarma, T.; Lester, R.L. *J. Biol. Chem.* **1960**, *235*, 3309.

[9] Kerckhoffs, J.M.C.A.; Ishi-I. T.; Paraschiv, V.; Timmerman, P.; Crego-Calama, M.; Shinkai, S.; Reinhoudt, D.N. *Org. Biomol. Chem.* **2003**, *1*, 2596.

[10] Krasowski, Matthew D.; Hong, Xuan; Hopfinger, A.J.; Harrison, N. L. *J. Med. Chem.* **2002**, *45(15)*, 3210.

[11] Chetia, B.; Iyer, P. K. *Tetrahedron Lett.* **2007**, *48*, 47.

[12] Armarego, W. L. F.; Perrin, D. D. *Purification of Laboratory Chemicals*; Butterworth-Heinemann: Burlington, MA, **2002**.

[13] Addison, A. W.; Burke, P. J. *J. Heterocycl. Chem.* **1981**, *18*, 803.

[14] Addison, A. W.; Rao, T. N.; Wahlgren, C G. *J. Heterocycl. Chem.* **1983**, *20*, 1481.

[15] Chou, P. T.; Wu, G.R.; Wei, C.Y.; Cheng, C.C.; Chang, C.P.; Hung, F.T. *J. Phys. Chem. B* **2000**, *104*, 7818.

Chapter B4

SELF ASSEMBLING METALLO-SUPRAMOLECULAR POLYMER AND FOLDAMER GELS ASSISTED BY ALKALI AND TRANSITION METAL

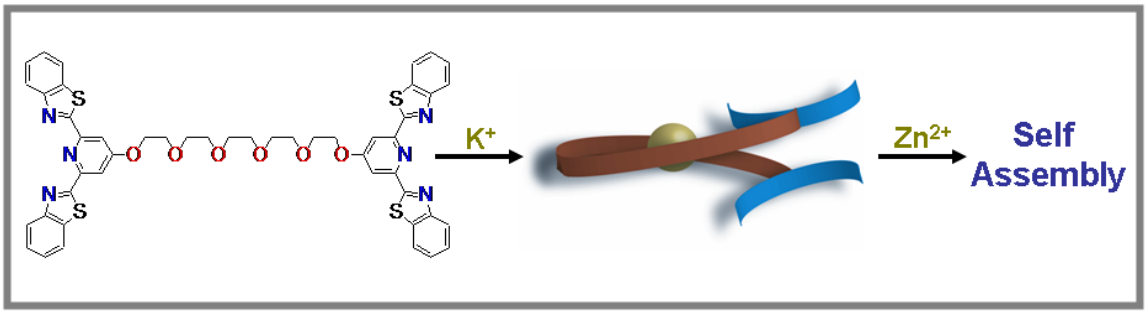

A novel ditopic ligand having benzothiazole based binding site and pentaethylene glycol chain as a spacer shows remarkable propensity to fold in solution by supramolecular interaction selectively upon addition of K^+. Monomer – K^+ folded unit self assemble upon addition of Zn^{2+} ion results supramolecular polymeric system. UV visible spectroscopy, fluorescence spectroscopy and viscosity measurements were used to follow the whole self assembly process. The 1: 1: 1 complex of Monomer : K^+ : Zn^{2+} in high concentrations results in gel formation. This gel was characterized by morphological studies by FESEM macrograph and EDX measurements. Structure optimization of the Monomer – K^+ folded system and energy optimization of the binding site after Zn^{2+} complexation were done using DFT calculations to support our experimentally observed results.

B4.1 Prologue

Nature relies on large molecules to carry out sophisticated chemical operations, such as catalysis, tight and specific binding, directed flow of electrons, or controlled crystallization of inorganic phases. The polymers entrusted with these crucial tasks, mostly proteins but sometimes RNA, are unique relative to other biological and synthetic polymers in that they adopt specific compact conformations that are thermodynamically and kinetically stable [1]. Nowadays, inspired by folding properties of the biological molecules like proteins and others, chemists are actively engaged in the design, synthesis and detailed characterization of artificial systems that utilize non covalent forces to modulate folding and assembly [2-4]. Towards these goals, chemists have endeavored to intentionally generate unnatural oligomeric sequences that take on well-defined conformations in solution [5]. A term 'foldamer' is used for some synthetic oligomers that adopt ordered conformations in solution due to noncovalent interactions [6]. They often possess unique functionality resulting from their folded structures, similar to biological macromolecules [7-9]. Foldamers provide important insights into the fundamentals of noncovalent folding, which is of primary importance for understanding biological systems and developing novel self-assembling materials. The literature so far available in this comparatively new area report indirect solution phase spectroscopic methods supported by theoretical studies as the basic methodology to establish foldameric systems [10-11].

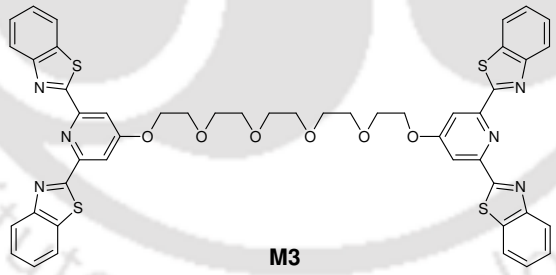

Figure 1 Ditopic monomer M3 comprising of 2,6-di(benzo[d]thiazol-2-yl)pyridine as binding site.

This work explains, selective binding of alkali metal and this alkali metal mediated folding of a monomer with non covalent interaction. The folded system further could be successfully self assembled by transition metal mediation to form novel supramolecular polymeric system. Monomer M3, synthesized in our lab, folds up at the ethereal spacer part on addition of K^+ ion (Figure 1). Subsequent self assembly of the M3 - K^+ folded system on further addition of Zn^{2+} ion resulted a novel metallo-supramolecular polymeric system.

B4.2 Experimental Section

B4.2 .1 Chemicals and solvents

All chemicals unless otherwise mentioned, were used as received. All solvents including chloroform and methanol were used after purification by standard purification techniques [12].

B4.2 .2 Instrumentation

UV-Visible spectra were recorded on a Perkin-Elmer Lambda 25 UV Visible spectrophotometer at room temperature. Photoluminescence studies were done using a Varian photoluminescence spectrophotometer. Scanning electron microscopic images were recorded in a field emission scanning electron microscope. Samples were prepared on small glass plate wrapped with aluminum foil. The samples were next dried under vacuum. Before analysis the samples were coated with gold. Transmission electron microscopic studies were done using a JEOL 2100 transmission electron microscope. Viscosity measurements were done in micro molar concentration using a m-VROC RheoSense, Inc viscometer.

B4.2 .3 Preparation of bis-p-Tosyl-penta(ethyleneglycol) from pentaethyleneglycol

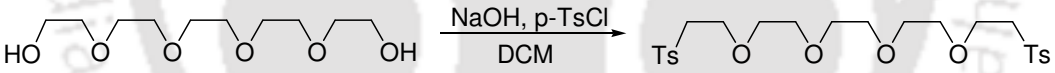

Scheme 1

Pentaethylene glycol (1.13 g, 4.74 mM) was dissolved in DCM and in ice cold condition p-TsCl (3.0 g, 15.73 mM) was added to it and stirred for 20 mins. Then in cold condition powdered NaOH (3.0 g) was added and stirred. After 12 hrs, ice cold water and DCM was added to the reaction mixture. The organics were collected and the water part was extracted with DCM repeatedly. Solvents were evaporated and the residue was dried under vacuum. The product was purified via column chromatography (100:0 Hexane : Ethylacetate, upto 50:50 Hexane : Ethylacetate) to give 2.4 g of the product. (93% yield)

^{1}H NMR (400 MHz, CDCl3): δ 7.77 (d, 4H), 7.32 (d, 4H), 4.12 (t, 4H), 3.66 (t, 4H), 3.55-3.57 (m, 12H), 2.41 (s, 6H).

^{13}C NMR (400 MHz, CDCl3): δ 144.7, 132.7, 129.7, 127.8, 70.6, 70.5, 70.3, 69.1, 68.4, 21.5.

B4.2 .4 Preparation of bisiodo(ethylene glycol)

Bis-p-Tosyl-penta(ethylene glycol) (1.00 g, 1.83 mM) was dissolved in acetone and slowly

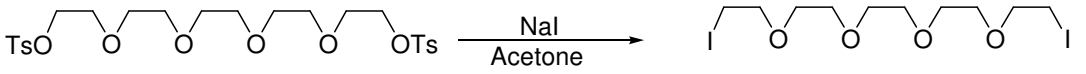

Scheme 2

NaI was added to the solution and stirred for 48 hrs. Water was added after removal of the solvent and the product was extracted using chloroform. The solvent was evaporated to give the product to yield 0.8 g of product as a liquid. (96% yield)

^{1}H NMR (400 MHz, CDCl3): δ 3.73 (t, 4H), 3.24 (t, 4H), 3.64-3.65 (m, 12H)
^{13}C NMR (400 MHz, CDCl3): δ 70.6, 70.5, 70.3, 69.1, 68.4.

B4.2 .5 Preparation of monomer M3

2,6-bis-benzothiazol-2-yl-pyridin-4-ol ligand (2.0g, 5.53 mM) and bisiodopenta (ethylene glycol) (0.58 g, 1.26 mM) were dissolved into a solution of Na_2CO_3 (4.1 g) in 10 mL of DMSO and stirred at 90°C for 24 hrs. After removing from heat, the mixture was poured into 200 mL of half-saturated NH_4Cl and washed with 100 mL of chloroform. The

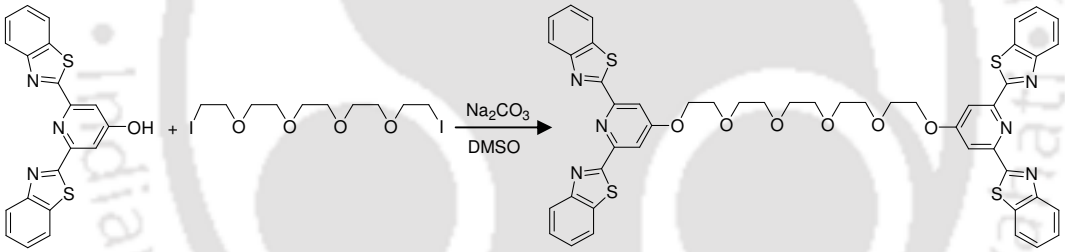

Scheme 3

organics were collected and extracted again from a mixture of water and chloroform. Solvents were evaporated and the residue dried under vacuum. The material was purified via column chromatography (100:0 CHCl3:MeOH 97:3 CHCl3:MeOH) to yield 0.8 g of product as a solid. (68% yield)

^{1}H NMR (400 MHz, CDCl3): δ 8.01 (d, 4H, J=8 Hz), 7.89 (d, 4H, J=6.4 Hz), 7.87 (s, 4H), 7.44 (t, 4H, J=6.6 Hz), 7.35 (t, 4H, J=7.4 Hz), 4.37 (t, 4H, J=6 Hz), 3.75 (t, 4H, J=6.2 Hz), 3.93 (t, 4H, J=6 Hz), 3.71-3.68 (m, 8H).
^{13}C NMR (400 MHz, CDCl3): δ 168.73, 166.08, 154.33, 152.70, 136.63, 126.37, 125.85, 123.81, 122.08, 108.39, 71.2, 70.8, 69.2, 68.4.

HR-MS(ESI): 924.1621 Analysis: C, 63.28; H, 4.52; N, 10.22; S, 15.34 λ_{max}: 322 nm $\lambda_{Emission\ Max}$: 387 nm (ex. 332 nm)

B4.2 .6 Metal titration studies

UV-visible spectra and photoluminescence spectra were recorded in solution phase at room temperature using 1:9 acetonitrile chloroform mixed solvent. For both UV visible and photoluminescence studies, solution of M3 in a mixture of $CH_3CN/CHCl_3$ (1: 9 v/v) was titrated with aliquots of KSCN in a solution of the same composition. Changes were monitored till 1: 1 ratio of M: K^+ is reached. At a 1:1 ratio of M: K^+, started adding aliquots of Zn^{2+} in increment of 0.1 equivalents. The addition was done until 1:1:1 ratio of M: K^+: Zn^{2+} where a novel metallo-supramolecular complex has formed.

B4.2 .7 Computational work or structural optimization

Binding moiety orientation of M3 is the same as we discussed earlier in case of M1 and M2 in the Chapter B2.

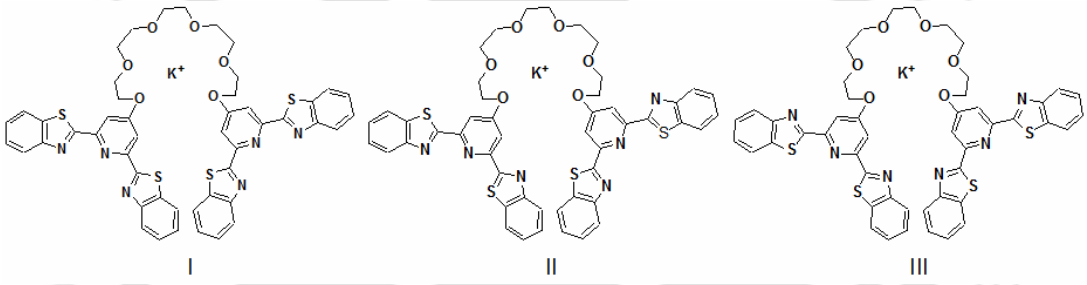

Figure 2 Three different configurations taken up for DFT calculation

The electronic structure calculations for M3-K^+ were performed by choosing three different binding atom orientations out of the all possible orientations (Figure 2) with density functional theory [13-14] applying the ONIOM methods [15-16]. We choose the two extreme possibilities, one with both the N atoms inside the binding site at each of the ends (I in Figure 2) and the other with both the S atoms inside the binding site at each of the ends (III in Figure 2). Another intermediate possibility is also considered for energy value comparison (II in Figure 2). The molecular system was divided into three layers for geometry optimization (Figure 3). In all the three layers, Becke's three parameter hybrid functional [17] with nonlocal correlation of Lee-Yang-Parr [18] was employed. Layer 1, 2 and 3 contains Model 1, Model 2 and Model 3. Model 3 is the real system (Figure 3). The model 1 was treated with 6-31G(d,p) basis set, model 2 with 6-31G(d) and the fully real model (model 3) was treated with 3-21G while the sulfur atoms were treated with 3-21G(d) basis set. Small difference in the basis sets between model 1 and model 2 was maintained as both are involved as active centers. Single point

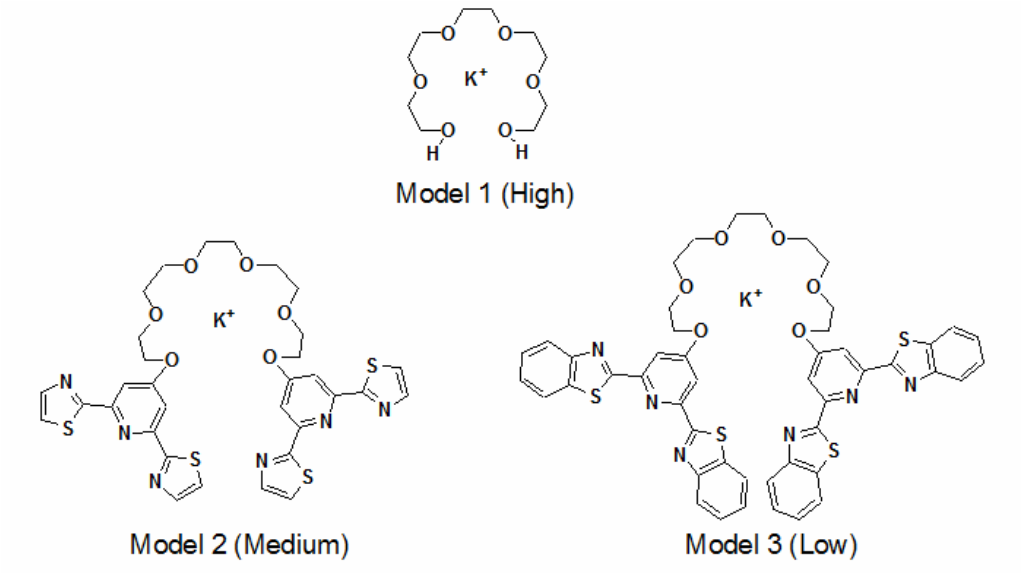

Figure 3 Division of the layers of molecular system for DFT calculation

calculations were performed with B3LYP/6-31+G(d,p) on the optimized geometries for energy correction. All the calculations were carried out using Gaussian 03W program [19].

B4.3 Result and discussion

B4.3.1 UV- visible spectroscopy

Different stages of interaction of M3 with metal ions are followed by UV-visible spectroscopy. The monomer M3 has absorption at λ_{max} 322 nm (Figure 2a). Addition of K^+ ion in increments of 0.1 equivalents gradually decreases the absorption of M3 at 322 nm and a new broad peaks starts growing at 365 nm with clear formation of an isosbestic point at 345 nm(the violet curves in the spectra). This observation establishes the formation of M-K^+ complex. While the M-K^+ reached near 1:1, the change in absorption become almost saturated, as evident from the titration profile (inset of Figure 2a). This indicates that at 1:1 the maximum interaction between the monomer and K^+ ion is possible. At this stage, to the M-K^+ complex, Zn^{2+} ion is added in increments of 0.1 equivalents. This further reduces the absorption intensity of M at 322 nm and the absorption at 365 nm is enhanced gradually. This implies interaction of M-K^+ complex with Zn^{2+} ion. The titration profile (inset of Figure 2a) shows this change is much more prominent than the change with K^+ ion. The same experiment was performed in the reverse order where Zn^{2+} ion is added in increments of 0.1 equivalents prior to addition of

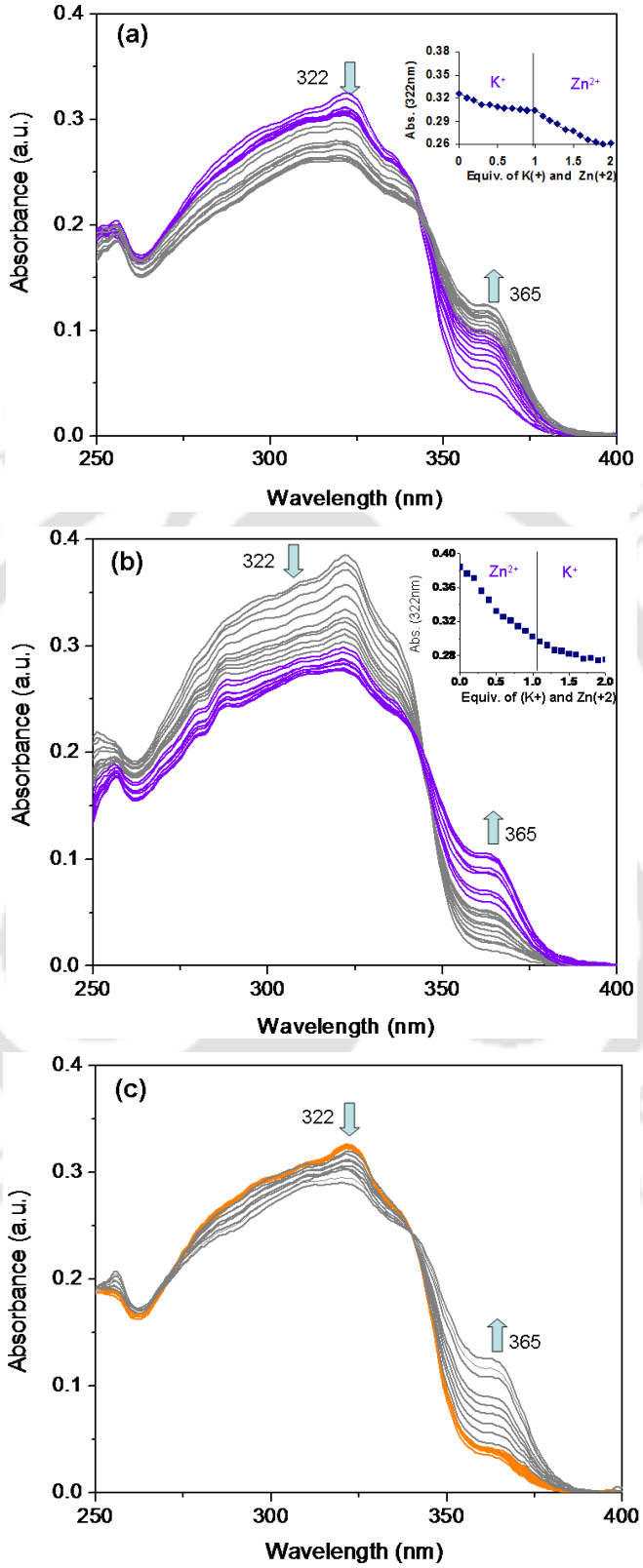

Figure 2 UV visible spectra of titration of (a) M3 with K^+ ion and then with Zn^{2+} ion (b) M3 with Zn^{2+} ion and then with K^+ ion (c) M3 with Na^+ ion and then with Zn^{2+} ion

K^+ ion (Figure 2b). Similar to the earlier case, absorption maxima at 322 nm decreases gradually with growing of a new broad peak at 365 nm with gradual addition of Zn^{2+}. The same peaks continue to grow while K^+ ion is added further. From the titration profile (Inset of Figure 2b) it is clear that Zn^{2+} changes the absorption maxima at 322 nm more in comparison to the K^+ ion. But growth of the new peak is influenced equally by both Zn^{2+} and K^+ ion. Another titration, adopting similar methods was done with Na^+ ion where neither significant change is absorption maxima at 322 nm nor growing of another peak is seen with addition Na^+ ion (Figure 2c). Further addition of Zn^{2+} again changes the absorption spectra similar to the earlier two experiments. This chemoselectivity of M3 towards K^+ ion is significant as selectivity of chemical species towards any among K^+ and Na^+ is of biological importance [20-21].

B4.3.2 Photoluminescence spectroscopy

To confirm the self assembly process further, photoluminescence spectroscopic studies were performed. Photoluminescence spectra of M3 show a peak at 387 nm (Figure 3a). The formation of supramolecular polymeric system in two steps is also followed by changes in photoluminescence spectra on addition of the metal ions. The photoluminescence intensity decreases gradually upon addition of K^+ ion is indication of an interaction between M3 and the K^+ ion. The original intensity significantly decreased from 577 to 407 nm. In the next step, while the M3-K^+ complex is further titrated with Zn^{2+} ion the intensity further decreased to 330 unit while the M3 : K^+ : Zn^{2+} ratio reaches 1:1:1. This gradual decrease in photoluminescence intensity of M3 upon addition of K^+ and Zn^{2+} respectively, put forward clear evidence of electronic interaction between the monomer and the metal ions. Similar results were obtained while we did the reverse experiment by adding Zn^{2+} ions before adding K^+ ion. Interestingly, Na^+ ion could not

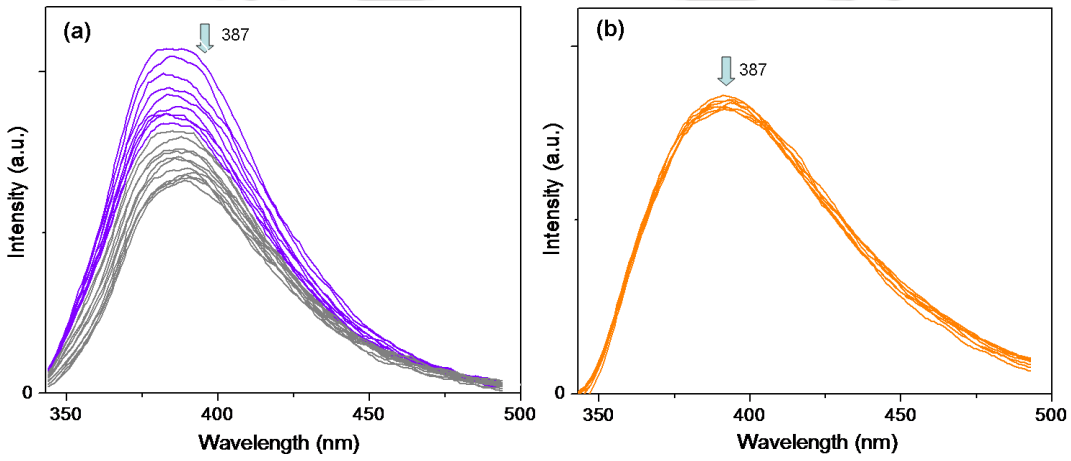

Figure 3 Pl spectra of titration (a) M3 with K^+ ion and then Zn^{2+} ion (b) M3 with Na^+ ion

change the photoluminescence intensity and there by again confirms the selectivity of the monomer towards K^+ ion (Figure 3b).

B4.3.3 Viscosity measurements

Viscosity measurements, in micro molar concentration, establish the different stages of complexation. Mixture solvent (1:9, acetonitrile : chloroform) has viscosity 0.50 mPa s (Figure 4). The micromolar solution of M3 in this solvent system shows viscosity of 0.66 mPa s. On gradual addition of K^+ ion to the monomer solution the viscosity gradually decreases and at 1:1 ration of M3 : K^+ it reaches a minima of 0.63 mPa s. This decrease of viscosity is in agreement with our prediction of folding of M3 upon addition of K^+ ion. The original surface area of M3 on folding decreases and it causes the decrease in viscosity of the system. Again while Zn^{2+} ion is added gradually to the M3- K^+ complex, the viscosity increases rapidly to a maximum of 0.80 mPa-s on addition of 1 equivalent of Zn^{2+}. This is evidence for the formation of supramolecular polymeric system by the M3 – K^+ complex. On further addition of Zn^{2+} ion, the viscosity again starts decreasing from the maximum value and at 2 equivalents it reaches 0.75 mPa s. This is because of the disassembling of the polymeric system which is common in case of metallo-supramolecular polymers. These observations lead to inference that M3-K^+ moiety self assemble with Zn^{2+} ion to form a novel metallo-supramolecular polymeric system.

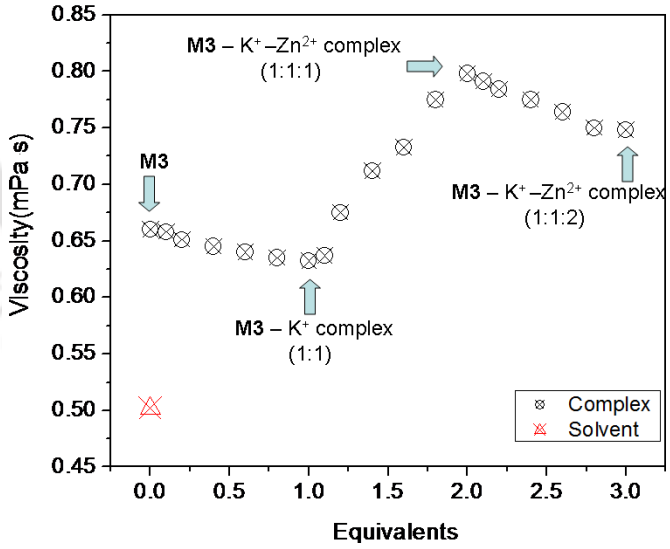

Figure 4 Changes of viscosity of M3 on addition of K^+ ion and then Zn^{2+} ion

B4.3.4 Gel Formation

The monomer M-K^+-Zn^{2+} assembly, in high concentration changes to gel form (Figure 5a). Heating the gel up to 45 °C changes it to sol form, which upon cooling forms back the gel reversibly (Figure 5b). The gel is characterized by FESEM micrographs. The common

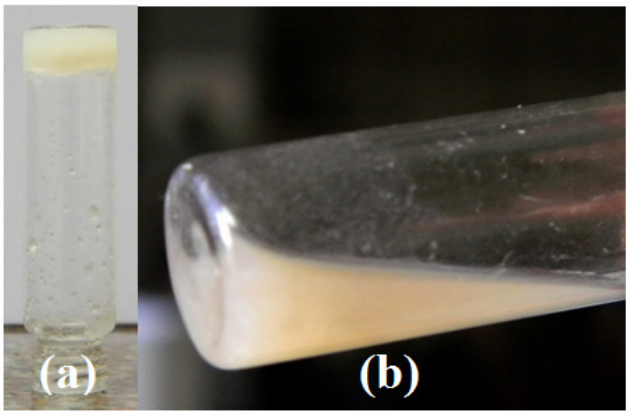

Figure 5 (a) Gel formation by 1:1:1 complex of M3 : K^+ : Zn^{2+} (b) Conversion of the gel to sol form upon treatment up to 45°C.

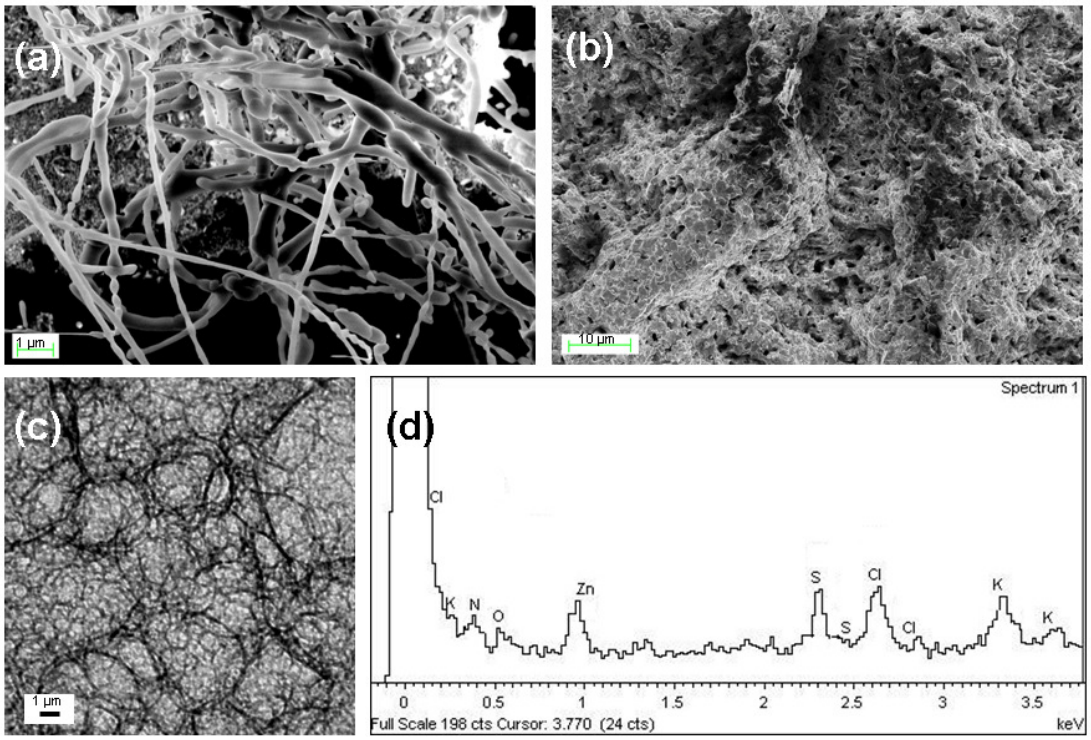

Figure 6 (a) FESEM image gel (b) FESEM image of dried gel (c) TEM image of gel and (d) EDX pattern of the gel formed by 1:1:1 complex of M3:K^+:Zn^{2+}

feature of fiber formation was very much prominent in the gel (Figure 6a). The xerogel, off white in color, is also characterized by FESEM micrograph (Figure 6b). TEM images also reveal the fiber like formation in the gel material (Figure 6c). EDX fitted with TEM showed the presence of the elements that compose the monomer (Figure 6d). The thermo reversible gel, on mechanical shaking also changes to sol form in a reversible manner (Add. Data 7, incorporated in the CD attached)

B4.3.5 Structure optimization (Calculated Results)

We have seen from the structural optimizations that monomer M3-K^+ moiety is resulted by folding of the monomer M3 at the ethereal part and trapping the K^+ ion inside (Figure 7). The M3-K^+ folded moiety, before addition of Zn^{2+} ion took a orientation, where the S atoms are inside the binding site at both the ends of the monomer (C in figure 7). This is similar to our observation in Chapter B2, where the binding moiety (being same as M1 and M2) S-atoms were inside the binding site when it is free. As mentioned in Chapter B2, the binding moiety of M3 changed its orientation while it formed complex with Zn^{2+} ion. In the Zn^{2+} complex of the binding moiety, the smaller N atoms oriented inside the binding site so that the repulsion is minimized (as N atoms are similar than S atom) and form bonds with Zn^{2+}. Similar must be the case while M3-K^+ moiety is involved in polymer formation by Zn^{2+} mediation. At both the ends, the N atoms must orient inside the binding site while the M3-K^+ folded system will involve in metallo-supramolecular polymer formation.

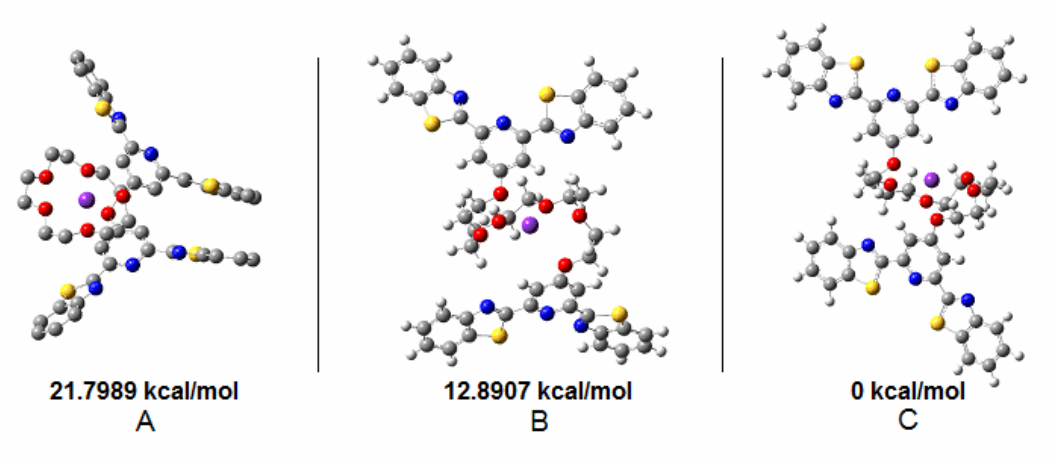

Figure 7 Optimized structures for M3-K+ complex with their respective relative energy values (Add. Data 8-10, incorporated in the CD attached)

B4.4 Concluding remark

The newly synthesized monomer M3 consists of two main structural parts. The spacer part pentaethyleneglycol, with its two ends attached to two aromatic heterocyclic (benzo[d]thiazol-2-yl)pyridine based moieties has total six oxygen atoms present in the spacer part. This makes the molecule open crown ether, which can interact with K^+ ion with its usual affinity. On the other hand the benzothiazol part is a good binding site for transition metal. Therefore, the folded M3-K^+ moiety when titrated with Zn^{2+} ion self assemble to give a novel metallo-supramolecular polymeric system. To confirm the whole

self assembly process of M3 with two different types of metal ions (alkali metal ion and transition metal ion) in two different binding sites and for structural optimization, DFT calculation method was applied and results found were very much supportive of the inferences taken from the experimental studies.

References

[1] Gellman, S. H. *Acc Chem Res* **1998**, *31, 173*.

[2] Seebach, D.; Matthews, J. *Chem Commun* **1997**, 2015.

[3] Kirshenbaum, K.; Zuckermann R. N.; Dill K. A *Curr Opin Struct Biol* **1999**, *9*, 530.

[4] Armitage B. A.; *Bioinspired organic chemistry*. *Annu Rep Prog Chem Sect B: Org Chem* **2000**, *96*,187.

[5] Hill, D. J.; Mio, M. J.; Prince, R.B.; Hughes, T. S.; Moore, J. S. *Chem*. Rev. **2001**, *101*, 3893.

[6] Kelley, R. F.; Rybtchinski, B.; Stone, M. T.; Moore, J. S.; Wasielewski, M. R. *J. Am. Chem. Soc*. **2007**, *129*, 4114.

[7] Cubberley M. S.; Iverson; B. L. *Curr. Opin. Chem. Biol*. **2001**, 5 (6), 650.

[8] Stigers, K. D.; Soth, M. J.; Nowick, J. S. *Curr. Opin. Chem. Biol*. **1999**, *3 (6),* 714.

[9] Patch, J. A.; Barron, A. E. *Curr. Opin. Chem. Biol*. **2002**, *6 (6),* 872.

[10] Nelson, J. C.; Saven, J. G.; Moore, J. S.; Wolynes . *P. G. Science* **1997**, *277 (5333),* 1793.

[11] Lee, O. S.; Saven, J. G. *J. Phys. Chem*. B **2004**, *108 (32*), 11988.

[12] Armarego, W. L. F.; Perrin, D. D. *Purification of Laboratory Chemicals; Butterworth-Heinemann: Burlington, MA*, **2002**.

[13] Hohenberg, P.; Kohn, *W. Phys. Rev. B*, **1964**, *136*, 864.

[14] Kohn, W.; Sham, L. *J. Phys. Rev. A* **1965**, *140*, 1133.

[15] Humbel, S.; Sieber, S.; Morokuma, K. *J. Chem. Phys*. **1996,** 105 (5), 1959.

[16] Svensson, Mats.; Humbe, S; Robert, D. J. F.; Matsubara, T.; Sieber, S.; Morokuma, K. *J. Phys. Chem*. **1996,** *100 (50),* 19357.

[17] Becke.; A. D. *J. Chem. Phys* **1993**, *98*, 5648.

[18] Lee, C.; Yang, W.; Parr, R. *G. Phys. Rev. B* 1988, 37, 785-789.

[19] Frisch, M. J.; Trucks, G. W.; Schlegel, H. B.; Scuseria, G. E.; Robb, M. A.; Cheeseman, J. R.; Montgomery, J. A . Jr.; T. Vreven; Kudin, K. N.; Burant, J. C.; Millam, J. M.; Iyengar, S. S.; Tomasi, J.; Barone, V.; Mennucci, B.; Cossi ,M.; Scalmani, G.; Rega, N.; Petersson, G. A.; Nakatsuji, H.; Hada, M.; Ehara, M.; Toyota, K.; Fukuda, R.; Hasegawa, J.; Ishida, M.; Nakajima, T.; Honda, Y.; Kitao, O.; Nakai, H.; Klene, M.; Li, X.; Knox, J. E.; Hratchian, H. P.; Cross, J. B.; Bakken, V.; Adamo, C.; Jaramillo, J.; Gomperts, R.; Stratmann, R. E.; Yazyev, O.; Austin, A. J.; Cammi, R.; Pomelli, C.; Ochterski, J. W.; Ayala, P. Y.; Morokuma, K.; Voth, G. A.; Salvador, P.; Dannenberg, J. J.; Zakrzewski, V. G.; Dapprich, S.; Daniels, A.D.; Strain, M.C.; Farkas, O.; Malick, D.K.; Rabuck, A.D.; Raghavachari, K.;

Foresman, J. B.; Ortiz, J. V.; Cui, Q.; Baboul, A. G.; Clifford, S.; Cioslowski, J.; Stefanov, B. B.; Liu, G.; Liashenko, A.; Piskorz, P.; Komaromi, I.; Martin, R. L.; Fox, D. J.; Keith, T.; Al-Laham, M. A.; Peng, C. Y.; Nanayakkara, A.; Challacombe, M.; Gill, P. M. W.; Johnson, B.; Chen, W.; Wong, M. W.; Gonzalez, C.; Pople, J. A. *Gaussian* 03, Revision E.01, Gaussian, Inc., Wallingford CT, **2004**.

[20] Tyerman, D. S.; Terry, R.B. *Plant Physiol* **1991**, 97, 598.

[21] Miler C. *Science* **1993**, 261(5129), 1692.

^{1}H NMR of P3HT (Chapter A2)

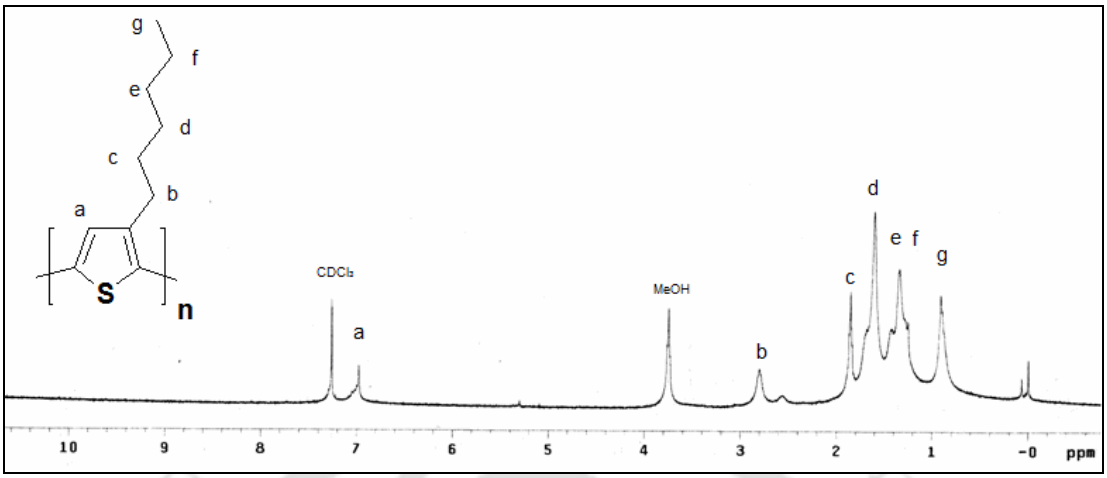

^{13}C NMR of P3HT (Chapter A2)

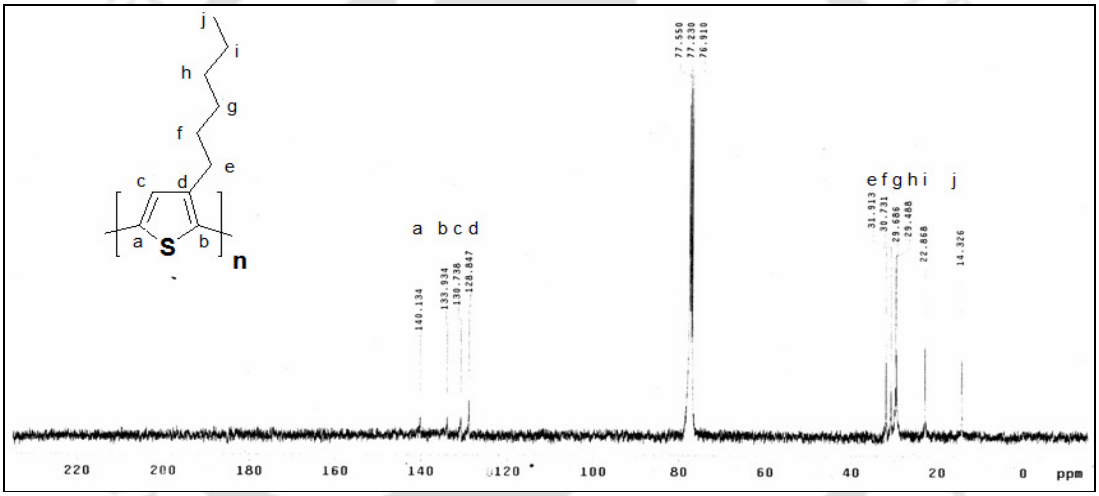

^{1}H NMR of M1(Chapter B2)

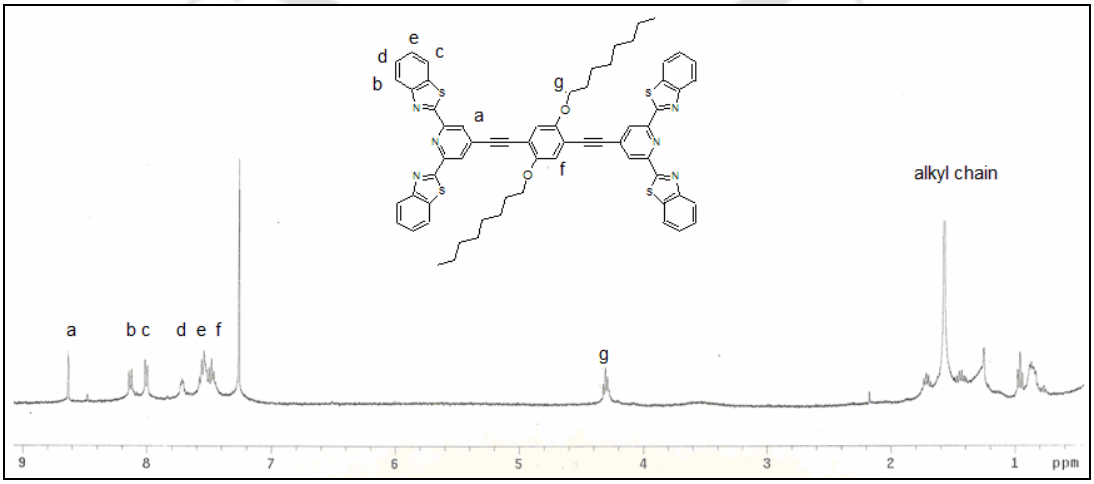

^{13}C NMR of M1 (Chapter B2)

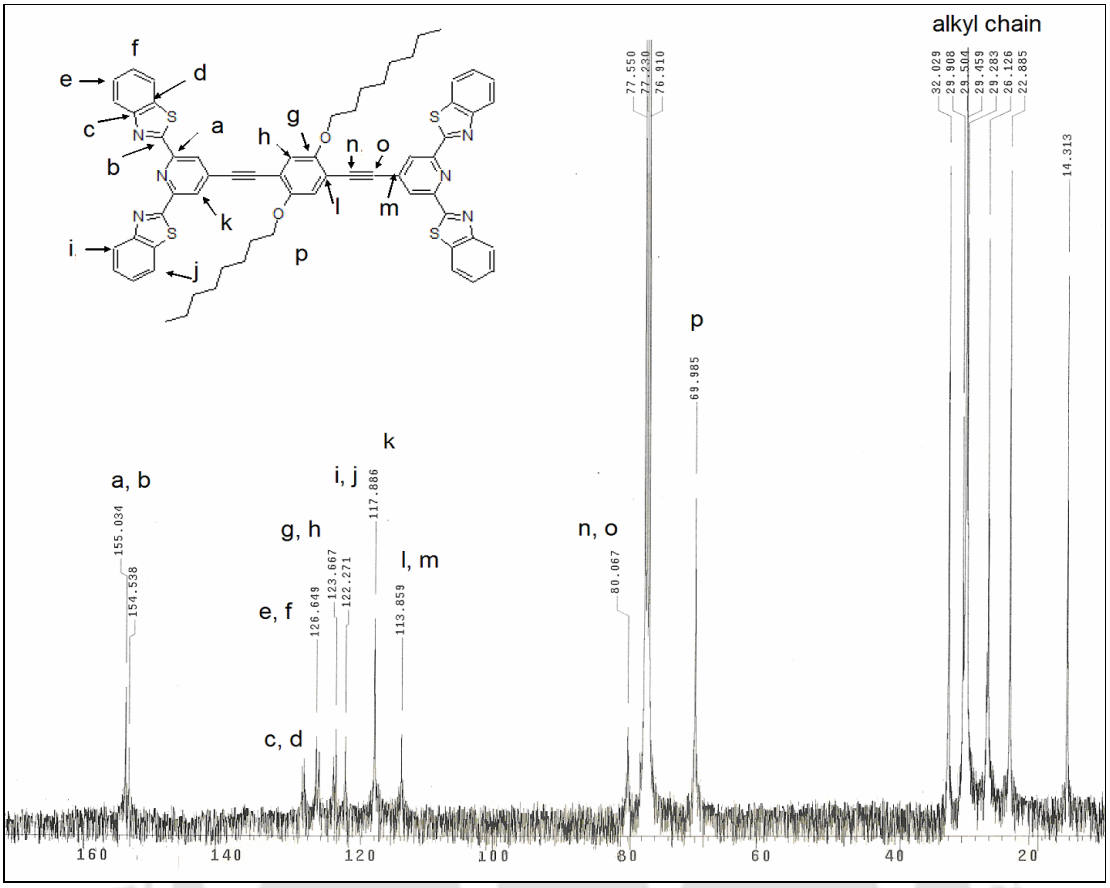

^{1}H NMR of M2(Chapter B2)

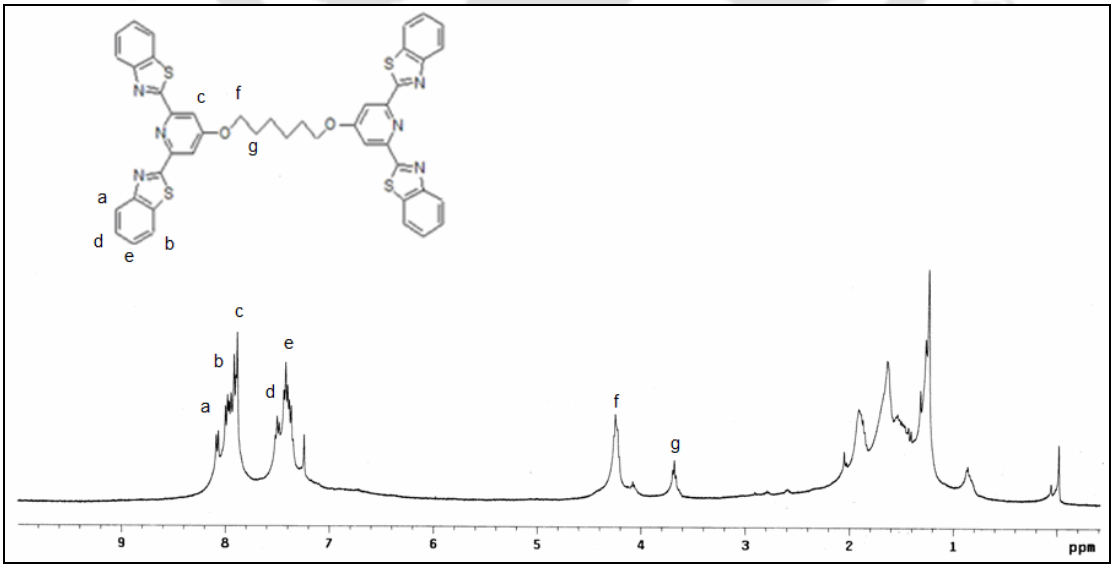

^{13}C NMR of M2 (Chapter B2)

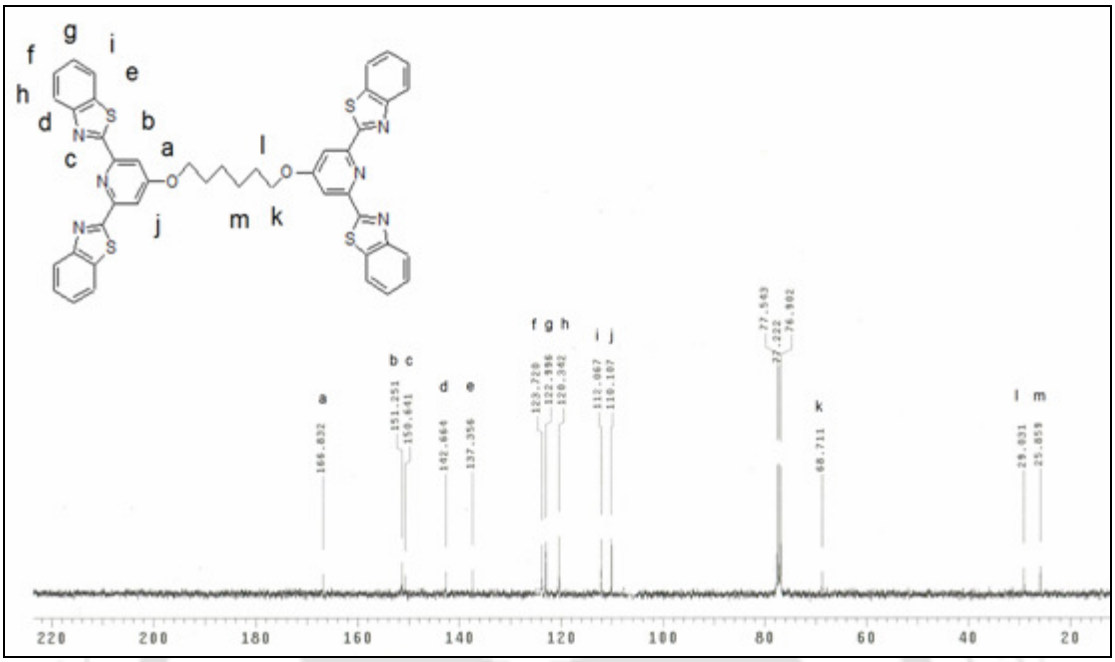

^{1}H NMR of M3(Chapter B4)

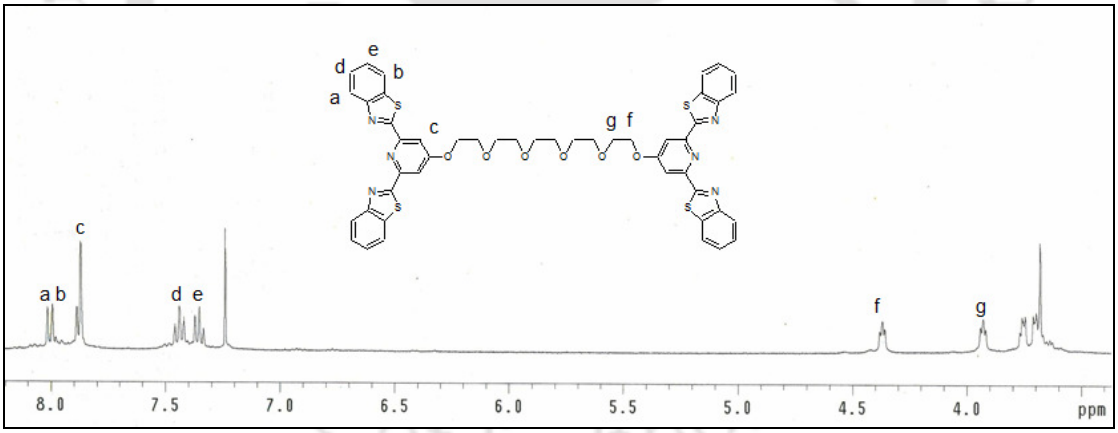

^{13}C NMR of M3 (Chapter B4)

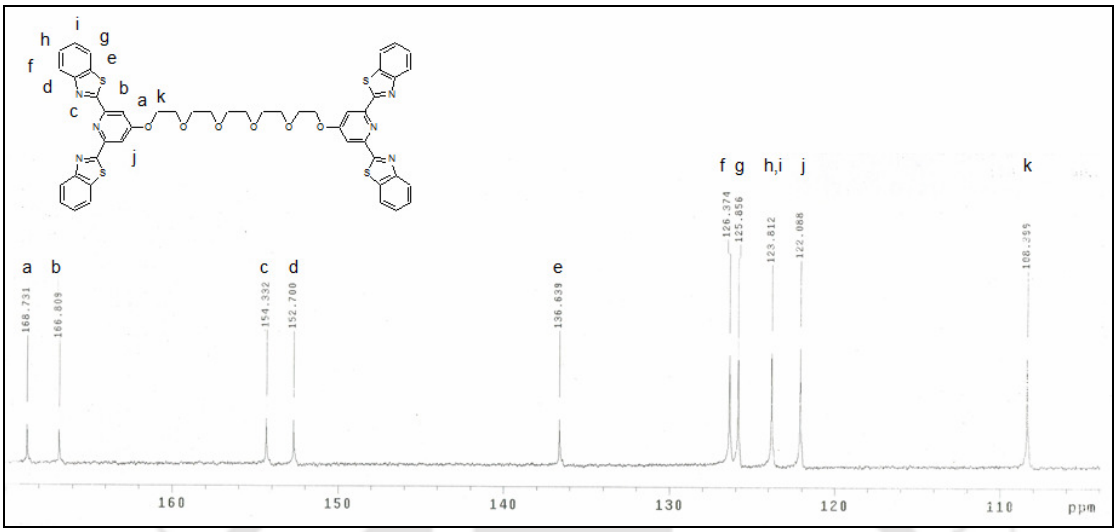

Publications

Journals

[1] *Mechanistic investigation, kinetic modeling and analysis parameters of poly(3-hexylthiophene) degradation to fullerenes* Reddy, P. K.; **Goutam, P. J.**; Singh, D. K.; Ghoshal, A. K. Iyer, P. K. *Poly Degrad Stab* **2009**, *94*, 1839.

[2] *Enhancing the photostability of poly(3-hexylthiophene) by preparing composites with multiwalled carbon nanotubes* **Goutam, P. J.**; Singh, D. K.; Giri, P. K.; Iyer, P. K. *J. Phys. Chem. B* **2011**, *115*, 919.

[3] *Photoluminescence quenching of poly(3-hexylthiophene) by carbon nanotubes* **Goutam, P. J.**; Singh, D. K.; Iyer, P. K. *J. Phys. Chem. C* **2012**, 116, 8196.

[4] *Proof of urea and thiourea recognition by 2,6-bis(2-benzimidazolyl) pyridine using spectroscopic techniques and DFT'* Chetia, B.; **Goutam, P. J.**; Chipem, F. A. S.; Iyer, P. K. (Communicated).

[5] *Self assembling metallo-supramolecular polymer and foldamer gels assisted by alkali and transition metal* **Goutam, P. J.**; Chetia, B.; Chipem, F. A. S.; Iyer, P. K. (Communicated).

[6] *Guest selective recognition of resorcinol by 1,6-bis(2,6-bis(benzothiazol-2-yl)pyridine-4-yloxy)hexane* **Goutam, P. J.**; Iyer, P. K. (Manuscript under preparation).

[7] *Photochemical stability enhancement in Poly(3-hexylthiophene)/PCBM nano composites by addition of MWCNT* **Goutam, P. J**. , Rath, R.; Iyer, P. K. (Manuscript under preparation).

[8] *Synthesis and optical properties of 2,6-bis(bezthiazolyl)pyridine based metallo-supramolecular polymers* **Goutam, P. J.**; Iyer, P. K. (Manuscript under preparation).

Book chapter

[1] *Photostability of Poly-(3-hexylthiophene)-Multiwalled Carbon Nanotube Nanocomposites* **Goutam, P. J.**; Singh, D. K.; Giri, P. K.; Iyer, P. K. *Electroactive Polymers: Materials and Devices*, Vol III, Macmillan, **2009**.

Vitae

Prasanta Jyoti Goutam was born in Assam, India. He obtained his Bachelors in Chemistry from Govt. Science College, Jorhat, and completed Masters in Chemistry from Indian Institute of Technology Guwahati. Under the supervision of Dr. Parameswar Krishnan Iyer, he started his research career at the Department of Chemistry, Indian Institute of Technology Guwahati. His current research interests include design and development of polymeric materials for optoelectronic applications, metallo-supramolecular polymers and sensors.